JOURNAL OF APPLIED PHYSICS

JOURNAL
OF
APPLIED PHYSICS

Vol. 18, No. 9 SEPTEMBER, 1947

In This Issue

Page

Microwave Dielectric Measurements T. W. Dakin and C. N. Works 789

Electron Beam Deflection. Part II. Applications of the Small-Angle Deflection Theory R. G. E. Hutter 797

70-Mev Synchrotron F. R. Elder, A. M. Gurewitsch, R. V. Langmuir, and H. C. Pollock 810

Cathode-Ray Presentation of Three-Dimensional Data Otto H. Schmitt 819

Least-Square Application to Relaxation Methods O. L. Bowie 830

X-Ray Diffraction Study of the Silver-Magnesium Alloy System Harold R. Letner and S. S. Sidhu 833

Erratum: The Torsion of a Rubber Cylinder R. S. Rivlin 837

Preliminary Analysis of Microwave Transmission Data Obtained on the San Diego Coast Under Conditions of a Surface Duct C. L. Pekeris and M. E. Davis 838

Letters to the Editor:

Modified Cavity Oscillator for the Generation of Microwaves George G. Bruck 843

Particle "Growth" in the Electron Microscope V. E. Cosslett 844

Ultrasonic Modulation of a Light Beam R. F. Humphreys, W. W. Watson, and D. L. Woernley 845

Films, Resistant to Organic Solvents, for Use in the Electron Microscope S. G. Ellis 846

Note on the Reduction of Microphonics in Triodes Victor W. Cohen and Abraham Bloom 847

Comments on "Sound-Velocity Determination of Molecular Weights" G. J. Dienes 848

Preliminary Measurements Relative to the Onset of Thermal Convection Currents in Unconsolidated Sands H. L. Morrison 849

Attachments for Aligning a Console Electron Microscope Henry C. Froula 850

In Every Issue

New Books 851

New Booklets 851

Here and There 852

Calendar of Meetings 854

Index to Advertisers xxx

BOARD OF EDITORS

Elmer Hutchisson, *Editor*

Associate Editors

R. Bowling Barnes
Otto Beeck
W. F. Busse
Selig Hecht
W. James Lyons
Philip Morrison
Paul E. Sabine
Frederick Seitz
J. R. Townsend
John Von Neumann

Publication of the American Institute of Physics

ADMINISTRATIVE STAFF

Henry A. Barton, *Director*

Cleveland Norcross, *Assistant Director*

Ruth F. Bryans, *Publication Manager*

Theodore Vorburger, *Business Manager*

John T. Tate, *Adviser on Publications*

GOVERNING BOARD

George R. Harrison, *Chairman*

Wallace Waterfall, *Secretary*

George B. Pegram, *Treasurer*

E. U. Condon
A. J. Dempster
W. F. Fair, Jr.
Floyd A. Firestone
Harvey Fletcher
R. C. Gibbs
K. S. Gibson
Paul E. Klopsteg
A. H. Pfund
John T. Tate
M. W. White
A. G. Worthing

The Journal of Applied Physics, published monthly at Prince and Lemon Sts., Lancaster, Pa., is devoted to physics in its role as the science basic to other natural sciences and to the arts and industries. Previous to 1937 this publication was known as Physics. The Journal of Applied Physics publishes editorials, news of physicists, and reviews, as well as technical papers of applied physics.

Manuscripts should be submitted to Elmer Hutchisson, Editor, Case School of Applied Science, Cleveland 6, Ohio.

Subscriptions and orders for back numbers should be addressed to Prince and Lemon Streets, Lancaster, Pa. or to the American Institute of Physics, 57 East 55 Street, New York 22, N. Y.

Subscription Price

	U.S. and Canada	Elsewhere
To members and associate members of the American Institute of Physics	$6.00	$7.00
To all others	8.00	9.00

Back Number Prices

Complete set: Vol. 1, July, 1931–Vol. 17, 1946—$124.00
Yearly back number rate: $10.00
Single copies: $1.00 each.

Changes of address and proofs should be addressed to the Publications Manager.

Advertising rates supplied on request. Orders, advertising copy, and cuts should be sent to the American Institute of Physics.

Entered as second class matter January 22, 1937, at the Post Office at Lancaster, Pennsylvania, under the Act of March 3, 1879. Accepted for mailing at the special rate of postage provided for in the Act of February 28, 1925, authorized May 2, 1932.

Copyright 1947, by the American Institute of Physics.

Journal
of
Applied Physics

Volume 18, Number 9 September, 1947

Microwave Dielectric Measurements

T. W. Dakin and C. N. Works
Westinghouse Research Laboratories, East Pittsburgh, Pennsylvania

(Received March 7, 1947)

The method of measurement of the dielectric properties of solid dielectrics described by S. Roberts and A. von Hippel has been applied with 3-cm wave-length waves in a rectangular wave guide. In this method the dielectric sample is placed at a short circuited end of the transmission line, and the dielectric properties of the sample, calculated from the position of a minimum of the standing wave and the ratio of the minimum field strength to the maximum field strength of the standing wave. A simplified procedure for calculating the dielectric properties from the measurements is presented. Values are given of the dielectric properties of some common plastic and ceramic materials at 10-cm wave-length and 3-cm wave-length, which were measured with this method.

INTRODUCTION

At microwave frequencies the dielectric properties of a material can be obtained accurately only by measuring the wave-length in the material or its reflecting power and the attenuation of the wave in the material. There are many experimental ways in which the problem can be attacked. A summary of the experimental work in this field up to 1927 is given by Romanoff.[1] His summary includes the pioneering work of Drude,[2] who proposed two methods, the first of which consisted of measuring the wave-length directly in the dielectric media surrounding a resonant section of a pair of lecher wires, and the second of which consisted of measuring the capacitance of a small capacitor containing the dielectric and closely attached to the resonant section of lecher wires. Drude's second method contains inherent errors, when applied at very short wave-lengths, because of the inaccuracy of considering a capacitor as a lumped capacitance at these wave-lengths. Drude's second method has, however, been used by many investigators[3] even up to recent years. Modifications and improvements of Drude's first method, including experiments where only a part of the resonant section of a transmission line is filled with dielectric, have been made by many investigators[4] since the summary of Romanoff. In more recent work, enclosed coaxial or hollow

[1] W. Romanoff, *Handbuch der Physik* (Julius Springer Verlag, Berlin, 1927), Vol. XV, p. 491.

[2] Paul Drude, Zeits. f. physik. Chemie **23**, 267 (1897). Ann. Physik und Chemie **55**, 633 (1895); *ibid.* **61**, 466 (1897).

[3] W. Hemple, Elekt. Nachr.-Techn. **14**, 33 (1937); J. W. Miller and B. Salzberg, R.C.A. Rev. **3**, 486 (1938); R. Odenwald, Ann. d. Physik **35**, 690 (1939); H. Slatis, Ann. d. Physik **36**, 397 (1939); C. Klages, Physik. Zeits. **43**, 151 (1942).

[4] M. Seeberger, Ann. d. Physik **16**, 77 (1933); H. Kaufmann, Hoch: tech. u. Elek: akus. **53**, 61 (1939); J.; Malsch, Ann. d. Physik **12**, 865 (1932); *ibid.* **19**, 707 (1934); *ibid.* **20**, 33 (1934); M. Ardenne, Otto Groos, and G. Otterbein, Physik. Zeits. **37**, 533 (1936); R. King, Rev. Sci. Inst. **8**, 201 (1937); K. Slevogt, Ann. d. Physik **36**, 141 (1939).

transmission lines have been used.[5] Optical methods where the transmission through slabs of the dielectric and reflection from the dielectric surface are measured have also been used[6] with microwaves. Direct measurement by probes of standing waves set up within liquid dielectrics and in front of dielectric surfaces by reflection have also been used to obtain dielectric properties.[7] Resonant-cavity methods where all or part of the cavity is filled with dielectric are an extension of the resonant-transmission line idea and these have been used at microwave frequencies.[8]

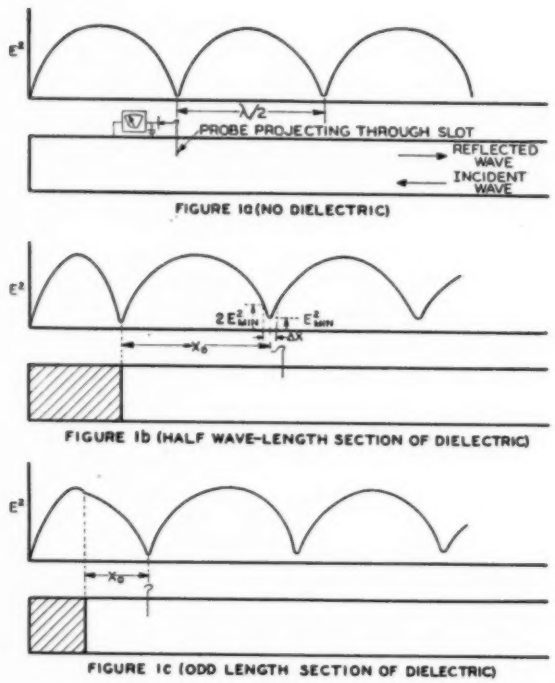

FIG. 1. Standing-wave patterns in short circuited wave guide.

[5] W. I. Kalinin, Physik. Zeits Sowjetunion **10**, 257 (1936); H. R. L. Lamont, Phil. Mag. **7–29**, 521 (1940); *ibid.* **7–30**, 1 (1940); W. Kusters, Hoch: tech. u. Elek: akus. **59**, 129 (1942); G. Fejer and P. Scherrer, Helv. Chim. Acta. **15–7**, 645 (1942); G. Williams, Phil. Mag. **7–35**, 283 (1944); J. Benoit, J. de phys. et rad. **8–5**, 173, 203 (1944); C. R. Englund, Bell Sys. Tech. J. **23**, 114 (1944).

[6] J. D. Tear, Phys. Rev. **21**, 611 (1923); Zeits. f. Physik **113**, 415 (1939); W. Kebbel, Hoch: tech. u. Elek: akus. **53**, 81 (1939), G. Baz, Physik. Zeits. **40**, 394 (1939); L. Palmer and G. Forrester, Proc. Phys. Soc. London, **53**, 479 (1941); L. H. Ford and R. Oliver, Proc. Phys. Soc. London **58**, 265 (1946).

[7] M. Velasco and G. L. Hutchinson, Proc. Phys. Soc. London **51**, 689 (1939); A. N. Soos, Comptes rendus Acad. Sci. U.R.S.S. **33**, 310 (1941); W. P. Conner and C. P. Smyth, J. Am. Chem. Soc. **65**, 382 (1943).

[8] F. Borguis, Naturwiss. **29**, 516 (1941); C. N. Works, T. W. Dakin, and F. W. Boggs, Trans. A. I. E. E. **63**, 1092 (1944); D. L. Hollaway, J. Inst. Eng. Aust. **21**, 79 (1940); W. R. MacLean, J. App. Phys. **17**, 558 (1946).

[9] S. Roberts and A. von Hippel, J. App. Phys. **17**, 610 (1946).

MEASUREMENT TECHNIQUE AND CALCULATIONS

The method using standing-wave measurements in the transmission line in front of the dielectric sample proposed by S. Roberts and A. von Hippel[9] has been developed for the measurement of solid dielectrics to a more practical state than any other method in recent years. This is the method which is used and discussed in this paper. This method consists of reflecting the wave at normal incidence from a slab of the dielectric which is placed against a perfectly reflecting surface. The process of reflection sets up standing waves in the space region in front of the sample as a result of the superposition of the incident and reflected waves (See Figs. 1a, 1b, 1c). The electric field direction is maintained at right angles to the direction of propagation of the wave (TE wave).

In actual practice the wave and the dielectric sample are restricted to an enclosed hollow or coaxial wave guide, although this is not in principle a necessary restriction. The same equations are valid in principle for a measurement using lecher wires or free space with a parallel beam of radiation, although it is more difficult in practice to do measurements under those conditions.

The separation of the first minimum from the face of the sample will depend on the wavelength of the wave in the sample and its thickness, since the first minimum will be an integer number of half-waves from the reflecting surface behind the sample (See Fig. 1b). In Figs. 1b and 1c the shortening of the wave-length in the sample is shown. Insertion of the dielectric shifts the minima of the standing wave toward the end. The separation of the first minimum of the standing wave from the surface of the sample is a measure of the dielectric constant.

If there is any attenuation in the dielectric, there will be a reduction in the standing-wave ratio E_{max}/E_{min}, since all the incident wave intensity would not be reflected. There is, of course, a finite standing-wave ratio with no dielectric present, because of the slight attenuation by the copper- or silver-walled transmission line. The measured value of E_{max}/E_{min} is mathematically

related to the attenuation constant and the dielectric constant of the slab of dielectric by the relation (1) which was derived by S. Roberts and A. von Hippel.[9]

$$\frac{\frac{E_{min}}{E_{max}} - i\tan\frac{360x_0}{\lambda_g}}{1 - i\frac{E_{min}}{E_{max}}\tan\frac{360x_0}{\lambda_g}} \cdot \frac{\lambda_g}{2\pi d i} = \frac{\tanh\gamma_2 d}{\gamma_2 d}. \quad (1)$$

Where x_0 is the distance from the first electric field strength minimum of the standing wave to the face of the sample, d is the thickness of the sample, and λ_g is the wave-length along the wave guide outside the sample. E_{min}/E_{max} is the ratio of the electric field strength at an adjacent maximum point. γ_2 is the propagation constant of the wave in the wave guide and within the sample.

The most general procedure is to solve the above complex transcendental equation for $\gamma_2 d$ after the measured values of E_{min}/E_{max}, λ_g, d, and x_0 are obtained. The solution of this equation can be obtained directly only by the use of charts of the complex function: $\tanh\gamma_2 d/\gamma_2 d$. Such charts have been prepared by Professor von Hippel and co-workers.[10] A convergent series solution has also been obtained by them for the case where $360x_0/\lambda_g$ is near to 90° or an odd multiple of 90°, and E_{min}/E_{max} is small. But this direct method of solving the complex transcendental equation is very laborious.

A simpler solution, usually of sufficient accuracy, can be obtained when the value of the dissipation factor of the dielectric is less than 0.1 by separating Eq. (1) into its real and imaginary parts and equating them separately, remembering that $\gamma_2 = \alpha_2 + \beta_2 i$. Equation of the real parts gives:

$$\frac{-\lambda_g \tan\frac{360x_0}{\lambda_g}\left(1 - \frac{E^2_{min}}{E^2_{max}}\right)}{2\pi d\left(1 + \frac{E^2_{min}}{E^2_{max}}\tan^2\frac{360x_0}{\lambda_g}\right)} = \frac{\beta_2 d\tan\beta_2 d(1-\tanh^2\alpha_2 d) + \alpha_2 d(1+\tan\beta_2 d)\tanh\alpha_2 d}{(\alpha_2^2 d^2 + \beta_2^2 d^2)(1+\tanh^2\alpha_2 d\tan^2\beta_2 d)}. \quad (2)$$

When $\alpha_2 d$ and E_{min}/E_{max} are small, the above equation reduces to:

$$\frac{-\lambda_g \tan\frac{360x_0}{\lambda_g}}{2\pi d} = \frac{\tan\beta_2 d}{\beta_2 d}. \quad (3)$$

This is an equation involving no complex numbers which may be readily solved for $\beta_2 d$ by reference to a table of $(\tan\theta)/\theta$ for radian arguments. Such an abbreviated table exists in Jahnke Emde's *Funktionentafeln*. A more complete table has been prepared at the Westinghouse Research Laboratory, and another by the Laboratory for Insulation Research at MIT.[11] The values on the left side of Eq. (3) are measured quantities, and after $\beta_2 d$ has been obtained the dielectric constant can be calculated from the following equation:

$$\epsilon' = \frac{1/\lambda_c^2 + \frac{(\beta_2 d)^2}{(2\pi d)^2}}{1/\lambda_c^2 + 1/\lambda_g^2}, \quad (4)$$

where ϵ' is the dielectric constant, λ_c is the cut off wave-length of the wave guide. If coaxial wave guide is used, $1/\lambda_c^2$ is zero. The above equation is accurate only for materials having dissipation factors less than 0.1. The solution of Eq. (3) for $\beta_2 d$ is multi-valued and will give several values of ϵ'. If the correct one cannot be selected by previous knowledge of the material, a second measurement is necessary using a sample of different length, d.

An expression can now be obtained for the attenuation constant by equating the imaginary

[10] Report III by A. von Hippel, D. G. Jelatis, and W. B. Westphal, Laboratory for Insulation Research, MIT Contract OEMsr 191, N.D.R.C.

[11] Report IX by W. B. Westphal, Laboratory for Insulation Research, MIT Contract OEMsr-191 N.D.R.C.

parts of Eq. (1).

$$\frac{-\lambda_g \frac{E_{\min}}{E_{\max}}\left(1+\tan^2\frac{360x_0}{\lambda_g}\right)}{2\pi d\left(1+\frac{E^2_{\min}}{E^2_{\max}}\tan^2\frac{360x_0}{\lambda_g}\right)}$$

$$=\frac{\alpha_2 d\tan\beta_2 d-\alpha_2 d\tan h^2\alpha_2 d\tan\beta_2 d-\beta_2 d\tan h\alpha_2 d-\beta_2 d\tan h\alpha_2 d\tan^2\beta_2 d}{(1+\tan h^2\alpha_2 d\tan^2\beta_2 d)(\alpha_2^2 d^2+\beta_2^2 d^2)}. \quad (5)$$

When α_2 and $E_{\min}/E_{\max}$ are small, Eq. (5) reduces to:

$$\alpha_2 d\cong\frac{\beta_2^2 d^2\lambda_g}{2\pi d}\cdot\frac{E_{\min}}{E_{\max}}\frac{\left(1+\tan^2\frac{360x_0}{\lambda_g}\right)}{\beta_2 d(1+\tan^2\beta_2 d)-\tan\beta_2 d}. \quad (6)$$

Roberts and von Hippel[9] have shown that $E_{\min}/E_{\max}=\pi\Delta x/\lambda g$ where Δx is the width of the minimum of the standing wave to the double power points. After making this substitution, and putting in an equivalent value for α_2, Eq. (6) gives an analytical expression for the dissipation factor:

$$\tan\delta_2=\frac{\Delta x}{d}\left[\frac{(1/\lambda_c^2+1/\lambda_g^2)-1/\lambda_c^2\epsilon'}{(1/\lambda_c^2+1/\lambda_g^2)}\right]\times\frac{\beta_2 d\left(1+\tan^2\frac{360x_0}{\lambda_g}\right)}{\beta_2 d(1+\tan^2\beta_2 d)-\tan\beta_2 d}. \quad (7)$$

In the above equation the term within the brackets reduces to unity for coaxial wave guide, since $1/\lambda_c^2$ is zero in that case. In carrying out calculations it is first necessary to obtain $\beta_2 d$ and $\tan\beta_2 d$ from Eq. (3) before the dissipation factor is calculated using Eq. (7).

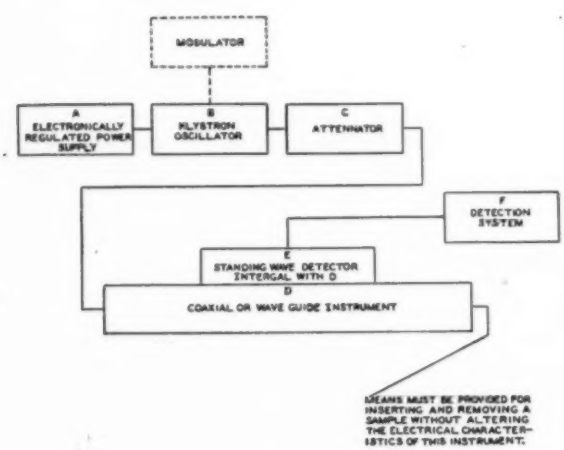

FIG. 2.

Since there is always some dissipation in the walls of the wave guide, a measurement of $E_{\min}/E_{\max}$ includes those losses together with the dielectric losses. These wave guide losses must be subtracted. The proper procedure is first to correct the measured value of $E_{\min}/E_{\max}$ for the loss due to the wave guide in front of the sample, between the sample face and the measured minimum. Then the total dissipation factor of the wave guide and sample are calculated from Eq. (7), and the dissipation factor of the wave guide subtracted from the result. The dissipation factor of the wave guide can be obtained from Eq. (7) after measuring the value of Δx with the wave guide empty. In this case ϵ' would be unity, d would be the distance from the measured minimum to the shorted end of the wave guide, and both $\tan(360x_0/\lambda_g)$ and $\tan\beta_2 d$ would be very large. Then Eq. (7) gives for the dissipation factor of the wave guide:

$$\tan\delta_w=\frac{\Delta x}{d}\frac{1}{1+\lambda_g^2/\lambda_c^2}. \quad (8)$$

Since the approximations involved in going from Eqs. (2) to (3) and from (5) to (6) are not readily obvious except in the limiting cases of very large $\tan(360x_0/\lambda_g)$ and $\tan\beta_2 d$ or of $\tan(360x_0/\lambda_g)$ and $\tan\beta_2 d$ less than unity, a numerical check of the validity of the approximations was made by substituting in typical measured values of Δx, d and $(360x_0/\lambda_g)$. It was verified by numerical calculation that Eq. (3) is accurate to about ± 1 percent in the dielectric

constant for dissipation factors less than 0.1. This numerical check was made for a wide range of values of $(360x_0/\lambda_g)$, varying from 0° to 120° and also a wide range of values of Δx and d by comparing values of ϵ' and $\tan\delta$ obtained from Eqs. (3), (4), and (7) with those obtained from a direct graphical solution of Eq. (1) for γ_2. The accuracy of the approximation increases with decreasing $\tan\delta$. Similar accuracy is also obtained in the calculation of $\tan\delta$

EXPERIMENTAL

The complete electrical system is shown in schematic form in the block diagram, Fig. 2. Figures 3 and 4 show the standing-wave detector and sample holding section of the instrument. The cross section of the guide and the sample is 0.900″ by 0.400″. Typical samples vary in length from about $\frac{1}{8}$″ for high loss and high dielectric constant materials to about $1\frac{1}{2}$″ for low loss and low dielectric constant materials.

The position of the probe must be known with great precision, so a Gaertner comparator, No. 1658, 0–100 mm, which reads accurately to 0.001 mm, was used to carry the probe. The probe must have sufficient length to give sufficient signal at the minimum of the wave pattern; its presence should not disturb the field; it must be shielded so that it does not produce disturbing radiation.

The steel brackets shown as E and F in Fig. 3 enabled a careful adjustment of the comparator so that the probe would move parallel (within ±0.0001″) with the bottom of the wave guide. The wave guide was milled from two pieces of brass with the inside silver plated. The dimensions of the guide were held to a tolerance of ±0.0001″ with parallel top and bottom. The 13-cm slot which accommodates the probe was made narrow (0.070″) and deep (0.175″) to reduce the radiation from it. This choice of slot dimensions makes it possible to place one's fingers on the slot without changing the response of the detector.

Details of the probe assembly are shown in Fig. 4. The probe which extends into the guide is a silver-plated steel wire of 0.012″ diameter, and its extent of penetration into the guide is adjustable. The probe is tuned with an adjustable choke so that maximum energy will be transferred from the probe to the detector.

The wave guide instrument has been used both tuned and untuned. When operating untuned, a tapered non-reflecting attenuator is placed between the end where the power is introduced and the end where measurements are made. This requires the introduction of more energy for the same detector current than in the case where the guide is tuned with a shorting plunger at the end opposite where the measurement is made.

Two different reflex klystron tubes (WE 721A and Sperry 2K25) operating in the vicinity of 10,000 megacycles have been used with the wave-guide instrument.

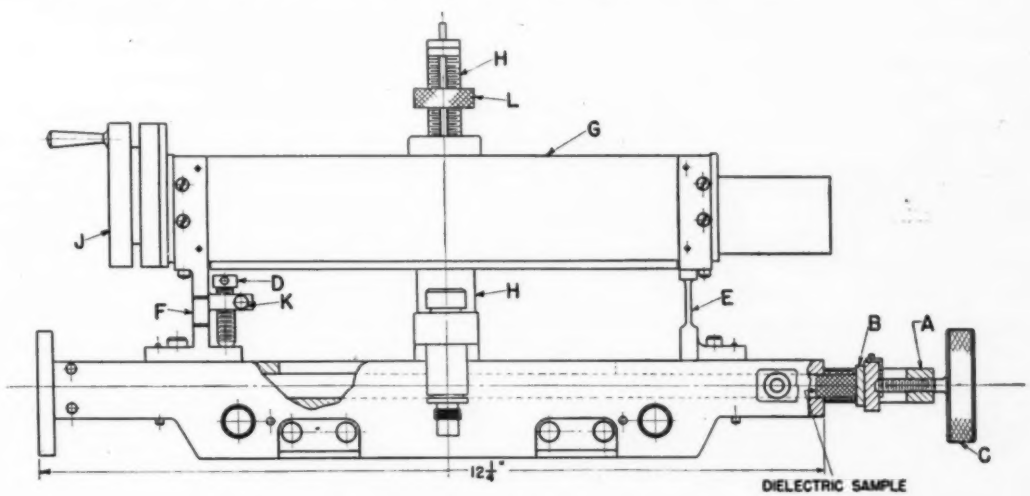

FIG. 3. The wave-guide instrument for dielectric measurements at 3 cm.

The power supplies for these tubes are of the conventional electronic voltage-regulated type.[12] The reflector voltage is pulse modulated by a square wave generator operating at an audiofrequency to amplitude modulate the microwave intensity. But where an automatic frequency control system was used to stabilize further the frequency of the oscillator tube for increased accuracy in the measurement of low loss materials, the microwave intensity was usually not modulated and a d.c. detector was used.

The crystal d.c. current from the 1N21 crystal detector shown in Fig. 4 was assumed to be proportional to the square of the radiofrequency electric field in the wave guide for low currents at which it is used. Galvanometers have been used as crystal current meters when the microwaves are unmodulated. The galvanometer should have a sensitivity of at least 0.002 micro ampere per mm to give a deflection that is readable with sufficient accuracy for measurements at the minimum voltage region.

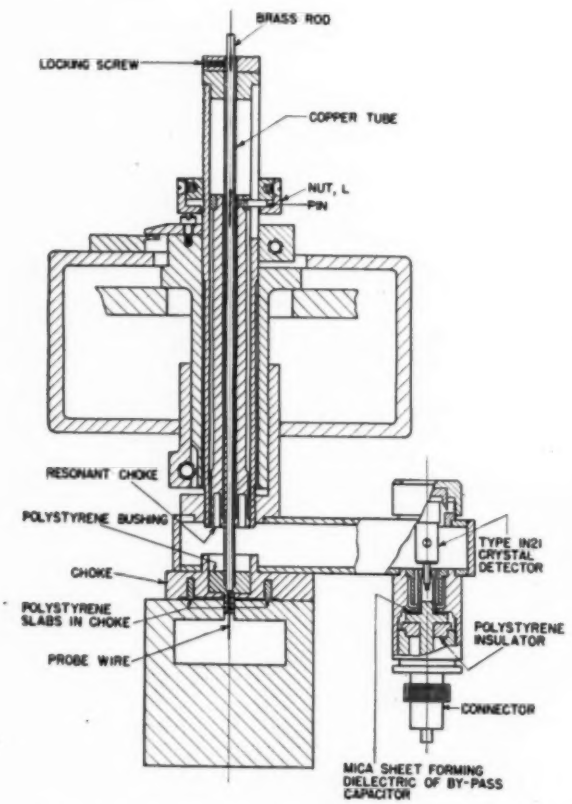

FIG. 4. Cross section through probe assembly and wave guide.

The rapid response of an a.c. amplifier makes it preferred over a galvanometer as a crystal-current indicator. When the microwave power is pulse modulated at an audiofrequency, a sensitive tuned audiofrequency amplifier is used with a panel output meter. The amplifier must be linear so that the output meter reading is always proportional to crystal current. Use of a reasonably high audiofrequency-tuned amplifier also has the advantage of largely eliminating spurious noise developed in the crystal.

SOURCES OF ERRORS IN THE MEASUREMENTS

(1) Errors Due to Change in the Frequency of the Oscillator

Changes in frequency may result during the measurement as a result of too close coupling between the oscillator tube and the measuring wave guide, or because of inadequate regulation of the electrode voltages on the tube. This, of course, results in changes in position of the voltage minima in the wave guide.

(2) Errors Due to Excessive Projection of the Probe into the Wave Guide

If the probe projects too far into the wave guide, it causes an error in both the position of the minimum and the value of Δx. If the detecting system and the standing wave detector are adjusted for maximum sensitivity, the required projection of the probe to obtain a satisfactory deflection of the indicating instrument should be such that no error is introduced. When very high loss samples are in the wave guide, it is well to check against this source of error by increasing or decreasing the projection of the probe into the wave guide by about 1/64 inch and again measuring the location of the minimum and the value of Δx. No change should be observed.

(3) Errors Due to Frequency Modulation

It has been found that appreciable frequency modulation of the source causes the value of Δx to be increased. This effect is analyzed by M. G. Haugen and W. B. Westphal.[13]

[12] F. E. Terman, *Radio Engineers Handbook* (McGraw-Hill Book Company, Inc., New York, 1943), p. 614.

[13] M. G. Haugen and W. B. Loss, "The design of equipment for measurement of dielectric constant and loss with

TABLE I.

Type of wave guide	Max. dimension for lowest TE mode only**	Min. dimension for lowest TE mode**	λ_c	Wave-length in sample λ_s	Characteristic impedance
Coax					
r_0 = outer radius	$r_0 - r_1 \lesssim \frac{\lambda}{2}$	none	∞	$*\lambda_a/(\epsilon')^{\frac{1}{2}}$	$\frac{*138}{(\epsilon')^{\frac{1}{2}}} \log_{10}\frac{r_0}{r_1}\left(\frac{1}{1-i\tan\delta}\right)^{\frac{1}{2}}$
r_1 = inner radius	$r_0 + r_1 \lesssim \frac{\lambda}{\pi}$				
Rectangular					
a = smaller width	$\frac{1}{a^2}+\frac{1}{b^2} > \frac{4}{\lambda^2}$	$b > \frac{\lambda}{2}$	$\lambda_c = 2b$	$*\frac{\lambda_c\lambda_a}{(\lambda_c^2\epsilon' - \lambda_a^2)^{\frac{1}{2}}}$	$***376.6\left(\frac{\mu}{\epsilon'}\right)^{\frac{1}{2}}\frac{\lambda_s}{\lambda_a}\left(1+\frac{i\epsilon''}{2\left(\epsilon'-\frac{\lambda_s^2}{\lambda_c^2}\right)}\right)$
b = greater width	$b < \lambda$				
Cylindrical					
r = radius	$r < \frac{\lambda}{2.61}$	$r > \frac{\lambda}{3.41}$	$\lambda_c = 3.41r$	$*\frac{\lambda_c\lambda_a}{(\lambda_c^2\epsilon' - \lambda_a^2)^{\frac{1}{2}}}$	$***376.6\left(\frac{\mu}{\epsilon'}\right)^{\frac{1}{2}}\frac{\lambda_s}{\lambda_a}\left(1+\frac{i\epsilon''}{2\left(\epsilon'-\frac{\lambda_s^2}{\lambda_c^2}\right)}\right)$

* $\tan\delta < 0.1$ and neglecting conductor losses.
** Divide λ by $(\epsilon')^{\frac{1}{2}}$ where guide is filled with dielectric.
*** Not comparable to characteristic impedance of coax ($\mu = 1$ for most dielectrics).
λ_a = free space wave-length.

However, if the wave form of the square wave signal used to modulate the oscillator is properly adjusted so that it reaches maximum value in a very short time and has a flat top or, in other words, approaches an ideal square wave closely, the frequency modulation introduced in this way will be so small that the error in the value of Δx will be less than the precision with which this quantity may be measured, because of mechanical limitations in the design of the standing wave detector.

(4) Errors Due to Faulty Tuning

Changes in the apparent value of the width of the minima have been noted when the wave guide is tuned slightly off resonance. This does not occur when operating with a non-reflecting attenuator and an untuned section of the guide.

(5) Higher Transmission Modes in the Dielectric

It is possible to have higher modes than the lowest TE mode within the dielectric at the end of the wave guide, even though the wave guide is beyond cut off for those modes in that part of the guide filled with air. The existence of other modes within the dielectric will cause a spurious reflection at the surface of the dielectric and lead to erroneous results in the dielectric constant and dissipation factor.

From the relations in Column 2 of Table I, it can be seen that when a dielectric is present, the wave-length should be longer if only the lowest TE mode is desired. Probably resonant lengths of dielectric samples, i.e., ones which are a multiple of $\frac{1}{4}$ or $\frac{1}{2}$ wave-length (in the sample) for the higher mode, should be avoided, for these lengths are more likely to give the higher modes. The values of λ given by the expressions in Column 2 of Table I give the cut off wave-lengths for the next higher modes. From these the wave-length in the guide in the dielectric sample can be calculated for the higher mode of transmission. The effect of higher modes on the accuracy of measurements has not been thoroughly investigated. Care should be taken especially with high dielectric constant materials where the possibility of higher modes is increased. Even with the coax instrument, the possibility of higher modes is prevalent.

MEASUREMENTS—DATA

Dielectric measurements at 3-cm wave-length and 10-cm wave-length have been made on a variety of plastic and ceramic materials during a

standing waves in wave guides," Laboratory for Insulation Research, Massachusetts Institute of Technology, Cambridge, Massachusetts, National Defense Research Committee, Contract OEMsr-191, Report XII.

TABLE II. Dielectric properties at 3-cm wave-length.

Material	ϵ'	tanδ	α, Nepers per meter, coax or free space*	D.B. per meter, coax or free space*	N, refractive index	Power-reflection coefficient normal incidence
Polyethylene	2.29	.00032	0.051	.44	1.514	.042
Polystyrene	2.43	.00036	0.060	.52	1.59	.052
Teflon	2.05	.00025	0.038	.33	1.431	.031
NaCl crystal	5.78	.0002	0.05	.43	2.40	.17
Insanol**	7.96	.0042	1.24	10.8	2.82	.228
Corning glass 704	4.79	0.0063	1.45	12.6	2.19	.139
Corning glass 707	4.05	0.0022	0.46	4.0	2.01	.113
Micarta 199†	4.03	0.0624	13.14	114.3	2.01	.113
Micarta 496†	3.58	0.054	10.7	93.	1.89	.095
Micarta 254†	3.36	0.039	7.47	65.	1.83	.086
Micarta 299†	4.61	0.0211	4.75	41.3	2.15	.133
Micarta 259†	5.36	0.041	9.95	86.6	2.32	.158
Micarta 273†	3.56	0.0686	13.57	118.0	1.89	.095
Cerex resin	2.69	0.0031	.53	4.6	1.64	.059
Polydichlorstyrene	2.63	0.0005	.085	.74	1.62	.056
Nylon	3.09	0.0106	1.95	17.0	1.76	.076
993 Silicone	2.90	0.0050	.89	7.7	1.70	.067
Fosterite 80–20	2.57	0.0048	.81	7.0	1.60	.053
Fosterite 35–65	2.58	0.0144	2.43	21.1	1.61	.055
Molded Micarta 192a	4.34	0.0093	2.03	17.6	2.08	.123
Kraft board***	3.55	.121	23.8	207.	1.88	.093
Kraft board, dry	2.99	.05	9.1	79.	1.73	.072
Dense Kraft board***	3.82	.122	24.9	217.	1.95	.104
Dense Kraft board, dry	3.20	.05	9.4	82.	1.79	.080
Ivory, walrus tusk	6.98	.0934	25.8	225.	2.64	.204

* Divide values in this column by $(1-\lambda^2/\epsilon'\lambda_c^2)^{\frac{1}{2}}$ for attenuation in wave guide.
** Westinghouse product similar to Mycalex.
*** At 30 percent humidity.
† Micarta 199 is a chopped cotton cloth filled phenol formaldehyde plastic. Micarta 273 is a fine weave cotton cloth phenol formaldehyde resin laminate. Micarta 259 is a glass cloth melamine formaldehyde resin laminate. Micarta 254 is a Kraft paper cresol formaldehyde resin laminate. Micarta 299 is a glass cloth cresol formaldehyde resin laminate. Micarta 496 is a medium weave cotton cloth phenol formaldehyde resin laminate.

period of several years. These results have been reported to interested persons when they requested the information, but have not been contained in any previous report in a tabulation. These data are now collected together with this paper.

The measurements were all made according to the method outlined in this paper, and the dielectric properties calculated according to the scheme outlined in this paper. The results of these measurements are tabulated in Table II along with useful attenuation and reflection constants of these materials for those frequencies.

The values for 10-cm wave-length were obtained on the MIT designed coaxial wave guide instrument (Reference 10) with the same technique in measurement as with the hollow rectangular wave guide.

In some cases, the materials are quite variable

TABLE IIa. Dielectric properties at 10-cm wave-length.

Material	ϵ'	tanδ	α, Nepers per meter in coax or free space	DB. per meter in coax or free space	N, index of refraction	Power reflection coefficient normal incidence
Polyethylene	2.29	0.0002 to 0.0006	0.0095 to 0.028	0.083 to 0.25	1.506	0.041
Polystyrene	2.50	0.0003	0.015	0.13	1.58	0.050
Insanol	7.95	0.006	0.53	4.6	2.82	0.23
Corning glass 704	4.80	0.004	0.275	2.4	2.19	0.14
Corning glass 707	3.96	0.0013	0.081	0.70	1.99	0.11
Corning glass 774	4.45	0.0051	0.34	3.0	2.11	0.13
Micarta 199	4.31	0.0860	5.6	49.	2.08	0.12
Micarta 254	3.66	0.0632	3.8	33.	1.91	0.10
Micarta 496	4.20	0.0988	63.	55.	2.05	0.12
Micarta glass filled	4.29	0.0243	1.58	13.7	2.07	0.12
Pork meat	62.6	0.30	74.	640.	7.9	0.60

in composition, and deviations from the values reported in Table II might be found. In some cases, the dissipation factor and dielectric constant are quite sensitive to moisture. In these cases, the conditions of humidity or dryness of the materials when the samples were measured are given.

SUMMARY

A method of measurement of the dielectric properties of solids at microwave frequencies has been discussed. A rectangular wave-guide apparatus for performing measurements in the vicinity of 10,000 megacycles has been described in detail. A simplified method of calculating the results of the wave-guide measurements is presented. Included in the paper are values of the dielectric properties of some common plastics and ceramics measured at 10-cm wave-length and 3-cm wave-length.

The authors wish to acknowledge guidance they obtained through the prior and simultaneous work in this field carried out at the laboratory for insulation research at the Massachusetts Institute of Technology under the direction of Professor A. von Hippel. Appreciation is also expressed to members of the Electronics Department of the Westinghouse Research Laboratory, who introduced us to some of the microwave apparatus which we have applied.

Electron Beam Deflection

Part II. Applications of the Small-Angle Deflection Theory

R. G. E. HUTTER*

(Received February 26, 1947)

The theory developed in Part I is applied to a number of typical deflection fields such as the fields produced by parallel plates, parallel cylinders, semi-infinite co-planar sheets, and bent-plates. Graphs for the magnitude of deflection are given. An electrolytic tank potential-plotting device is described which was used for the determination of the potential distribution of some of the deflection fields.

The theory shows that the deflection is a function of the initial conditions of the electron beam before entering the field and that it is a slightly non-linear function of the field strength. It follows that the fluorescent spot and the pattern produced on the screen of cathode-ray tubes will show distortions. These distortions were calculated for several deflection fields and electron beam shapes; the results are shown graphically.

The problem of the reduction of these distortion effects is discussed.

A. THE DEFLECTION BY TYPICAL ELECTRIC DEFLECTION FIELDS

ELECTROSTATIC deflection systems are ordinarily designed by experienced personnel. Since no design formulae or charts of reasonable accuracy exist to aid the inexperienced person, he must therefore use the deflection formula for the parallel-plate deflection field without edge effects[1] as a guide. He may then correct the resultant error by adjustment of the deflection potential. This means that deflection amplifiers having a wide gain adjustment must be provided. It is the purpose of this paper to present design charts for a number of typical electric deflection systems.

The paper "Electron Beam Deflection," Part I,[2] contained a mathematical expression for the deflection in terms of the accelerating potential ϕ and the axial field-strength distribution $E(z)$ (Part I, Eq. (31)). It is (assuming $x_0=y_0=x_0'=y_0'=0$):

$$d=Y(z_i)=Y_i=-(1/2\phi)\int_{z_0}^{z_i}d\zeta\int_{z_0}^{\zeta}E(u)du, \quad (1)$$

where z_0 is a point on the axis on the entrance side of the deflection field and z_i is the coordinate of the screen position; z_0 and z_i are ordinarily in regions where the field-strength of the deflection field is nearly equal to zero. (The deflection electrodes are assumed to be of infinite extent in the x direction.)

If Eq. (1) is used to determine the deflection, the axial field-strength distribution $E(z)$ must be known. Some electrode configurations exist for which $E(z)$ may be determined mathematically. In most cases, this distribution must be obtained by an experimental method, e.g., one which makes use of an electrolytic tank. Electrode systems of the first type are parallel plates with and without fringing fields, parallel cylinders or wires, and semi-infinite co-planar sheets. A field of the second type is that produced by the commonly employed bent-plate electrode system.

Before going into the discussion of these fields it should be mentioned that an alternative method might be used to determine the deflection d by such fields. This method is based on a formula derived by H. G. Rudenberg[3] which expresses the deflection d in terms of the capacitance per unit width of the deflection system. The derivation of this formula may be based on Eq. (30) of Part I for $Y(z)$ which led to Eq. (1). The slope of the electron path is given by (assuming $y_0'=0$)

$$Y'(z)=-(1/2\phi)\int_{z_0}^{z}E(u)du=\tan\theta. \quad (2)$$

* Sylvania Electric Products, Inc., 34–10 Linden Place, Flushing, New York.

[1] I. G. Maloff and D. W. Epstein, *Electron Optics in Television* (McGraw-Hill Book Company, Inc., New York, 1938), p. 198.

[2] R. G. E. Hutter, J. App. Phys. **18**, 740 (1947).

[3] H. G. Rudenberg, J. App. Phys. **16**, 279 (1945).

If the field is essentially different from zero only between the axial coordinates z_1 and z_2, the angle at z_2 for small deflection angles will be given by

$$\theta_2 = -(1/2\phi)\int_{z_1}^{z_2} E(u)du. \qquad (3)$$

Rudenberg has shown by an application of Gauss' theorem that Eq. (3) is equivalent to

$$\theta_2 = (1/2\phi)\rho/\epsilon_0,$$

where ρ is that portion of the charge density on the deflection electrodes which is active in producing the deflection, and ϵ_0 is the dielectric constant of free space. The charge density ρ, the capacitance c per unit width of the deflecting electrodes, and the deflection potential $\Delta\phi$, are related by

$$\rho = c \cdot \Delta\phi.$$

Hence,

$$\theta_2 = c\Delta\phi/2\phi\epsilon_0. \qquad (4)$$

The deflection at the screen becomes

$$d = (z_i - z_2)\cdot\theta_2 = (z_i - z_2)\cdot(c\Delta\phi/2\phi\epsilon_0). \qquad (5)$$

For some electrode configurations it is possible to determine the capacitance per unit width mathematically; in most cases this quantity would have to be measured.

It is apparent that both expressions for the deflection d (Eq. (1) and Eq. (5)) will yield the same result if z_i is greater than z_2. The formula given by Eq. (5), however, cannot be used to determine the deflection at the coordinate of the exit side of the electrode configuration because of the contribution of the fringing field on that side of the electrodes to the value of the capacitance c. The magnitude of the deflection at that point is important in deciding the question of whether or not an electron beam hits the electrodes. It may be determined by means of Eq. (1).

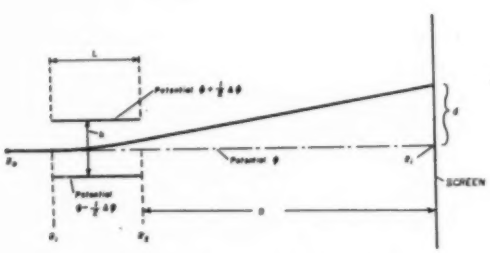

FIG. 1. The parallel-plate deflection field.

1. Mathematically Obtained Field Distributions

a. *Parallel Plates without Fringing Effects*

The field that can most easily be treated mathematically is an idealized one which, however, cannot be produced in practice if the electrodes are of finite length. It is that between two parallel plates which are at the potentials $\phi+\frac{1}{2}\Delta\phi$ and $\phi-\frac{1}{2}\Delta\phi$. The geometry of this field is shown in Fig. 1. The idealization is expressed by making the following assumption regarding the field-strength distribution:

$$E(z) = \left\{ \begin{array}{lll} 0 & \text{For} & z < z_1, \\ -\Delta\phi/h & \text{For} & z_1 \leqq z \leqq z_2, \\ 0 & \text{For} & z > z_2. \end{array} \right\} \qquad (6)$$

If $E(z)$ of Eq. (6) is substituted in Eq. (1), one obtains the familiar formula

$$d = (\Delta\phi/2\phi)(1/h)L(D+\tfrac{1}{2}L), \qquad (7)$$

where $z_2 - z_1 = L$, $z_i - z_2 = D$, h is the distance between the electrodes, ϕ is the accelerating potential (potential of the last anode) and $\Delta\phi$ is the potential difference between the electrodes.

Because of the idealization of the field-strength distribution, large errors occur if Eq. (7) is applied to actual parallel-plate deflection systems.

b. *Parallel Plates with Fringing Effects*

An application of the Schwartz transformation of the theory of functions of a complex variable yields an expression for the equipotential distribution at the edge of semi-infinite parallel plates.[4] It is, therefore, possible to obtain a mathematical expression for the axial field-strength distribution of such an edge field. In order to obtain the axial field-strength distribution of parallel plates of finite length two expressions for a single edge may be used. If the axial coordinates of the entrance and exit edge of the parallel plates are given by z_1 and z_2, respectively (Fig. 1), the axial field strength may be written as:

$$E(z) = -(\Delta\phi/h)(1/1+r), \qquad (8)$$

where r is given in terms of the axial coordinate

[4] R. Rothe, F. Ollendorff and K. Pohlhausen, *Theory of Functions* (Technology Press, Massachusetts Institute of Technology, Cambridge, 1942), p. 138.

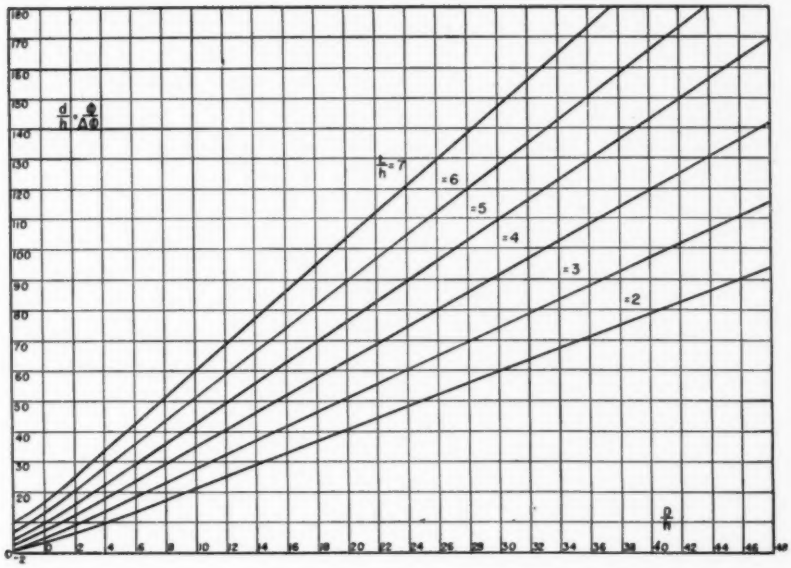

FIG. 2. The deflection by parallel plates (1 form).

by:

$$\left.\begin{aligned} z&=z_1+h/2\pi[1+r+\ln r] \\ &\qquad \text{For} \quad -\infty<z\leqq z_1+z_2/2, \\ z&=z_2-(h/2\pi)[1+r+\ln r] \\ &\qquad \text{For} \quad z_1+z_2/2\leqq z<+\infty. \end{aligned}\right\} \tag{9}$$

Measurements have shown that Eqs. (8) and (9) describe the axial field-strength distribution well for plates for which the field strength $E(z)$ is very nearly $-\Delta\phi/h$ at $z=\frac{1}{2}(z_1+z_2)$. This was found to be the case for parallel plates with ratios of L/h larger than two.

The integration indicated by Eq. (1) must be performed in two steps corresponding to the two branches of the axial field-strength distribution. The resultant mathematical expression for the deflection is unwieldy, hence the deflection is better presented in the form of a graph. Any quantity except h can easily be determined from Fig. 2 if the other quantities are known. It is possible to replot the graph and obtain a new one (Fig. 3) which permits the determination of h with ease if the other quantities are known.

c. *Parallel Cylinders or Wires*

The method of conformal mapping yields in this case a mathematical expression for the axial field distribution.[5] The geometry is shown in Fig. 4. With the notation explained in this figure, the axial field-strength distribution becomes

$$E(z)=-\frac{2\Delta\phi}{cq/2}\,\frac{1}{\ln\dfrac{1+q}{1-q}}\cdot\frac{1}{1+\left(\dfrac{z}{cq/2}\right)^2}. \tag{10}$$

Substituting Eq. (10) in Eq. (1), the deflection d is given by

$$d=\frac{\Delta\phi}{\phi}\cdot\frac{cq}{2}\cdot\frac{1}{\ln\dfrac{1+q}{1-q}}\left[\frac{z_i}{\dfrac{cq}{2}}\arctan\frac{\dfrac{z_i}{cq/2}-\dfrac{z_0}{cq/2}}{1+\dfrac{z_iz_0}{(cq/2)^2}}+\tfrac{1}{2}\ln\frac{1+\left(\dfrac{z_0}{cq/2}\right)^2}{1+\left(\dfrac{z_i}{cq/2}\right)^2}\right], \tag{11}$$

which is shown graphically in Fig. 5. $[z_0/(cq/2)]$ was assumed to be equal to -30. At this point $E\cong(1/900)E(0)$.

This deflection field was discussed by G. Rudenberg.[3]

d. *Semi-Infinite Co-planar Sheets*

Another field for which the axial field-strength distribution may be determined accurately by the method of conformal mapping is that produced

[5] K. Kupfmüller, *Einführung in die Theoretische Elektrotechnik* (Julius Springer Verlag, Berlin, 1932), p. 71.

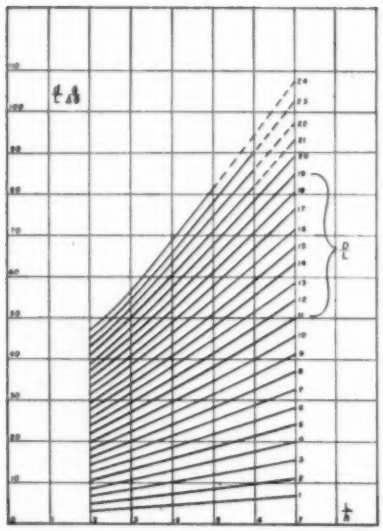

FIG. 3. The deflection by parallel plates (2 form).

by two semi-infinite co-planar sheets.[6] The geometry is shown in Fig. 6. With the use of the notation indicated in this figure, the axial field-strength distribution becomes

$$E(z)=(1/\pi)\Delta\phi(1/a)1\Big/\left[1+\left(\frac{z}{a}\right)^2\right]^{\frac{1}{2}}. \quad (12)$$

The deflection is then given by

$$d=\frac{a}{2}\frac{\Delta\phi}{\pi\phi}\left\{\frac{z_i}{a}\ln\frac{z_i/a+[1+(z_i/a)^2]^{\frac{1}{2}}}{z_0/a+[1+(z_0/a)^2]^{\frac{1}{2}}}-\left(\frac{z_i}{a}-\frac{z_0}{a}\right)\right.$$
$$\left.-\left(\frac{1}{z_i/a+[1+(z_i/a)^2]^{\frac{1}{2}}}-\frac{1}{z_0/a+[1+(z_0/a)^2]^{\frac{1}{2}}}\right)\right\}. \quad (13)$$

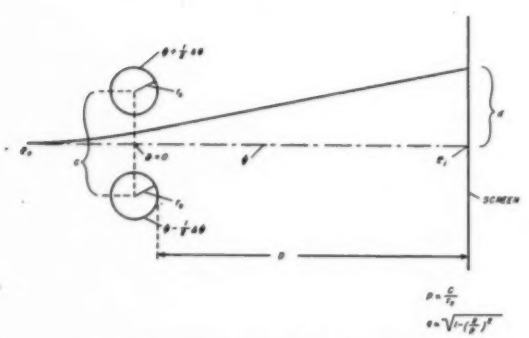

FIG. 4. The parallel-cylinder deflection field.

[6] W. R. Smythe, *Static and Dynamic Electricity* (McGraw-Hill Book Company, Inc., New York, 1939), p. 89.

This expression is shown graphically in Fig. 7. z_0/a was assumed to be equal to -900. At this point $E\cong(1/900)E(0)$.

2. An Experimental Method to Determine the Field Distribution

In general, it is not possible to determine the axial field distribution mathematically. It may, however, be determined experimentally with sufficient accuracy by means of an electrolytic tank. This instrument is useful in many electron-optical investigations and is available in many electronic laboratories in one form or another.

The theory underlying the use of the tank has been presented many times in the literature[7,8] and will, therefore, not be repeated here. The following paragraphs will give a brief description of the instrument, developed in the Research Laboratories of Sylvania Electric Products, Inc., and its application to a number of problems of deflection systems.

a. *The Electrolytic Tank Potential-Plotting Apparatus.*

Figure 8 is a photograph of the entire set-up which consists of two electrolytic tanks (T_1, T_2), a plotting board (B), an instrument rack (I.R.), a plotting mechanism, and an arrangement for positioning the electrodes to be investigated.

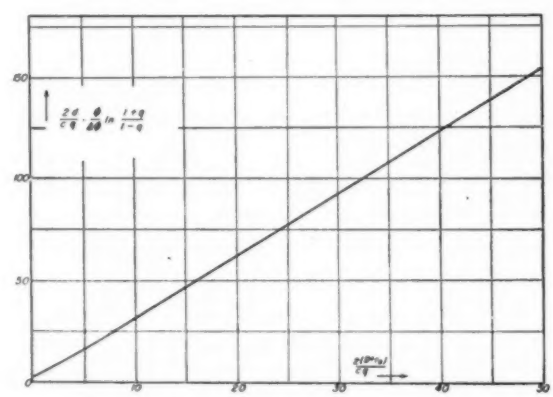

FIG. 5. The deflection by parallel cylinders $\left(z_0/(cq/2)=-30,\quad E\left(\frac{z_0}{cq/2}\right)\cong\frac{1}{900}E(0)\right)$.

[7] V. K. Zworykin and G. A. Morton, *Television* (John Wiley and Sons, Inc., New York, 1940), p. 73.

[8] V. K. Zworykin, G. A. Morton, E. G. Ramberg, J. Hillier, and A. W. Vance, *Electron Optics and the Electron Microscope* (John Wiley and Sons, Inc., New York, 1946), p. 389.

These tanks are constructed of lava slabs; the inside dimensions of tank T_1 are $30'' \times 30'' \times 60''$, and $5'' \times 30'' \times 30''$ for tank T_2. Ordinary tap water is used as the electrolyte in tank T_2, while deionized water is used in tank T_1. The plotting mechanism consists of two rails (R.R.) extending the full length of both tanks. A carriage C_1 is provided which travels on the rails R.R., and is provided with another pair of rails r.r., at right angles to R.R., upon which is mounted a second carriage C_2. The second carriage carries the probe (P) and a long beam member (b) which holds the stylus (S). A close-up view of the tank T_2 and the components C_2, b, and P is shown in the photographs, Fig. 9. The probe is a 5-mil platinum wire which is sealed into one end of a glass tube which is enclosed in a metal tube for shielding purposes. The probe may be brought to any point on the water surfaces of either of the two tanks by turning two hand wheels which operate—through gears—the motion of both carriages. Stylus and probe are rigidly connected and trace out identical curves. Figure 9 also shows a larger sized view of the electrode holders. The electrodes under investigation (in Fig. 8—two bent plates) are supported by adjustable arms (L.L.) which slide on two flat rails (R_1, R_2). The heads (H.H.) of the support mechanism can be tilted in two directions and the electrodes can be adjusted in the vertical direction. The instrument rack (I.R.) above the tanks holds three units: the potential source (O), a single vacuum-tube voltmeter (VTVM), and a unit comprising 5 vacuum-tube voltmeters (5 VTVM's). The potential source is a 500 cycle/sec. resistance-capacitance oscillator which provides a signal of about 50 volts r.m.s. across 500 ohms without distortion of the wave shape. The circuits of all six vacuum-tube voltmeters are alike, the circuit diagram being shown in Fig. 10. The meter reads zero if the signal from the probe is equal to the potential across the calibrated potentiometer.

A block diagram of the complete wiring circuit is shown in Fig. 11. The writing pen is operated electromagnetically from a push button near the hand wheels on the carriage C_1.

b. *Procedure and Measurements*

The large tank, T_1, may be used for the study of focusing fields or for the determination of axial field-strength distribution of deflection fields which are not of infinite length in any direction. The shallow tank, T_2 is convenient for the investigation of two-dimensional electric fields. The problem of determining the axial field-strength distribution, E, for a given electrode system may be solved by measuring two equipotential lines near the axis. The field strength, $E(z)$, is computed as the ratio of the potential difference between the lines to the distance between them at every point z. A comparison between mathematical and experimental results is shown in Fig. 12 for the case of two parallel cylinders; the agreement is quite satisfactory. The same tank can also be used for the inverse problem of determining electrode shapes producing a prescribed field-strength distribution $E(z)$. By means of Eq. (20), Part I,[2] two equipotential lines near the axis are computed. The convergence of the series is generally good for small values of y. Then the five probes—connected to the unit consisting of five VTVM's—are placed in the tank along the computed equipotential line, and the electrode shapes varied

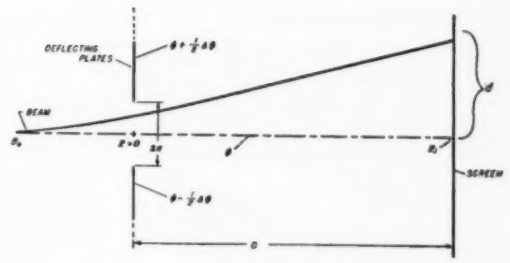

FIG. 6. The semi-infinite co-planar-sheet deflection field.

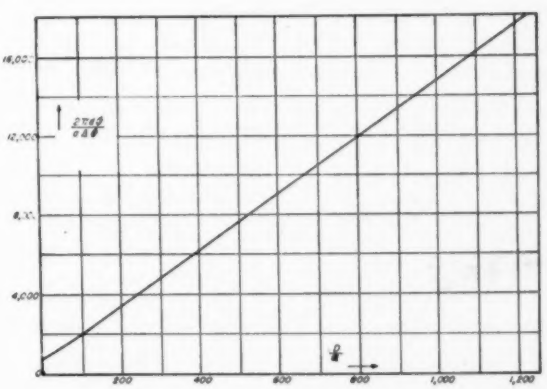

FIG. 7. The deflection by semi-infinite co-planar sheets ($z_0/a = -900$; $E(z_0/a) \leqq (1/900)E(0)$).

FIG. 8. Potential-plotting tank (Sylvania Electric Products, Inc.).

until all five meters read the potential value of the line simultaneously.

In order to increase the versatility of the tank set-up, an arrangement T tilts the tank T_2, thus producing a wedge-shaped volume of electrolyte. In this manner the tank may be used to investigate so-called "Pierce-guns."[9] The five VTVM's are employed to measure the potential distribution along the edge of the electron beam, which is, in this case, represented by an insulator shaped in the form of the desired beam.

3. Bent-Plate Deflection Systems

The axial field-strength distributions of a number of bent-plate deflection systems were measured in the manner described in Section 2-b. The geometry of the electrodes and the notation are shown in Fig. 13. The parameters L_1/h, L_2/L_1, and θ were chosen to cover a range sufficient to compute the deflection for other values than those for which the graphs are given by interpolation. The integrations according to Eq. (1) were performed by means of a planimeter and the results are plotted in Figs. 14 and 15.

B. DEFOCUSING AND DISTORTION EFFECTS OF TYPICAL ELECTRIC AND MAGNETIC DEFLECTION FIELDS

Crossed deflection fields, as used in cathode-ray and television tubes, produce undesirable effects of two kinds. One is the beam deformation causing a change in size and shape of the luminous spot on the fluorescent screen of the tube. The other is the distortion of the "pattern." The "pattern" may be the rectangular scanning pattern of the television tube or a Lissajou figure on the screen of a cathode-ray tube in an oscilloscope. Many factors may contribute, and usually do, to the pattern distortion. Only one of these will be investigated here, namely that due to the electric or magnetic field distribution. Discussion of other factors, such as wave-shape of driving circuits, frequency response of the amplifiers, coupling between circuits, or coils of the magnetic deflection yoke, etc., will be omitted.

Idealizations concerning the electron beam and the focusing system mentioned in Part I[2] will be used here.

This method of investigation permits one to distinguish defects caused by the deflection fields from those caused by other components of the device employing such fields. It then becomes possible to attribute a certain observed defect to the proper component.

There are a number of elementary explanations for the mechanism of both types of defects. All of them are qualitative in nature with one exception —that of electron-ray tracing. The electron trajectory through a given potential or field-strength plot is determined by means of numerical or graphical methods of integration. However, unless this method is used with extreme care, the results are not very reliable. In the language of this work, the deflection of an electron at the screen must be determined accurately to distances which are small compared with the quantities here called Δx_i and Δy_i, which in turn are

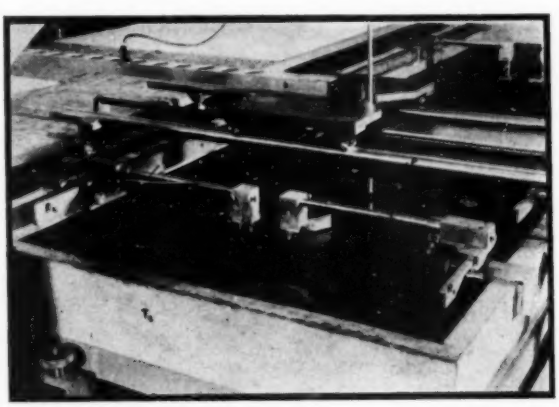

FIG. 9. Partial view of potential-plotting tank.

[9] J. R. Pierce, J. App. Phys. **2**, 548 (1940).

small compared with the first-order deflection $Y(z_i)$. In order to achieve this accuracy it is necessary to proceed in very small steps in the determination of the trajectory, increasing the amount of numerical work considerably and requiring a very accurate equipotential line or field-strength plot. Furthermore, it is difficult to apply this method to initially deflected electrons and to magnetic deflection fields. In the search for better deflection fields only qualitative hints, at best, were obtained.

The theoretical procedure outlined in Part I, Section 2[2], avoids the difficulties mentioned above. It will now be applied to a number of special deflection fields.

1. Special Electric Deflection Fields

The electric deflection fields discussed in this section are those produced by parallel plates (including the fringing fields), parallel cylinders, and bent plates. A comparison of the defocusing and distortion effects of these fields is of interest. In order to make such a comparison it will be necessary that some basis be chosen upon which to compare the defects which are the functions of the accelerating potential ϕ, the deflection potential $\Delta\phi$, the electrode-to-screen distance, the deflection d, and the geometry of the deflection electrodes which determines the axial field-strength distribution $E(z)$. It is possible to formulate various bases of comparison. One way, for instance, requires that the potentials ϕ and $\Delta\phi$, the deflection d, the distance from the exit side of the electrodes to the screen, and the minimum separation between the electrodes should be the same for otherwise different fields which are being compared. This basis was chosen for the examples discussed below. A better basis might be the following which also requires that ϕ, $\Delta\phi$, and d should be the same, but which replaces the before-mentioned condition concerning the electrode-to-screen distance and electrode separation by another one. The field-strength distribution will ordinarily be such that $E(z) < E_{\max}/n$ for all axial coordinates z smaller than a value z_2 and larger than a value z_1, where n may be arbitrarily chosen, so that one could say that the essential part of $E(z)$ lies between the coordinates z_1 and z_2 (e.g. n a value between 10 and 100). Fields may then be compared for which ϕ, $\Delta\phi$, d, $z_2 - z_1 = L$, and $z_i - z_2$ are the same. Again, keeping ϕ, $\Delta\phi$, and d equal, fields produced by electrodes occupying a given volume may be compared. The choice of a basis is, therefore, arbitrary and should be made to suit one's particular requirements.

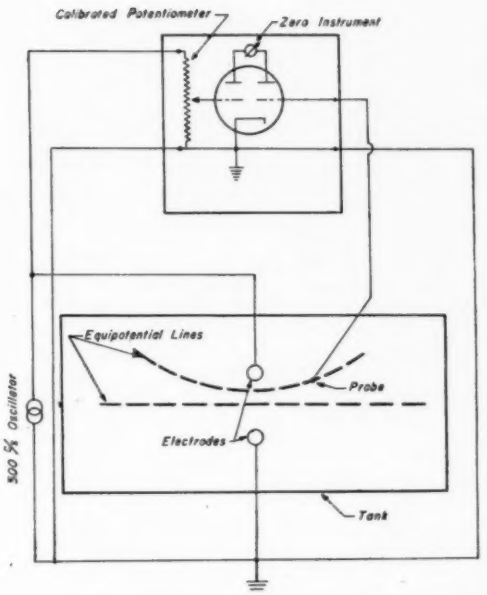

FIG. 11. Block diagram of electrical circuit.

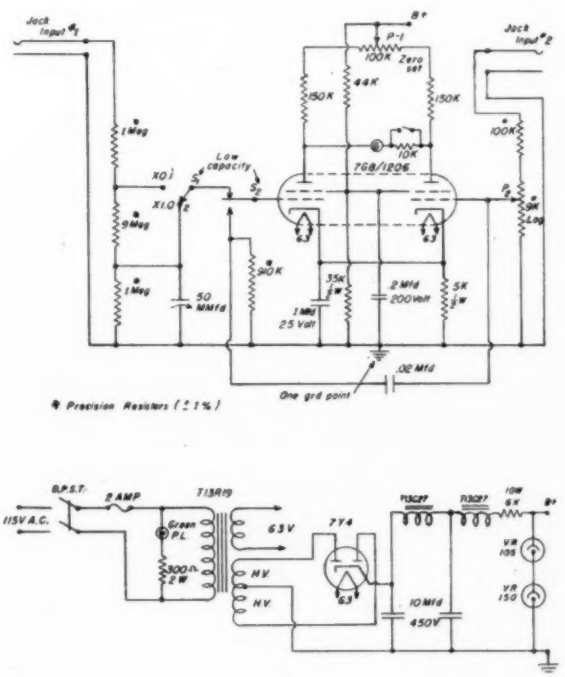

FIG. 10. Circuit diagram of the vacuum-tube voltmeter.

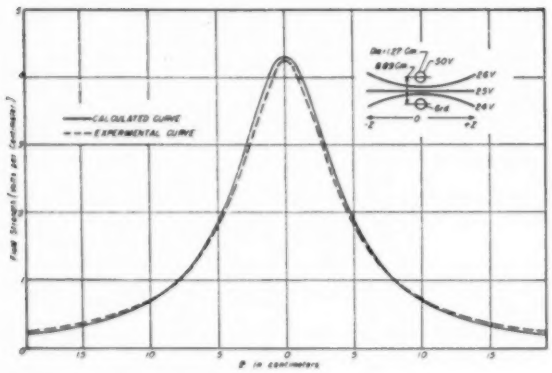

FIG. 12. Comparison between a measured and a computed axial field-strength distribution (parallel-cylinder deflection field).

Figure 16 shows the electrode geometry of three two-dimensional electric deflection fields whose defocusing and distortion effects were computed. This figure shows that the minimum distance between deflecting electrodes was kept nearly the same in all three cases.

Figure 17 shows the spot distortion for the case of a cylindrical beam whose diameter was assumed to be 0.08 inch. The figures show the focusing effect of the deflection field, demonstrating the statement[2] made that electron prisms are always joined to weak cylinder lenses.

Figure 18 shows pattern and spot distortions of a conical beam produced by parallel-plate and parallel-cylinder deflection fields. The deflections were assumed to be those produced by electrodes of dimensions shown in Fig. 16, the horizontal deflection fields preceding the vertical ones. The horizontal deflection potential could be reduced to $\Delta\phi = 140$ volts for a 2.5-inch deflection due to the larger electrode-to-screen distance. The electrode-to-electrode spacings of the horizontal and vertical fields in the axial direction were one inch

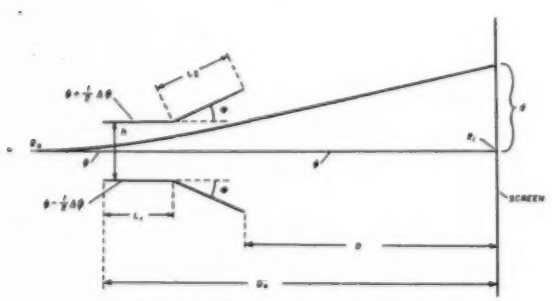

FIG. 13. The bent-plate deflection field.

for the parallel plates and 0.266 inch for the parallel cylinders. The diameter of the conical beam before entering the fields was 0.08 inch, and the apex of the cone was at the center of the fluorescent screen when undeflected. It should be mentioned that the calculations of spot and pattern distortion take into account the defocusing which is caused by a flat screen.

In the cases investigated so far, it was assumed that perfect alignment of the focusing and deflection systems existed. The distortion figures were therefore mirror-symmetrical with respect to the x_i and y_i axes. In actual tubes, distortions of the spot are observed which do not show this type of symmetry. It was thought that some kind of misalignment of gun and deflection system might be the cause of this. Calculations were made assuming the circumference of the electron beam at z_0 to satisfy the equation

$$(x_0 - r_b)^2 + (y_0 - r_b)^2 = r_b^2,$$

with r_b again equal to 0.04 inch. The beam was point-focused at the center of the screen. The resulting pattern and spot distortions are shown in Fig. 19 for the case of the parallel-plate field. The distorted spots are shown as little polygons, the corners of which are the points on the circumference of the beam for which the Δx_i and Δy_i were determined. Actually, the corners will appear rounded off.

a. *The Parallel-Cylinder Deflection Field*

Most electrically deflected cathode-ray and television tubes use either parallel or bent plates as deflection electrodes. A discussion of such fields with regard to the change of their defocusing effects with the electrode geometry would require many tables. Instead, a textbook-type of example of a deflection field will be discussed here in greater detail. It is that of the parallel cylinders or wires, which was suggested for use where electron transit time and capacitive-shunting effects begin to influence the operation of a cathode-ray tube.[3] It is possible to describe the defocusing effects of parallel-cylinder deflection fields with one set of reduced distortion coefficients for all radii and distances between the wires. These coefficients are given in Table I for various reduced screen distances $[z_i/(cq/2)]$. For

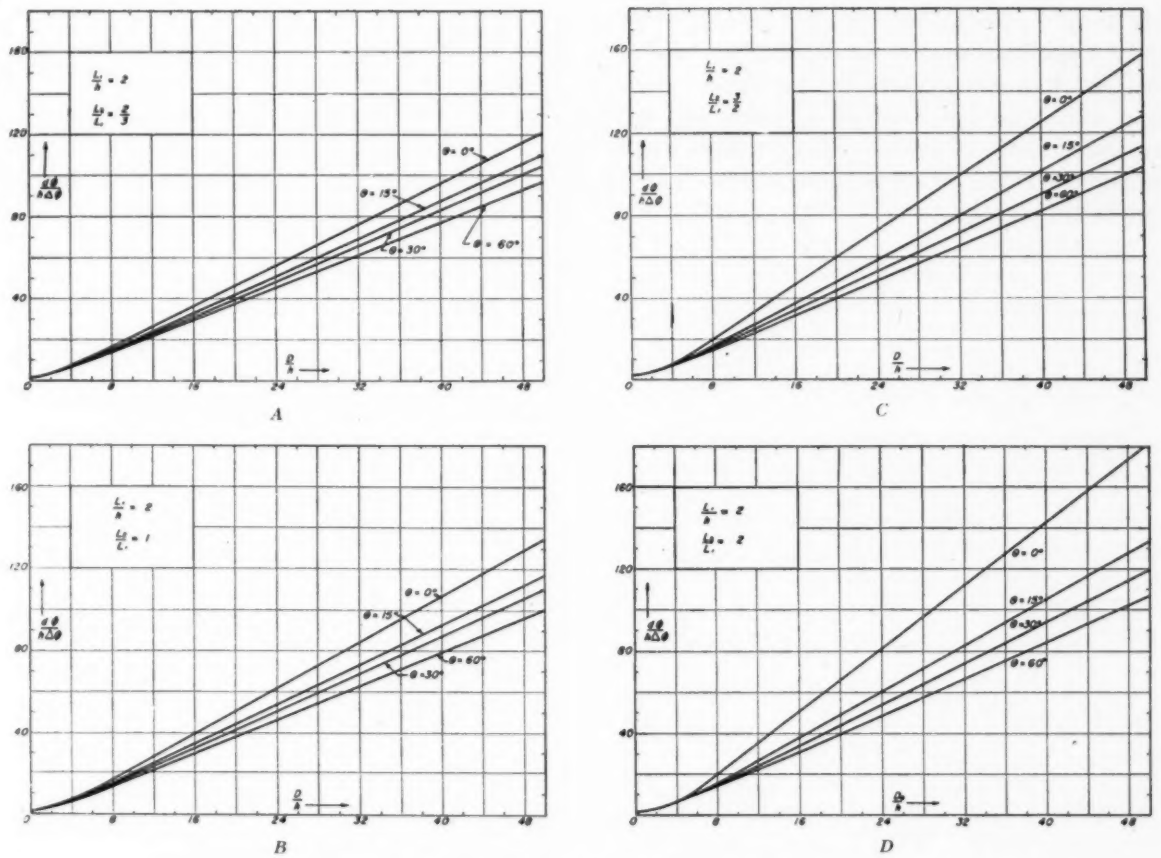

FIG. 14. The deflection by bent plates *A*, *B*, *C*, *D*.

large values of $[z_i/(cq/2)]$ some coefficients are straight lines on linear graph paper, others on logarithmic paper which simplifies the problem of extrapolation.

The notation is the same as was used in Part I.[2] Here c is the center-to-center distance between the cylinders which have the radius r_0, and z_i is the distance from the center-to-center plane to the fluorescent screen; z_0 is the axial coordinate of a point where the field strength is relatively small compared with that of the maximum at $z=0$. The quantity $(z_0/(cq/2)]$ was chosen as -30, i.e.,

$$E_{z_0}=(1/901)E_{\max}.$$

The use of the Table to determine a coefficient is simple. As an illustration, one may take

$$\beta_{0000}=\{-31.48\epsilon^3+334.34\epsilon^5-1773.69\epsilon^7\}\cdot c\cdot q,$$

for

$$2(z_i/cq)=30.$$

The deflection field for the parallel cylinders had the following dimensions: $c=.178''+2\cdot r_0$, $r_0=.598''$, $\Delta\phi=173\,V$, $\phi=2000\,V$, $z_i=10.198''$, and $Y_i=2.5''$. If the minimum distance between the surfaces of the cylinders is kept fixed (0.178") and the radius is varied in steps from $r_0=.0565''$ to $r_0=23.3''$, the half-width of the field-strength curve $(cq=c[1-(2r_0/c)^2]^{\frac{1}{2}})$ varies between 0.268" and 4.08". In order to keep the deflection constant at $Y_i=2.5''$, the deflection potential $\Delta\phi$ will be decreased with increasing value of r_0. Keeping the beam dimension the same as in the example shown in Fig. 16, it is found that the aberration coefficients α_{0010}, β_{0000}, β_{0100}, β_{0001}, β_{0002} decrease rapidly with increasing r_0, while β_{0020} remains constant over the range of values for r_0 given above.

Instead of keeping the distance between the cylinders constant and varying the deflection sensitivity, the latter may be kept fixed and the distance between the cylinders varied, hence

$\Delta\phi$, ϕ, z_i, Y_i are kept constant. The larger distance then corresponds to the larger radius. A computation of the distortion coefficients shows that the defocusing effects become less with increasing radius. Similar considerations can be applied to other electrode systems, i.e., if all dimensions except the distances z_i and Y_i are multiplied by an arbitrary factor, an improvement of the defocusing effects is obtained. (See paragraph 2.)

It becomes apparent that it is difficult to compare the defocusing effects of different types of electrode systems. It is necessary to introduce assumptions concerning the actual physical size

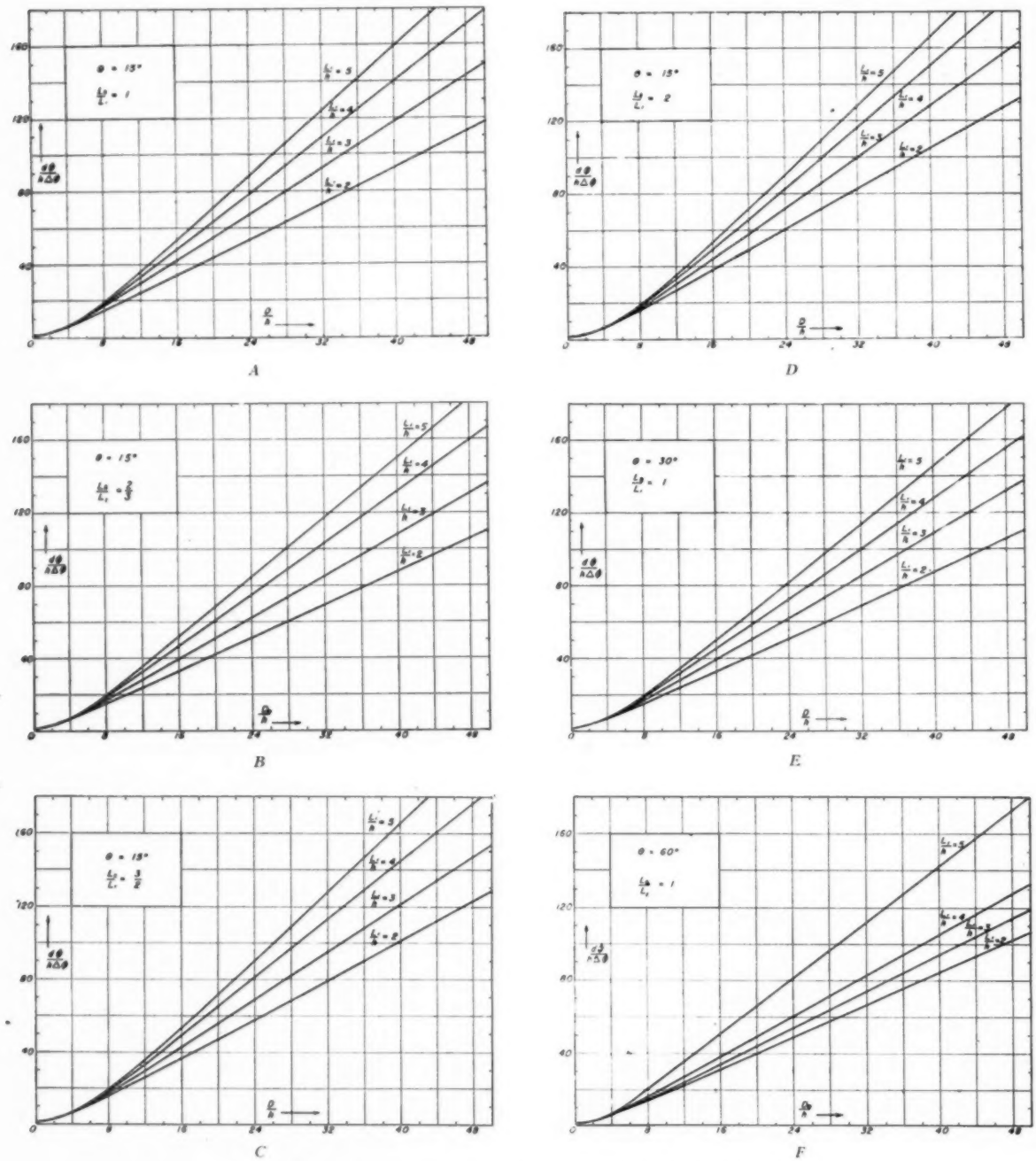

FIG. 15. The deflection by bent plates *A*, *B*, *C*, *D*, *E*, *F*.

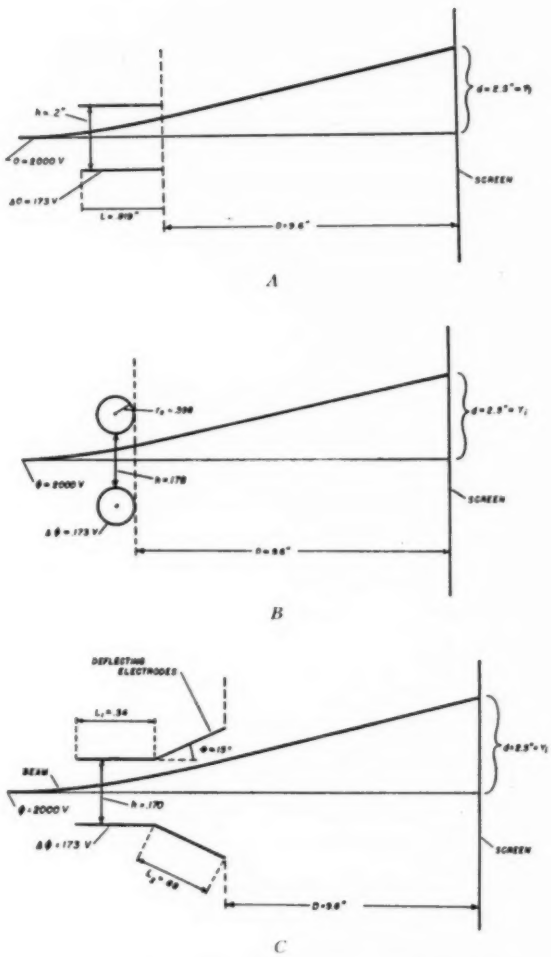

A

B

C

FIG. 16. The geometry of three two-dimensional electric deflection fields.

of the electrodes which are being compared; such assumptions are hard to formulate for electrodes of different shapes.

b. *A Magnetic Deflection Field*

Pattern and spot distortion were also computed for a special magnetic deflection field. The axial field-distributions of the two crossed fields were assumed to be of the form

$$H_x^v = -\frac{H_m}{1+(z/b)^2+(y/a)^2},$$

$$H_y^h = \frac{H_m}{1+(z/b)^2+(x/a)^2}.$$

The superscripts v and h indicate the vertical and horizontal fields, respectively. The assumption about H_x^v means that the field-strength distribution of the x component is a bell-shaped function with a half-width of $2b$ along the z axis and a half-width of $2a$ along the y axis. The half-width in any other direction $y=cz$ in the (y, z) plane will be $[2ab(1+c^2)^{\frac{1}{2}}]/[(a^2+c^2b^2)^{\frac{1}{2}}]$. This half-width is measured in terms of the coordinate $w=(z^2+y^2)^{\frac{1}{2}}=z(1+c^2)^{\frac{1}{2}}$ along the line $y=cz$. A similar interpretation holds for the horizontal deflection field for H_y^h in the (x, z) plane. Pole pieces or coil arrangements producing exactly such a distribution were not determined. The magnetic field everywhere else in space is uniquely determined. The functions V_0, V_2, H_0, H_2 of the series expressions for the components of $\vec{H}$ (see Part I[2] Eq. (55)) may be determined by expanding H_x^v and H_y^h in the manner shown for H_x^v:

$$H_x^v = -H_m\left\{\frac{1}{1+(z/b)^2} - \frac{1}{a^2}\frac{1}{[1+(z/b)^2]^2}y^2 - + \cdots\right\}.$$

Hence

$$V_0 = H_m/1+(z/b)^2,$$

$$V_2 = -1/a^2[H_m]/[1+(z/b)^2]^2.$$

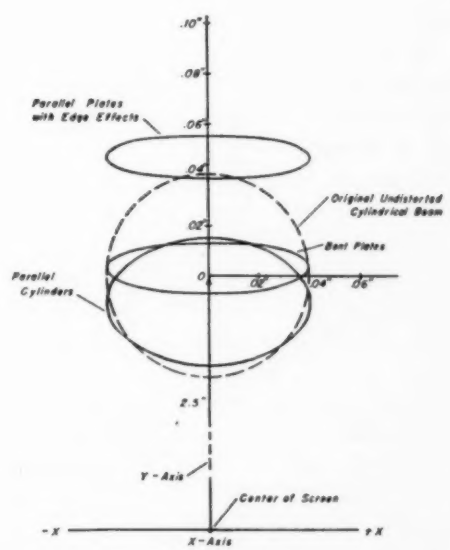

FIG. 17. The spot distortions by three two-dimensional electric deflection fields. (The electrode geometry of these fields is shown in Fig. 1.)

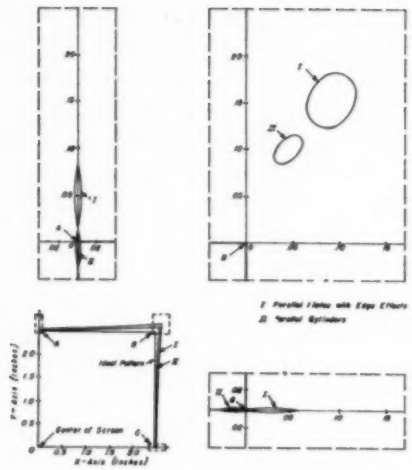

FIG. 18. Pattern and spot distortions by two special crossed electric deflection fields. (The electrode geometry and the shape and dimensions of the electron beam are described in the text.)

and similarly for H_0, H_2

$$H_0 = H_m/1+(z/b)^2,$$

$$H_2 = -1/a^2[H_m]/[1+(z/b)^2]^2.$$

The distortions are shown in Fig. 20 for the following set of parameters: $\phi = 2000$ v, $H_m = 35.4$ gauss, $b = 0.34''$, $z_i = 10.198''$, $z_i/b = 30$, and two values of a, namely, $a_1 = 1.36''$, $a_2 = 0.68''$. The maximum deflections on the screen were $d_v = 2.5''$, $d_h = 2.5''$. The electron beam was assumed to be of cylindrical shape with $r_b = 0.04$ inch.

It can be seen from these graphs that the spot distortion increases if the half-width of the field-strength distribution curve, which is in the direction of deflection, is decreased. For very small half-widths, $2a$, the defocusing quantities Δx, Δy become so large that the aberration theory can no longer be applied. A condition similar to that for electrostatic fields Eq. (27) Part I[2] could be formulated for magnetic fields. It is this condition which is violated by allowing $2a$ to become too small.

The graph also shows an elongation of the spot in the direction of the deflection at the corner points of the pattern. This is surprising when compared with the action of one single magnetic field for which an over-focusing is observed in the direction of deflection. A single vertical deflection field over-focuses because the upper edge of the beam passes through weaker portions of the field than does the lower part of the beam. An explanation of the under-focusing of two crossed fields is found when it is discovered that the field-strength function along the line of deflection, $y=x$, $z=0$, is saddle-shaped, hence causing the outer portions of the beam to pass through stronger fields than the inner parts.

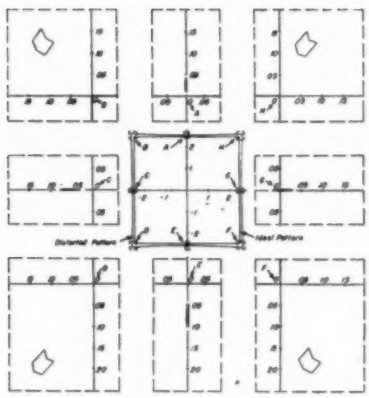

FIG. 19. Pattern and spot distortions by a special parallel-plate field. (Electron gun and deflection system were assumed to be misaligned. The electron beam was assumed to point-focus at the center of the screen.)

2. *The Problem of Reducing the Defocusing Effects*

At this time only an outline of a method can be given which might lead to deflection fields with less defocusing and distortion.

Each of the coefficients α_{abcd} and β_{abcd} determines a characteristic distortion. It was found that α_{0010}, β_{0000}, β_{0020} are the important coefficients which determine pattern distortion, while β_{0100}, β_{0001}, β_{0002} are of primary importance in describing the spot distortion produced by electric deflection fields. It is, therefore, unnecessary to graph every distortion since the magnitude of the coefficients gives the information.

These coefficients may be computed for a number of different fields. A comparison will show which of these is the best so far as they concern defocusing effects. One can then proceed to modify the axial distribution of this field in order to obtain another, having smaller distortion coefficients. The form of the coefficients reveals the "direction" of modification.

The field-strength function obtained in such manner determines the proper configuration of the deflection electrodes or magnets. In case of

electric deflection fields, this problem may be solved relatively easily; it is a difficult one in the case of magnetic fields.

In routine design work the method just outlined will not be of much help and is carried out more properly by the development and research groups. A paper written by H. Moss[10] states a theorem which "is of fundamental importance in the design of all-electrostatic cathode ray tubes, since it indicates a general method by which the beam width, and therefore the spot density, can be increased, without an increase in deflection defocusing. Large deflectors and a large neck diameter to accommodate them are used." This theorem reads:

"If the beam width and scale of the whole deflectors (including their spacing) are multiplied by k, then the increase of spot size on deflection through a constant angle is unchanged, provided the distance between the screen and the center of deflection is also unchanged."

The proof of this theorem was based on theories of scale, energy, dimensional homogeneity, and experiment. A more rigorous proof showing at the same time some limitations of the scaling process can be based on the theory developed here.

Consider a point-focused (conical) electron beam. The defocusing effects will be given to a first approximation by

$$\Delta y_i = \beta_{0000} + \beta_{0001} y_{iu}'.$$

If *all* dimensions are now increased by a factor k (keeping all potentials constant), the deflection d will very nearly increase by this factor k as long as the electrode-to-screen distance is sufficiently large. The coefficients β_{0000} and β_{0001} will also increase by the same factor and, since y_{iu}' remains unchanged, Δy_i will increase to $k \cdot \Delta y_i$. If the screen is now brought back to its original

TABLE I. Distortion coefficients of the parallel-cylinder deflection field.

$$\left[\epsilon = \frac{\Delta\phi}{\phi}\,\frac{1}{\ln(1+q/1-q)}\right].$$

Coefficient	$[z_i/(cq/2)]=5$	$[z_i/(cq/2)]=10$	$[z_i/(cq/2)]=20$	$[z_i/(cq/2)]=30$	Factor
$\frac{1}{cq}\cdot\alpha_{0010}$	3.24	13.14	35.12	57.93	ϵ^2
	6.09	6.31	6.51	6.56	ϵ^4
α_{0110}	−2.91	−3.01	−3.06	−3.08	ϵ
	5.70	5.77	5.78	5.79	ϵ^3
$\frac{1}{cq}\cdot\alpha_{0011}$	15.53	31.53	61.58	92.25	ϵ
	−13.36	−27.79	−56.72	−85.69	ϵ^3
$cq\cdot\alpha_{0210}$	1.57	1.57	1.57	1.57	ϵ^2
α_{0111}	−7.82	−15.70	−31.42	−47.13	ϵ^2
$\frac{1}{cq}\cdot\alpha_{0012}$	10.10	39.59	157.62	353.75	ϵ^2
$\frac{1}{cq}\beta_{0000}$	−2.80	−8.10	−19.63	−31.48	ϵ^3
	34.61	94.16	213.71	334.34	ϵ^5
	−282.44	−580.45	−1177.06	−1773.69	ϵ^7
β_{0100}	−5.53	−15.80	−37.59	−59.36	ϵ^3
	−12.70	−6.07	+3.70	+13.77	ϵ^4
	−460.13	−936.38	−1888.88	−2841.38	ϵ^6
$\frac{1}{cq}\beta_{0001}$	38.78	122.37	459.89	1013.95	ϵ^2
	50.27	88.68	101.69	10.93	ϵ^4
	1122.94	4614.19	18,752.00	42,317.00	ϵ^6
$cq\cdot\beta_{0200}$	−.0038	+.0369	+.01242	+.00888	ϵ
	−26.81	−51.78	−101.44	−151.16	ϵ^3
	−251.85	−508.35	−1021.35	−1534.35	ϵ^5
$\frac{1}{cq}\cdot\beta_{0020}$	7.77	15.77	30.79	46.13	ϵ
	−6.68	−13.89	−28.36	−42.85	ϵ^3
$\frac{1}{cq}\beta_{0002}$	−.055	+2.005	3.705	5.36	ϵ
	−157.13	−1320.73	−10,407.92	−34,747.84	ϵ^3
	−1552.28	−12,556.28	−101,329	−343,229	ϵ^5
β_{0101}	2.87	2.93	2.74	2.66	ϵ
	133.93	527.09	2061.97	4599.98	ϵ^3
	1246.80	5047.80	20,329.8	45,886.8	ϵ^5
$(cq)^2\beta_{0300}$	−10.40	−20.80	−41.60	−62.40	ϵ^2
	−46.00	−94.00	−191.00	−288.00	ϵ^4
β_{0120}	−3.91	−7.85	−15.71	−23.57	ϵ^2
β_{0102}	−183.21	−1536.11	−12,432.3	−41,968.2	ϵ^3
	−884.55	−7094.10	−57,388	−194,533	ϵ^4
$\frac{1}{cq}\beta_{0021}$	10.10	39.59	157.62	353.75	ϵ^2
$cq\cdot\beta_{0201}$	76.45	310.45	1246.37	2806.37	ϵ^2
	348.00	1413.00	5733.00	12,963	ϵ^4
$\frac{1}{cq}\beta_{0003}$	140.82	2520.36	41,322	210,054	ϵ^3
	755.74	11,897.48	191,590	973,326	ϵ^4

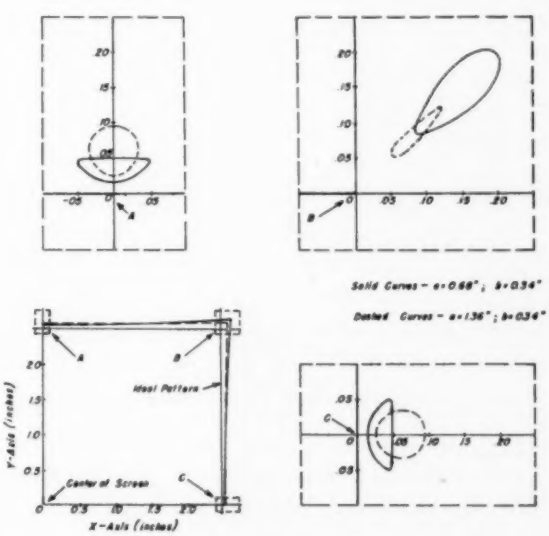

FIG. 20. Pattern and spot distortions by a special pair of crossed magnetic fields. (The fields are given by: $H_x^v = -\frac{H_m}{1+(z/b)^2+(y/b)^2}$, $H_y^h = \frac{H_m}{1+(z/b)^2+(x/a)^2}$)

[10] H. Moss, J. Tel. Soc. 4, 206 (1946).

position and the electron beam is refocused to a point at the center of the screen, the deflection will again be equal to d. The angle y_{iu}', however, will be k times its original value (for small angles). An inspection of the coefficients β_{0000} and β_{0001} shows that β_{0000} is a linear function of the electrode-to-screen distance, while β_{0001} is a quadratic function of this distance (for large electrode-to-screen distances). Decreasing the electrode-to-screen distance restores, therefore, β_{0000} to its original value. Since β_{0001} increased to k times its original value, and since β_{0001} is a quadratic function of the electrode-to-screen distance, $\beta_{0001} \cdot y_{iu}'$ will reduce to its original value when this distance is decreased to its original value. Hence Δy_i has the original value.

ACKNOWLEDGMENT

I would like to thank Mr. L. H. McKee for his assistance in the experimental work, and Miss Gloria Glaston and Mrs. Shirley Harrison for their help with the computations. I also would like to thank Dr. R. M. Bowie, Manager of Research of the Sylvania Electric Products Research Laboratory, for helpful discussions and constant encouragement in our work.

A 70-Mev Synchrotron

F. R. Elder, A. M. Gurewitsch, R. V. Langmuir, and H. C. Pollock
Research Laboratory, General Electric Company, Schenectady, New York

(Received April 22, 1947)

A synchrotron for the production of 70-Mev x-rays has been built and tested. The general mode of operation, and various features of its design and construction, are discussed. Some preliminary information on the characteristics of the electron and x-ray beams is included. This work has been supported by the Office of Naval Research.

I. INTRODUCTION

SOON after the synchrotron principle was proposed by Veksler[1,2] and McMillan[3] for the acceleration of electrons to high energies, the construction of a 70-million-volt machine, using betatron injection,[4] was begun. The completed synchrotron (Fig. 1) has been in operation at the 70-Mev level for several months. The results obtained with it confirm and extend the experimental results of Goward and Barnes[5] with an 8-Mev machine. The synchrotron provides a satisfactory means of producing high energy electrons and x-rays. By varying the important parameters of the present machine, information is being acquired to facilitate the design and construction of larger units.

The general theories of both the betatron and the synchrotron have been described in earlier publications.[6–10] This particular machine may be regarded as a betatron during the initial portion of each cycle of the magnet. The electrons, after their injection, are accelerated by the changing magnetic flux carried by iron laminations within their orbit. Later, these central flux bars of the magnet begin to saturate and the acceleration is supplied instead by the electric field at the gap of a radiofrequency resonator.

The magnet is driven at 60 cycles from an induction regulator. The magnetizing coils are resonated with a 3000-kva capacitor bank. As the magnetic field begins to increase, electrons are injected into the vacuum tube from a betatron-type gun pulsed with a voltage of the order of 40 kv. The gun filament is pulsed negative for 2 to 3 microseconds in each cycle, the timing of

[1] V. I. Veksler, Comptes rendus U.S.S.R. **44** [9], 365 (1944).
[2] V. I. Veksler, J. Phys. U.S.S.R. **9**, 153 (1945).
[3] E. M. McMillan, Phys. Rev. **68**, 143 (1945).
[4] H. C. Pollock, Phys. Rev. **69**, 125 (1946). H. C. Pollock, R. V. Langmuir, F. R. Elder, J. P. Blewett, A. M. Gurewitsch, and R. L. Watters, Phys. Rev. **70**, 798 (1946).
[5] F. K. Goward and D. E. Barnes, Nature **158**, 413 (1946).
[6] D. W. Kerst, Phys. Rev. **60**, 47 (1941).
[7] D. W. Kerst and R. Serber, Phys. Rev. **60**, 53 (1941).
[8] D. Bohm and L. Foldy, Phys. Rev. **70**, 249 (1946).
[9] N. H. Frank, Phys. Rev. **70**, 177 (1946).
[10] D. M. Dennison and T. H. Berlin, Phys. Rev. **70**, 58 (1946).

the pulse being adjustable from $t=0$, when $B_0=0$, to $t=20$ microseconds. This timing is accurately controlled by a multivibrator circuit which is initially triggered from a permalloy peaking strip mounted across the magnet gap. Since the central flux bars do not possess uniform permeability during the betatron acceleration, the betatron orbit is slowly shrinking as t increases. It matches the theoretical synchrotron orbit, which is slowly expanding, at about 200 microseconds. At this time, when the electron energy is about 2 Mev, and the electron velocity 97 percent that of light, another multivibrator circuit turns on a radiofrequency oscillator which excites a 163-megacycle cavity, forming a part of the vacuum envelope. The electrons become bunched in orbital distribution by the electric field at the gap of the resonator, and on successive revolutions they are held in synchronism with the r-f field with a stability which is characteristic of the synchrotron. Following the turn-off of the cavity resonator, the electron energy will remain essentially fixed. If the magnetic guide field has not reached its peak, the electron beam contracts to strike a tungsten-wire target placed within the tube inside the synchrotron orbit. If the field has passed its peak when the resonator is turned off, the beam expands to hit the back of the injection gun and accordingly the x-ray beam comes from the gun.

When the magnet is fully excited, the peak value of B, at the orbit radius of 29.3 cm, is 8100 gauss, which permits a peak electron energy of 70 Mev. At present the x-ray yield in the center of the beam at 1 meter from the tungsten target is 50 roentgens per minute as measured by a Victoreen thimble in a $\frac{1}{8}''$ thick lead shield. This output undoubtedly will improve as the many variables of the equipment are adjusted to their optimum settings.

II. THE MAGNET

The 70-Mev synchrotron magnet (Fig. 2) resembles in general design and construction the betatron magnets which have been built in this laboratory.[11,12] The total weight of the magnet and coils is approximately 8 tons.

[11] W. F. Westendorp, Phys. Rev. **71**, 271 (1947).
[12] W. F. Westendorp and E. E. Charlton, J. App. Phys. 16, 581 (1945).

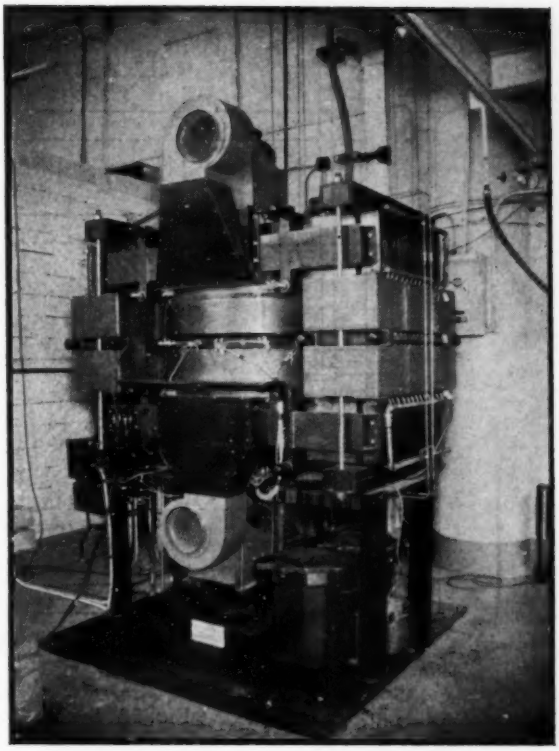

FIG. 1. Photograph of 70-Mev synchrotron.

The shape of the pole face was determined by using a half-scale model made of solid steel. The magnetic field intensity in the plane midway between pole faces varies inversely as the $\frac{3}{4}$ power of the radius. The width of the pole face near the orbit is 4″, and the gap at the 23″ diameter orbit is $2\frac{3}{4}''$.

The pole pieces were assembled from approximately 4° sectors made of enamelled punchings of dynamo-grade silicon steel 0.014″ thick. Each sector was impregnated with permafil and baked while held in a special clamp. The individual punchings, which were properly profiled, varied from 1″ to 12″ wide in steps of 1″. To avoid excessive eddy currents in the pole pieces, a total of 3 sheets of 0.005″ paper was equally spaced between bunches of laminations during the stacking of each sector. A 2″ wide copper sheet, which extended about $\frac{1}{4}''$ beyond the inner end of the iron stack, was placed in the middle of each sector. To assemble accurately pole pieces of 27″ O.D., the sectors were placed on a ground steel plate of this diameter and clamped together with a Textolite ring. The ring, fabricated from

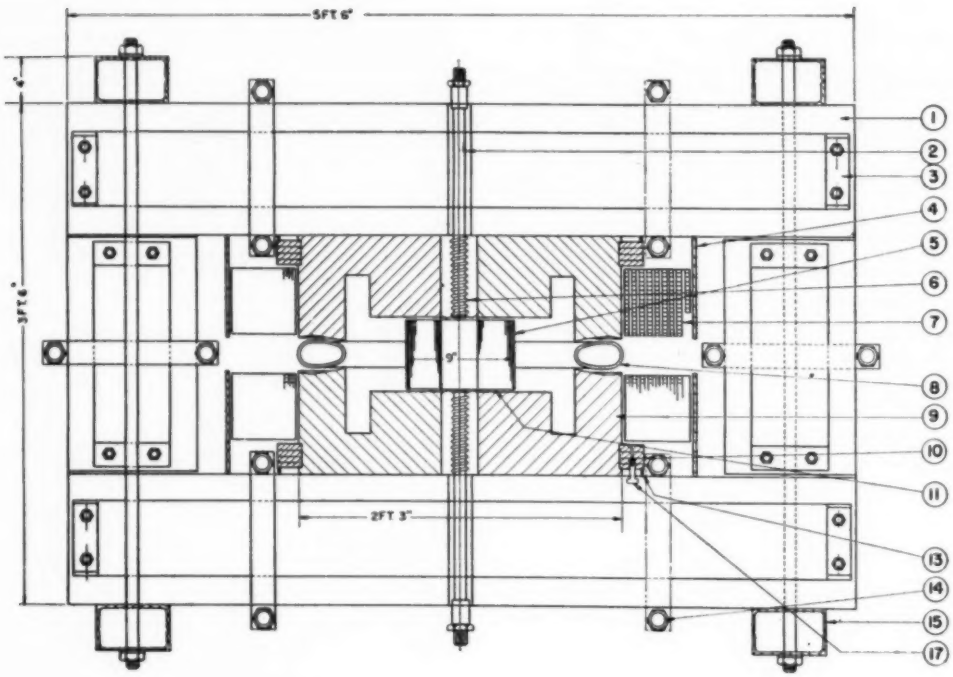

FIG. 2A. Synchrotron magnet—front view.

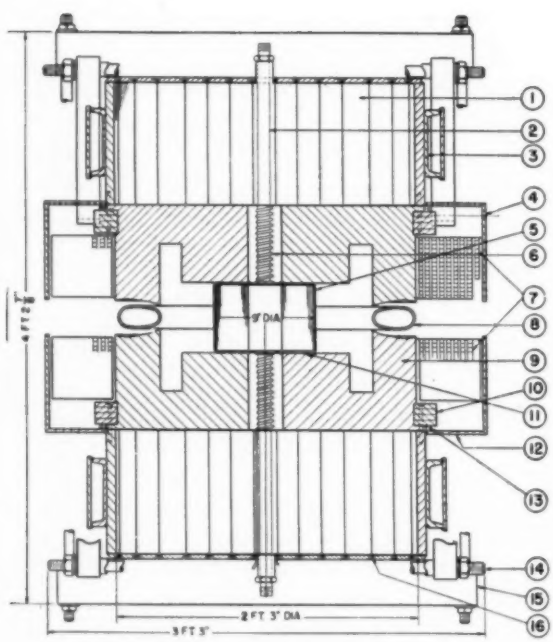

FIG. 2B. Synchrotron magnet—end view.

1. Laminated magnet yoke
2. Brass pipe
3. Clamping beam
4. Herkolite coil housing
5. Flux bars
6. Cooling spiral
7. Magnetizing coils
8. Vacuum tube
9. Pole piece
10. Textolite clamping ring
11. Adjustable gap
12. Cooling opening
13. Exciting coil
14. Clamping bolt
15. Clamping beam
16. Cooling pipe
17. Hanger

6 semicircular pieces, was fastened together with brass pins after assembly in the rectangular groove at the outer edge of the sectors. The joints in the ring were staggered by 120°.

In the central 3″ diameter hole of the pole piece was inserted a spiral cooling coil of copper together with a $\frac{3}{4}$″ brass pipe inside the coil. The space between the brass pipe and sectors was filled with soft solder to provide heat transfer from the copper fins in the sectors to the spiral coil. The brass pipe, long enough to extend through a 2″×2″ hole through the yokes, then served as a support for the central part of the pole piece.

For the yokes and legs of the magnet, enamelled transformer-grade silicon steel .014″ thick was used. For the purpose of cooling, pairs of .030″ copper sheets were distributed at appropriate intervals during the stacking of the yokes and legs. Water flowing through copper tubes, soldered in a V groove formed by bending the outside edges of the copper sheets, serves to remove the heat produced in the iron. The cooling fins also provide a means of attaching the pole pieces to the yokes. This was accomplished by punching T-shaped notches in the sheets into

which beryllium-copper hangers were inserted during stacking. By spacing the fins suitably, and by varying the distance of the notches from the center line of each yoke, the hangers were arranged to lie at equal intervals on the circumference of a circle. The circular pole pieces were then attached securely to the yokes with thirty-two brass bolts through each of the Textolite clamping rings, previously assembled in a rectangular groove in the pole piece.

The flux bars of 0.004″ enamelled strip steel consist of twenty-four bundles of strips, $5\frac{15}{16}$″ long. Each bundle contains approximately 120 strips of average width 2″ and is supported in a Textolite holder. Two spacing disks, of about 0.128″ thickness, position the holder between the pole pieces. A stream of air introduced through one of the brass pipes cools the flux bars.

III. THE COILS

The magnetizing coils, placed around the pole pieces, carry current to produce both flux through the orbit and guiding field at the orbit. Approximately 35,000-ampere turns r.m.s. are needed for 70-Mev operation. The apparent power is furnished at 22,900-volts r.m.s. from a capacitor bank through a high voltage cable to the coils. The two coils are connected in series (Fig. 3) and each contains 130 turns of cable. The cable which consists of 12 strands of 0.050″ × 0.150″ Formex-covered copper wire is taped together in a bundle while being wound. Glass

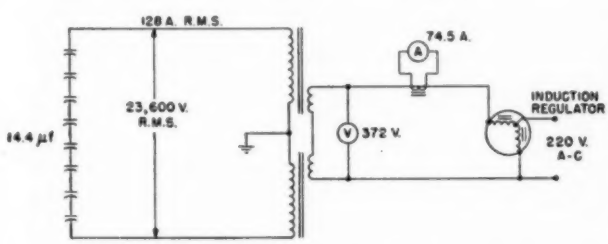

FIG. 3A. Main power circuit.

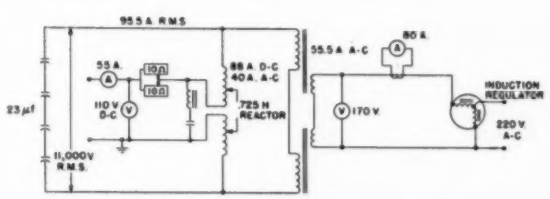

FIG. 3B. Main power circuit with d.c. bias.

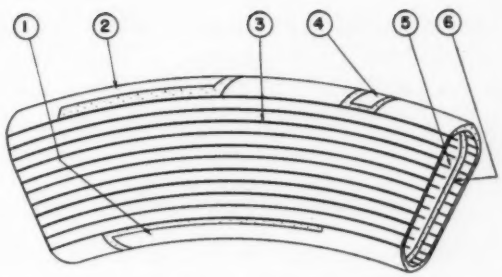

FIG. 4. Pictorial view of cavity.

1. Tuning strip
2. Coupling strip
3. Slots in silver to reduce eddy currents
4. Insulated patch for voltage monitor
5. Connection between adjacent strips
6. Accelerating gap

cloth spacers, treated with permafil, serve to provide insulation between coil layers and to form ducts for forced air cooling. After the coils were wound, they were impregnated in vacuum with permafil and then baked to produce a rigid structure. The coils are supported and held in place inside Herkolite cylinders by insulating blocks bolted to the cylinders. The cylinders, which are fastened to the yoke structure by four brackets, carry through the coils the air flow from two ½-hp blowers.

The exciting coils are connected across an induction regulator which supplies 74.5 amperes at 372 volts for 70-Mev operation of the synchrotron. Each coil has two turns of No. 2 insulated code wire wrapped around the pole piece between the Textolite clamping ring and the yoke, as is shown in Fig. 2.

The saturating coils, two of which are mounted on each leg of the magnet, are required for starting the machine. The inductance of the magnet varies during each cycle as the flux bars saturate. When the machine is not running, its inductance and the capacitor bank are in tune at approximately 40 cycles. Accordingly, in starting, the exciting coils draw an excessive current from the 60-cycle line. Therefore, the saturating coils are supplied with 60 amperes of d.c. which, by partially saturating the magnetic structure, tunes the circuit to 60 cycles for low power operation. As the excitation is increased, the d.c. is reduced by an automatic phase-sensitive control circuit which keeps the magnet-driving current and voltage nearly in phase. Finally, when the magnet is fully excited, no d.c. remains in the saturating coils. Each of the four coils has 46 turns,

wound in a single layer on an insulating frame. The individual coils are connected in series so that the a.c. voltages which are induced in them balance out and do not appear across the d.c. supply.

IV. THE CAPACITOR BANK

The 3000-kva capacitor bank, which supplies the apparent power for the magnetizing coils, consists of 121 units arranged with 8 banks in series. Seven banks have 15 units in parallel, and one bank 16 units in parallel. Each Pyranol-filled unit is rated at about 7 micro farads, 3 kv r.m.s., and 24 kva. The 8 insulated metal racks holding the capacitors are contained within a sheet-steel housing through which air is circulated by a low pressure blower. The power loss in the capacitor cabinet is $\frac{1}{3}$ of 1 percent of the voltamperes, or approximately 10 kw.

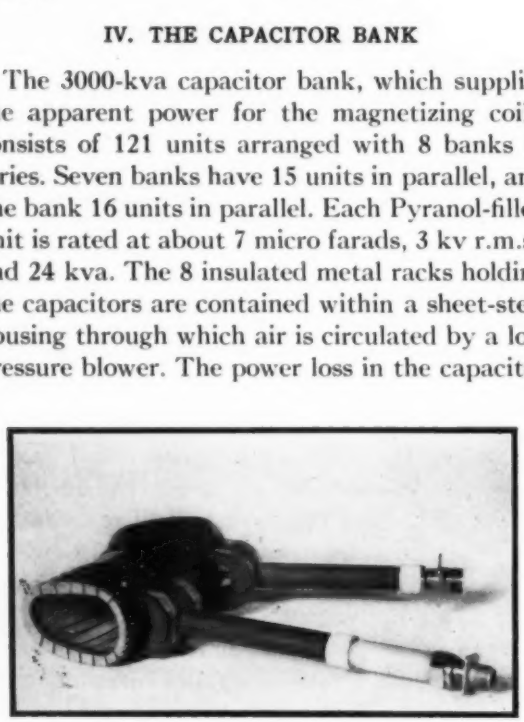

FIG. 5A. Photograph of r-f resonator.

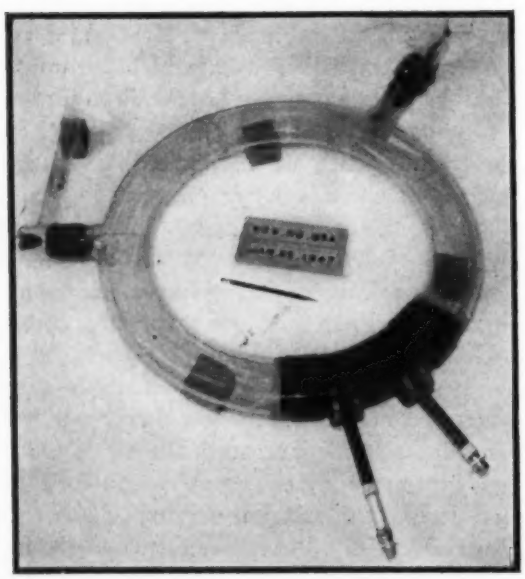

FIG. 5B. Photograph of resonator installed in vacuum tube.

V. VACUUM TUBE AND R-F CAVITY

The vacuum tube was molded by the Corning Glass Works of 774 Pyrex glass, $\frac{1}{4}''$ thick. It is of toroidal shape with an outside diameter of 27″, an inside diameter of 19″, and with a nearly elliptical cross section; the major axis is 4″ and the minor axis is $2\frac{1}{4}''$. Two side arms are provided 120° apart for gun and target, the pumping lead being on the target arm. From the tube, a 57° sector was removed by making radial cuts with an emery wheel. This sector was replaced by one of similar shape, but of 707-DG glass, the loss tangent of which at 163 megacycles is 0.0012, a value low enough to make this glass suitable for the radiofrequency resonator. The 707-DG glass sector, cast in the same mold as the original tube, had its ends ground so that it fitted tightly in the place of the sector which was cut out. The resonator (Fig. 4) was prepared in the following way. The low loss glass was coated appropriately with DuPont silver paint which was baked onto the glass at 500°C. In an electrolytic plating bath, the thickness of the silver coating was increased to 0.001″. A tungsten wheel, mounted on a rotating arm and connected to a current transformer, was then used as a tool for removing silver from the glass so as to subdivide the silver coating into narrow strips. This reduces the eddy currents produced in the coating by the a.c. magnetic field.

The complete cavity (Fig. 5) may be regarded as a $\frac{1}{4}$-wave concentric resonator which has been fore-shortened physically by the introduction of glass between inner and outer conductors. Voltage is developed across a $\frac{1}{8}''$ wide gap inside the sector close to one end. The r-f excitation from the oscillator is fed from a coaxial 50-ohm line. Coupling is achieved by having the central conductor of the cable make proper contact with a strip of the outer silver coating of the cavity. The coupling can be varied to secure a good match by moving the point at which the center conductor of the cable makes contact with the silver strip. This strip is only connected to the remainder of the silver coating at the extreme end of the cavity, away from the gap. It is not necessary to bring any metal leads through the

glass. For measuring the voltage across the gap, a calibrated probe and crystal is supported outside the glass near the gap. All the electrical connections are made by silver strips supported on Textolite blocks which are taped to the resonator by permafil-treated glass cloth.

Before the silvered cavity was inserted into the main tube, the inner surface of the tube was chemically coated in a uniform manner to obtain a resistance of 200 to 1000 ohms per square cm. When the cavity is permanently positioned, 0.002″ gaskets are used at the joints. Molded sleeves of butyl rubber hold cavity, gun, and target in position. These sleeves when painted with Glyptal insure vacuum-tight joints. A glass oil-diffusion pump of 20 liters per second capacity, backed up by a suitable fore-pump, keeps the tube pressure below 10^{-5} mm of mercury. This pressure, measured with an ionization gauge, is satisfactory for regular operation.

The cavity requires 250 watts to produce 1000 volts peak across the gap. As the duty cycle is normally 25 percent, considerably less average power is used. Operation of the cavity shows that the voltage can be developed across the gap without excessive heating of the dielectric or the rubber sleeves. The Q of the cavity has been measured as 375. It is possible to change the resonant frequency 10 percent by moving the position of a piece of foil attached to the tuning strip outside of the cavity. In practice, this tuning is done only to adjust a new cavity to the desired frequency. The power is supplied to the cavity by an 832-A oscillator driving an 829-B grid-modulated power amplifier.

VI. ORBIT LOCATION

The location of the betatron orbit is of interest only during the time that the magnetic field is low. The orbit is located by methods which are similar to those already published.[12] The voltage induced in a small coil placed at the desired orbit position is balanced against a fraction of the voltage from a single turn of wire of 23″ diameter on the pole face. A null-voltage indication on an oscilloscope enables the orbit position to be calculated. This null indication is observed on a sweep which is triggered when the magnetic field passes through zero. By varying the fraction of the single-turn voltage which is used, the null indication can be obtained at various times following $B=0$. Thus the location of the orbit as a function of time can be found. Adjustment of the betatron orbit is readily carried out by changing the paper shims between the yokes and legs of the magnet. Since the gap of approximately 0.25″ between the central flux bars and pole pieces varies more rapidly, relatively, than the main gap of 2.75″, the flux within the orbit can be altered by a large amount without appreciably affecting the flux density at the orbit. In this way, the betatron condition can be fulfilled in order to match the desired orbit diameter.

The orbit shrinks considerably as the flux bars begin to saturate. The contraction in orbit radius is about 1½″ in 350 microseconds, with most of the contraction occurring near the end of this period. This contraction does not prevent a satisfactory transition to the synchrotron condition. Indeed, the exact location of the betatron orbit in the center of the glass vacuum tube does not appear important. The orbit has been shifted over a wide region inside the tube with little change on the x-ray output. The synchrotron orbit is defined by the energy of the electrons and the frequency of the r-f oscillator.

VII. POWER CIRCUIT

A diagram of the main power circuit of the machine is shown in Fig. 3A. Power is supplied from a 220 volt 60-cycle a.c. line through a motor-controlled induction regulator to the exciting coils of the magnet. The Q of the resonant circuit is approximately 113. Variations in line frequency could have a relatively large effect on operation, but trouble from this source has rarely been observed with this installation. If the capacitor bank is cold, and hence the capacity high, the machine will be in resonance at a slightly higher power level because of the nonlinear inductance of the magnet. After ten minutes of running, the temperature of the capacitor bank has reached equilibrium. The power required to energize the machine fully is 26.5 kw.

The machine has also been run with d.c. bias on the magnetizing coils as is shown in Fig. 3B. The large increase in electron energy which is obtainable by biasing a betatron[13] of given

[13] W. F. Westendorp, J. App. Phys. 16, 657 (1945).

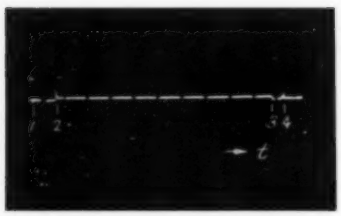

FIG. 6. Oscillogram showing operation of the machine; the trace is cut off every 100 microseconds. (1) marks the time of electron injection. At (2) the r-f voltage is turned on and at (3) it is turned off. (4) marks a signal from a photo-multiplier tube placed in the x-ray beam. For this trace the energy was about 20 Mev.

weight cannot be realized with a synchrotron. However with a biased synchrotron, for a given energy output, the voltage across the magnetizing coils may be reduced by nearly 50 percent and the effective value of the current by about 15 percent. Because of the lowered a.c. component of flux, the iron losses decrease to about $\frac{1}{3}$, which reduces the cooling requirement of the magnet. The a.c. power input is also lowered. Theoretically, the capacitor bank is reduced to about 30 percent of that required for full a.c. operation. The full saving in capacitor kva cannot be realized since it is necessary to compensate the inductance of the reactor required to introduce the d.c. bias current into the magnetizing coils. The net saving in practice may thus amount to about 50 percent. With the present machine, the cost of the reactor was comparable to that of the added capacitor kva required for full a.c. operation. For a higher energy machine, some saving in cost might be obtained by using bias.

With d.c. bias, it was somewhat more difficult to start up and get the machine on the line. The operation was also rather unstable. A large part of the instability was due to the regulation characteristics of the input circuit coupled with the non-linearity of the reactance of the magnet. Normally, the input lines have a small inductive reactance. When the magnetizing circuit is near resonance at the line frequency, the operation will be stable provided the power factor of the circuit is slightly lagging. A small change in the d.c. bias current can cause the power factor to swing from lagging to leading or *vice versa*. If the power factor becomes leading, then the voltage at the machine terminals rises because of the inductive reactance of the input lines. A rise of voltage on the exciting coils causes a higher effective inductance of the magnet, and hence a tendency for the power factor to become still more leading, since the capacitor bank has a fixed value. Obviously, under such conditions, the operation will be unstable. One way in which this difficulty can be overcome is by means of a series capacitor in the input circuit. This was tried and found to be reasonably effective. We are confident that stability can be obtained when it is desirable to use a biased magnet.

With full a.c. operation, there is stability. An increase of voltage at the input terminals decreases the effective inductance of the magnet, there by making the power factor more lagging, which tends to lower the input voltage.

VIII. OPERATION

The operation of the machine is quite simple. The sequence of events in each cycle is illustrated by Fig. 6. The final energy of the electrons is easily changed by a single knob controlling the time that the r-f cavity stays on. Figure 7 shows that the time at which the r-f is turned on is not very critical. The time at which the electrons are injected into the tube is critical as is shown by Fig. 8. Under good conditions, when the line frequency is stable, the injection timing multivibrator is adjusted perhaps once or twice a minute. It is easy to keep the intensity of the x-rays constant to within about 10 percent for long periods of time.

The transiton from betatron operation to synchrotron operation seems to be rather efficient.

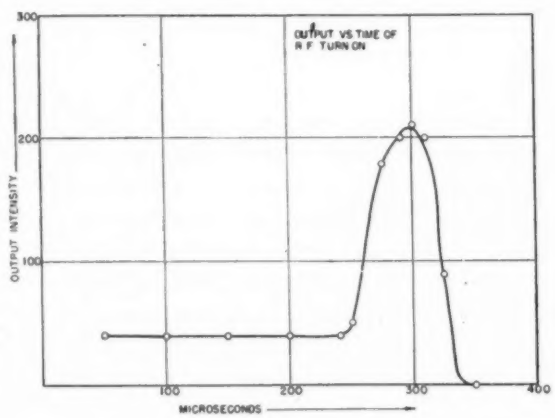

FIG. 7. Output *vs.* time r-f is turned on.

This is shown by operating the machine at a low intensity and observing the output by means of a Geiger counter. The pulses from the counter are displayed on an oscilloscope with a 60-cycle sweep. If the r-f oscillator is not turned on, a count is registered almost every cycle a few hundred microseconds after injection, at the sweep position where 3.5-Mev x-rays are expected. This is of course the betatron beam collapsing to the target as the central flux bars saturate. If the r-f is turned on, no betatron counts are observed, but higher energy quanta produce counts following r-f turn off. This indicates that a large fraction of the electrons which previously had collapsed to the target are bunched in the synchrotron orbit and are accelerated to high energy.

The rate of rise of the r-f envelope was varied from 2 to 20 microseconds and does not seem to affect the efficiency of the transition. Increasing the peak r-f voltage on the accelerating gap beyond twice the minimum voltage needed per turn does not increase the output appreciably (see Fig. 9). It is felt that further increase in x-ray output will result from improvement in betatron injection techniques rather than from changes in the synchrotron mode of operation.

Two types of electron gun have been used. One is a standard gun which has been used with betatrons for several years in this laboratory. It is quite similar to a gun described by D. W. Kerst.[14] A rather different gun, designed by J. P. Blewett, and initially studied on a rubber model, has been in use for a short time. The

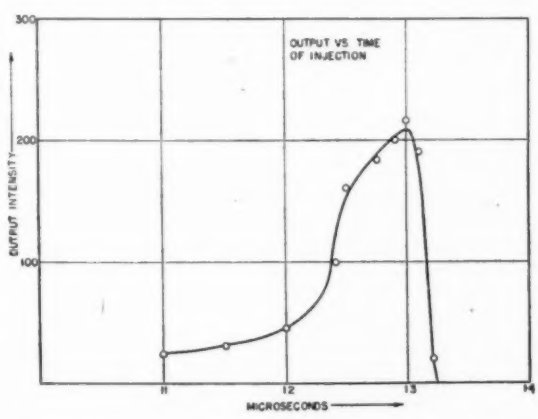

FIG. 8. Output *vs.* time electrons are injected by gun.

[14] D. W. Kerst, Rev. Sci. Inst. **13**, 387 (1942).

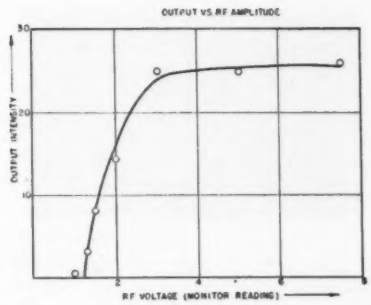

FIG. 9. Output *vs.* r-f accelerating volts. Monitor readings are directly proportional to peak voltage at the accelerating gap.

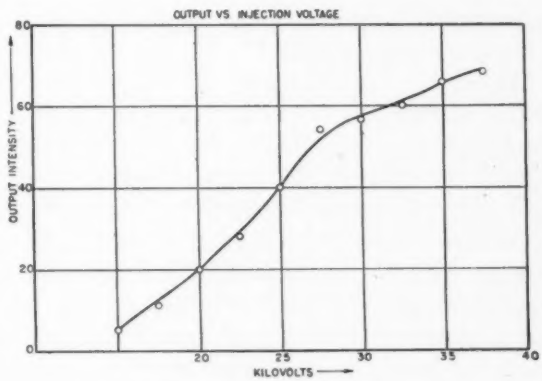

FIG. 10. Output *vs.* gun injection voltage.

required orbit contraction is less than that in the earlier guns. Initial comparative experiments indicate that this improved gun gives a larger output than the standard gun.

The electron gun is always mounted on a side arm of the tube through a metal bellows which allows the gun position to be easily varied. Maximum x-ray output always seems to occur when the gun is located at a position in the tube just outside that where the magnetic field falls off inversely with the radius. It can be shown that in this region the electron beam has no radial stability, and accordingly the electrons can rapidly spiral in towards the center of the tube. A typical plot of x-ray output *vs.* injection voltage is shown in Fig. 10.

The x-ray output can be considerably increased by slight changes in the azimuthal distribution of the magnetic field. This is accomplished by placing flat sector-shaped coils along the top and bottom pole pieces of the magnet. These coils are connected to variable resistors. When the machine is operating, the output can usually

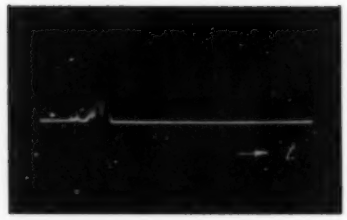

FIG. 11. Oscillogram of x-rays from internal target. The length of the sweep is 1000 microseconds. The trace begins at the time the r-f was turned off, when the electron orbit starts to contract. The irregular signal is from the output of a photo-multiplier tube placed in the emergent x-ray beam.

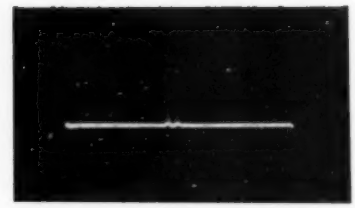

FIG. 12. Oscillogram of x-rays generated by electrons expanding to the gun as the magnetic field decreases. The 1000-microsecond trace is keyed at the time of r-f turn off. Two sharp pulses are registered by the photo-multiplier tube, about 50 microseconds apart.

be increased several-fold by varying the current flowing through these coils.

When the x-ray intensity is low, the output of the machine is observed by a Geiger counter. With higher output, it is convenient to monitor with a 931 photo-multiplier tube contained in a light-tight box, and set a few feet from the target in the center of the beam, which is approximately 3° wide. The 931 is followed by a single stage of amplification and a cathode follower whose output is observed on an oscilloscope. The circuit has good frequency response which permits details of the x-ray beam structure to be observed on a fast sweep of the oscilloscope. An ionization chamber and d.c. amplifier are used to measure the average output of the machine.

The structure of the x-ray beam as a function of time is rather complicated. The distribution of x-rays from a contracted electron beam, as determined by a photo-multiplier tube is shown in Fig. 11. Upon moving the target by means of a metal bellows, it was found that a contracted electron beam gives a single x-ray pulse if the target is placed at a radius where $n>0[n=-d(\log B)/d(\log r)]$. If the target is at a smaller radius than that at which $n=0$, the x-ray beam becomes very complicated, probably because the electron beam has no vertical stability in regions where $n<0$.

An expanded electron beam, striking the gun as a target, gives a single pulse unless the gun is placed at a radius larger than that at which $n=1$. In this case, the x-rays emerge in two well separated sharp pulses as shown in Fig. 12. This splitting of the expanded beam is not understood at present, but is being investigated further.

In these experiments, the ejection of the electron beam to a target is accomplished by turning off the r-f resonator and letting the beam expand or contract as the magnetic field changes. If an x-ray pulse of shorter duration is needed for experimental work, some faster method of electron ejection should be used.[15]

ACKNOWLEDGMENTS

The authors wish to acknowledge the many helpful suggestions made by Dr. E. E. Charlton, Dr. W. F. Westendorp, and Dr. J. P. Blewett. Mr. P. C. Noble, Mr. J. F. Tracy, Mr. R. L. Watters, and Mr. G. M. Kirkpatrick designed and tested many of the r-f components. Mr. F. Haber, Mr. G. N. Knowlton, and Mr. S. Sebis participated in much of the construction. This project has been supported throughout by the Office of Naval Research under Contract No. N5ori-178, task I.

[15] J. S. Clark, I. A. Getting, and J. E. Thomas, Phys. Rev. **70**, 562 (1946).

Cathode-Ray Presentation of Three-Dimensional Data*

OTTO H. SCHMITT
*Airborne Instruments Laboratory, Inc.,** Mineola, New York*
(Received March 24, 1947)

The cathode-ray oscilloscope is usually regarded as a means for displaying data in one or two variables as a function of time. By means of simple transformations which are easily performed electrically, it is possible to present three variable electrical data in the form of isometric or other conventional projections or as true perspective drawings. It is further possible to change the observer's viewpoint in the presentation coordinate system at will by turning range, elevation, and azimuth controls.

A more elaborate but similar set of transformations permits presentation of separate pictures to the two eyes. These pictures are optically superimposed but differ in such a way as to yield stereoscopically correct perspective pictures. These pictures are fully acceptable to the eye as patterns in space.

WHEN we are interested in examining an object of moderate size, we instinctively try to position it so that we look directly at it with both eyes from a distance ranging from a few inches to a few feet, depending upon the size of the object. We next turn the object or move about it so as to get several different views of it. Then, if we find certain details of the object particularly interesting, we move up and examine these details from a very short distance, sometimes even using a lens system to assist our eyes in focusing.

By the time we have completed such an examination we know pretty thoroughly what the object is like three-dimensionally, even though we have, in reality, seen only a series of pairs of the two-dimensional images formed on the retinas of our eyes.

The "realness" and "solidity" of an object in our field of view depends on a complex of subjective and objective factors, all of which our minds quickly and accurately put together into a mental image of the three-dimensional object. This mental picture is never a simple accumulation of the various retinal images: it is a real three-dimensional picture, nicely painted onto a framework provided by clues contained in the image pairs.

In this mental picture, missing details are neatly filled in, compromises are automatically made between various inconsistencies actually present in the data as seen, and errors resulting from optical and mechanical imperfections in the eye mechanisms are smoothed over.

Our visual apparatus is remarkably adaptable; if furnished with a few clues—even if some of them are contradictory—it will piece together a plausible, single clear picture, though this picture may not be the right one. When a wrong cue is taken and the data gets just too confusing, the eyes will try to find another picture that also fits the available data. The search for an intelligible picture will be repeated again and again before the eyes finally give up and register a blur.

This picture synthesis is the basis of many familiar optical illusions, especially those in which surfaces suddenly reverse or shift position. It is this process also that allows a skilled draftsman to convey a clear three-dimensional picture by a drawing on a flat sheet, using one of the systems of projection or perspective. In addition to having no real depth, these drawings may violently distort certain angles or lengths; yet so long as a few strong clues are given and the observer is trained to reject conflicting data, a clear picture can be formed.

In any scheme that proposes to present a three-dimensional picture to the eye in terms of one or a pair of flat pictures, we must attempt to suppress, or eliminate by education, the tendency for the eye to cling to features of the picture which reveal that it is "really" two-dimensional and we must emphasize those elements which

* Paper presented at the national convention of the Institute of Radio Engineers, March 3, 1947.
** Now at University of Minnesota, Department of Physics.

give the actually false impression of depth. Perception of depth by accommodation is subordinate to depth perception by binocular convergence, and depth perception by binocular convergence is subordinate to that by perspective. Consequently, a presentation that provides only perspective is convincing, whereas one that provides both perspective and stereoscopic view is very "real" indeed.

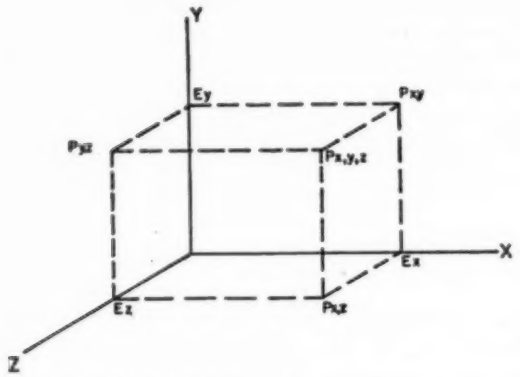

FIG. 1. Right-handed Cartesian coordinate system.

A cathode-ray tube provided with suitable deflecting and modulating voltages is capable of painting *any* two-dimensional picture within reasonable limits of brilliance, color, and grain size. It thus becomes obvious that a single cathode-ray tube can convey any three-dimensional-appearing picture that a perspective drawing can. In addition, two cathode-ray pictures, properly interrelated, can yield a real three-dimensional view if eye accommodation and comparison with surroundings are properly suppressed so that the eyes will be forced to rely on convergence and object shape for depth perception.

It is the purpose of this report to point out how easily the underlying principles of projective and perspective drawing and of stereoscopic photography can be applied to cathode-ray presentation so as to convert raw electrical data directly into vividly recognizable three-dimensional pictures.

Let us consider first the cases where both eyes look at the same picture. These are the projections and the perspective pictures familiar to every engineer and draftsman. In all these methods of presentation, a degree of three-dimensionality is given to the picture by having it resemble, in greater or less degree, the actual picture formed in the eye when viewing the object from some particular viewpoint, imaginary or real, the viewpoint in each case being chosen to bring out certain features of the picture.

In perspective drawing, some advantageous viewpoint is chosen and a serious attempt is made to develop, as accurately as is possible with simple rules of procedure, a picture like that which one eye would see if placed at that point. Projections, on the other hand, attempt to present as many as possible of the lines and angles of the picture in directly measurable form. Consequently, perspective drawings are easily recognized as three-dimensional even by the uninitiated, whereas projections tend to be distorted and often tax the eyes' ability to synthesize them into clear mental pictures, though great ingenuity has been shown in devising special projections that tend to neutralize the intrinsic distortions by counter-distortions.

To investigate the feasibility of presenting three-dimensional data on the cathode-ray tube let us start with the most general assumption: that we have at each instant three coordinate electrical data representing a point in our three-dimensional picture space, and that we also have a voltage specifying the spot brightness desired at that point, thus representing in a limited sense an additional parametric variable. We thus leave unrestricted the paths of the cathode-ray spot and are therefore able to deal with stationary or moving patterns made up of lines, spots, or surfaces; we need not consider separately whether the final picture is formed by scanning or by directed motion of the cathode-ray beam. (Remember, however, that direct, complete, three-dimensional scanning is ordinarily impractical because of the immense number of picture elements involved.)

Though coordinates other than Cartesian might obviously be used, we shall restrict ourselves to these for simplicity (Fig. 1). Let us call the three component voltages with which we are supplied E_x, E_y, and E_z, and let us think of X as directed to the right, Y as up, and Z as toward us—the three axes comprising a right-handed Cartesian system. The three component voltages taken

together represent a point P in the three-dimensional X, Y, Z space.

Plotting E_x against E_y, E_x against E_z, or E_y against E_z by means of a cathode-ray tube, we find that we get nothing new: we have one or another conventional cathode-ray presentation of part of the data. But looked at from the draftsman's standpoint, we have made standard multi-planar orthographic projection drawings: respectively, an elevation, a plan, and a profile projection of P on these three projection planes. Following this lead we undertake to produce the draftsman's more difficult but more illustrative presentations on the cathode-ray tube.

Each of the orthographic projections is based on projection of the "object" data on a single projection plane by rays perpendicular to that plane. It can easily be shown that there is a perfectly general and always linear transformation from the three-dimensional voltage components E_x, E_y, and E_z to the two-dimensional projection components on any specified projection plane. This transformation can be performed in the following manner.

Establish a new coordinate system X', Y', Z' (Fig. 2) in such a fashion that one of its coordinate planes, say the $X'Y'$ plane, coincides with the desired projection plane. Call the cosines of the angles which the new X' axis makes with the old X, Y, and Z axes, respectively, l_1, m_1, n_1, and the cosines of the angles made by the new Y' and Z' axes with the old axes, correspondingly, l_2, m_2, n_2 and l_3, m_3, n_3. The general transformation for rotation of axes now yields the three component voltages $E_{x'}$, $E_{y'}$, $E_{z'}$, resolved along the new prime axes:

$$E_{x'}=l_1E_x+m_1E_y+n_1E_z,$$
$$E_{y'}=l_2E_x+m_2E_y+n_2E_z,$$
$$E_{z'}=l_3E_x+m_3E_y+n_3E_z.$$

Because each of these represents the total resultant voltage along one of the new prime axes, any pair represents the projection on one of the coordinate planes.

Electrically the meaning of this is simple. If we take, with a potentiometer, a fraction l_1 of our incoming E_x voltage, add a fraction m_1 of E_y and n_1 of E_z, apply this to our cathode-ray tube as X deflection voltage, and use the corresponding fractions l_2, m_2, and n_2 of the original voltages for Y deflection voltage, our tube will automatically plot the projection of the data on a new arbitrarily rotated $X'Y'$ plane. Since all the direction cosines are constant for any specified projection and since sine-cosine potentiometers, which are now readily available, yield the cosine directly when only the angle is set on the dial, this transformation is really a very simple one. It is often further simplified in particular resolutions by the fact that some of the angles are 0° or 90° and hence have cosines of 1 or 0—in which event no potentiometer is needed, all or none of a particular component voltage being used.

A specific example will serve to illustrate the simplicity of this projection transformation. Isometric projection occurs when the object axes are all inclined at equal angles of 35° 16′ to the projection plane. If the Y projection is chosen to fall along the new Y' axis, the transformation is:

$$E_{x'}=\frac{\sqrt{2}}{2}(E_x-E_z)$$
$$=0.707(E_x-E_z),$$
$$E_{y'}=\sqrt{\frac{2}{3}}\left(E_y-\frac{E_x}{2}-\frac{E_z}{2}\right)$$
$$=0.816\left(E_y-\frac{E_x}{2}-\frac{E_z}{2}\right).$$

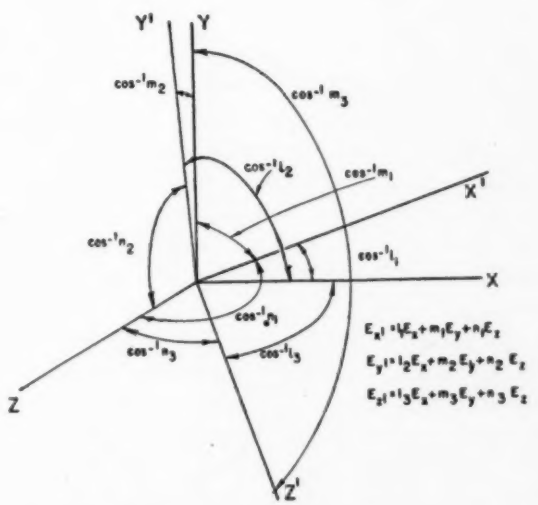

FIG. 2. General transformation for rotation of coordinates.

A little study will give values for the three coefficients for the X' and for the Y' that will yield any of the dimetric or trimetric projections.

Some of the most effective drawings are done in various "oblique projections." These are not

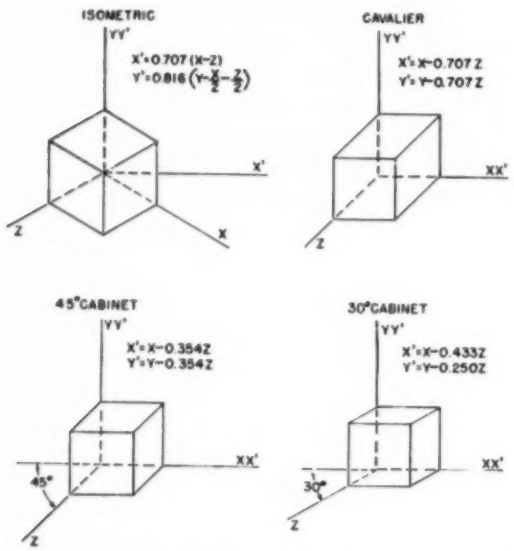

FIG. 3. Cube in isometric and various oblique projections with electrical transformation for each type of projection.

really projections in the simple sense but they make use of the eyes' compromising ability to permit use of very simple drawing rules while still retaining good metric properties.

Figure 3 illustrates several projections, with a sketch of a cube in each, and gives the corresponding electrical transformations. Working independently, Carl Berkley of the DuMont Laboratories has devised and investigated certain of these projections in detail, both theoretically and experimentally, and has obtained excellent results. They were reported at the national convention of the Institute of Radio Engineers on March 5, 1947, and I shall therefore not elaborate on them here.

In military problems, in radar problems, indeed in most cases other than purely geometrical ones, we are likely to know angles other than those from which the direction cosines are derived. The most common case will be that of Fig. 4, in which voltage data are presented in rectangular X, Y, Z coordinates. We wish (1) to take up our viewpoint at some little distance from the phenomenon, in a direction defined by an azimuth angle ϕ and an elevation angle θ; (2) to see the data presented as a projection on a normal plane passing through a chosen origin; and (3), to keep our projection plane so oriented that the picture is still level, i.e., so that the new X axis in the projection plane still lies in the old XZ plane.

As it turns out, the transformation of electrical data to this new and completely general projection is very simple. Using two two-gang potentiometers, we can provide two knobs, one directly calibrated in azimuth and another marked in elevation, which will allow us to set the viewpoint anywhere around a complete sphere.

The transformation is simple if done as two separate coordinate rotations in proper order, as follows (Fig. 5). Starting as usual with data given as E_x, E_y, E_z, transform this for a rotation in azimuth ϕ about the Y axis to give the E data in terms of new coordinates X', Y', Z':

$$E_{x'}=l_1E_x+m_1E_y+n_1E_z,$$
$$E_{y'}=l_2E_x+m_2E_y+n_2E_z,$$
$$E_{z'}=l_3E_x+m_3E_y+n_3E_z,$$

where l_1, m_1, n_1 are the direction cosines of the new X' axis with respect to the old axes and l_2, m_2, n_2 and l_3, m_3, n_3 are the direction cosines

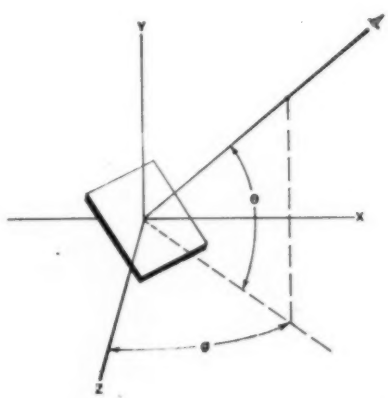

FIG. 4. Projection plane for viewpoint at azimuth ϕ and elevation θ.

of the new Y' and Z' axes. This yields:

$$E_{x'}=E_x\cos\phi-E_z\sin\phi,$$
$$E_{y'}=E_y,$$
$$E_{z'}=E_x\sin\phi+E_z\cos\phi.$$

Now rotate this new coordinate system to a double-prime position (Fig. 6), where the Z'' axis, which is the desired line of view, is swung to an elevation angle θ by a rotation about X'.

$$E_{x''} = E_{x'}$$
$$E_{y''} = E_{y'} \cos\theta + E_{z'} \sin\theta$$
$$E_{z''} = -E_{y'} \sin\theta + E_{z'} \cos\theta.$$

To obtain these data, we need from the azimuth control system:

$E_x \sin\phi$ and $E_x \cos\phi$
(sine-cosine potentiometer No. 1),

E_y (already available),

$E_z \sin\phi$ and $E_z \cos\phi$
(sine-cosine potentiometer No. 2).

For the second transformation, to put in elevation we need:

$E_{x'}$ (already available),
$E_{y'} \sin\theta$ and $E_{y'} \cos\theta$
(sine-cosine potentiometer No. 3),
$E_{z'} \sin\theta$ and $E_{z'} \cos\theta$
(sine-cosine potentiometer No. 4).

Since we desire to show the projection on the $X''Y''$ plane, we put the $E_{x''}$ and $E_{y''}$ voltages

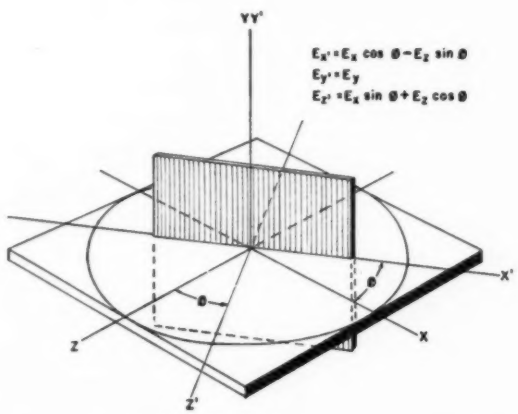

FIG. 5. Transformation by two separate coordinate rotations (rotation for azimuth angle ϕ).

on the oscilloscope deflection plates and therefore do not need the $E_{z''}$ voltage. (Notice, however, that no extra potentiometers are required to obtain $E_{z''}$ because sine and cosine can come from a single unit. We shall have reason to return to $E_{z''}$ later, in connection with perspective and stereoscopic presentations.)

All the transformations thus far considered result in ideal or in stylized projections that are useful where distances along certain axes must

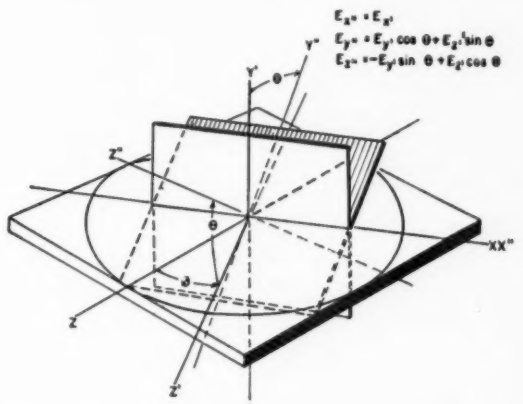

FIG. 6. Transformation by two separate coordinate rotations (rotation for elevation angle θ).

be linearly measurable. Their extensive use in drafting as compared with perspective drawings results largely from their metric properties and from the difficulty of making good perspective drawings, especially from arbitrarily defined viewpoints. In the electric case, the use of view-rotating potentiometers permits any viewpoint to be chosen. For a complete presentation, therefore, it remains only to solve the problem of displaying perspective convergence on the cathode-ray tube.

Return to the original case—where E_x, E_y, and E_z potentials are supplied directly or, what is equivalent, where the necessary rotations have already been accomplished—and consider how the picture would appear in perspective, looking along the Z axis toward the origin (see Fig. 7). All points along the Z axis project as a point at the origin O on the XY projection plane. Viewed from a distance d, the projection for a point $x=a$, $y=b$, $z=c$ would fall a distance $A=ad/(d-c)$ from the axis in the X direction and $B=bd/(d-c)$ in the Y direction. (This follows at once from inspection of similar triangles.) Since a and b are represented by the deflection voltages E_x and E_y, respectively, and d is a constant distance set on a dial, the multiplication indicated in the numerator can be accomplished by two simple

linear potentiometers ganged to the "distance-of-view" control shaft. These potentiometers multiply the incoming E_x and E_y voltages, respectively, by the d set on the dial. c is a constantly varying quantity proportional to E_z. The

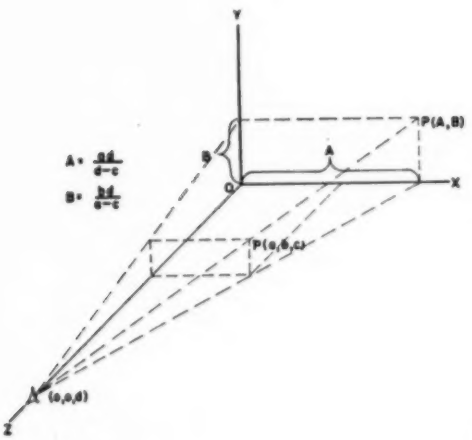

FIG. 7. Perspective projection presentation.

reciprocal $1/(d-c)$ is obtained by using a nonlinear amplifier. The d in the denominator presents no difficulty because it is merely a d.c. bias proportional to the distance setting and is obtained from a third linear potentiometer on that shaft. Several components can be used in common for both A and B since both use identical circuits and contain the same multiplying factor $d/(d-c)$. This system has not been completed, and its performance characteristics cannot yet be stated.

Adjustment of the distance-of-view control changes d—that is, it moves the observer's perspective viewpoint nearer or farther from the apparent object; since there is no focus problem here, it is equivalent to an ideal telephoto lens of adjustable magnification and corrected perspective.

Let us now consider what control over presentation we have, utilizing this perspective control combined with the azimuth and elevation controls previously described in connection with the orthogonal projection presentation. Let us take up a viewpoint a long way off and look over the data from all sides, as one does in inspecting an object visually. This we do by setting our perspective control for a long-distance viewpoint—just long enough, however, to permit us to see the whole picture at once. We now rotate the object—even though it may be actual radar data representing cubic miles of volume—by turning the two angular-selection controls. This permits us to select the one best viewpoint over the entire sphere of possible viewpoints. We now move ourselves nearer at will, going in among the data if this seems advantageous.

A word of caution should be injected at this point. It is feasible to utilize all the freedom just mentioned, but two factors must be remembered. On advancing the viewpoint into the field of data, data behind the observer may appear before him as a "negative." The occurrence of this phenomenon depends upon the design of the reciprocal amplifier and may in special cases require use of a special blanking circuit. However, this blanking circuit turns out to be quite simple.

The second factor concerns the apparent transparency of objects. It is obvious that no data can be presented which are not furnished electrically and, conversely, that all the data provided will be presented unless specifically blanked out. All "pictures" made by this process will then be "glass-block" pictures in which all surfaces of the object can be seen "through." This is generally desirable, especially when graphical or other line data are being presented. It may lead to optical illusions in certain cases, however, where the perspective picture shown is equivalent to another perspective picture of some other data configuration. Recall that in these pictures the eye is being asked to perceive depth solely by convergence of picture lines and cannot rely even on binocular convergence for a clue to real depth.

To investigate whether this one powerful aid to three-dimensional perception can be made to aid us in our attempt to present three-dimensional data realistically, let us see what further resolution of data would be needed to provide two suitably different sets of perspective data to be viewed by the two eyes separately to give the exact equivalent of stereoscopic, or perhaps even of enhanced stereoscopic, relief.

Ideal stereoscopic viewing presumes that both eyes look directly at the object from slightly separated points. In the language of our two

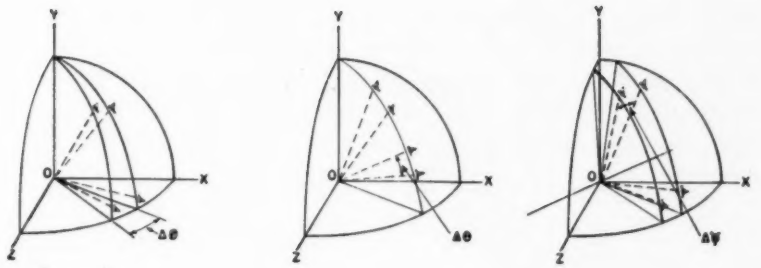

FIG. 8. Stereoscopic eyepoint separation by variation of ϕ, θ, and ψ.

angular-resolution potentiometers, this means that the tubes presenting data to the two eyes must be supplied with similar data for two slightly different viewpoints, and that this difference will depend upon the distance of the viewpoint from the data and upon the degree of stereoscopic enhancement desired.

As our coordinate transformation has been carried out, it is very simple to provide different viewpoints if those viewpoints differ by some simple and preferably constant amount in either ϕ or θ. An extra set of contacts on the potentiometers that establish these angles or, at worst, a duplicate set of potentiometers lagging at a properly set angle will give the additional viewpoint.

Unfortunately, though the equivalent eye separation provided by a small change $\Delta\phi$ in azimuth (Fig. 8) corresponds to a desirable *horizontal* separation of eyepoints, it varies in amount with the cosine of the elevation angle θ, since all the "longitude lines" converge.

Eyepoints produced by deviation of the elevation angle θ by a small amount $\Delta\theta$ are not subject to this error because lines of latitude are uniformly spaced. However, since they correspond to viewpoints above one another, the observer must view the picture as though lying on his side.

This problem can be ideally solved by a third re-resolution of the picture—this time by rotation about the Y'' axis—to give eyepoints that are usable for any azimuth or elevation without readjustment. This is not a complicated transformation; it requires only two additional potentiometers and is therefore justified in special cases.

$$E_{x'''} = E_{x''}\cos\psi - E_{z''}\sin\psi,$$
$$E_{y'''} = E_{y''},$$
$$E_{z'''} = E_{x''}\sin\psi + E_{z''}\cos\psi.$$

These equations can also be expressed as follows:

$$E_{x'''} = \cos\psi(E_x\cos\phi - E_z\sin\phi) - \sin\psi[-E_y\sin\theta + \cos\theta(E_x\sin\phi + E_z\cos\phi)],$$

$$E_{y'''} = E_y\cos\theta + \sin\theta(E_x\sin\phi + E_z\cos\phi),$$

$$E_{z'''} = \sin\psi(E_x\cos\phi - E_z\sin\phi) + \cos\psi[-E_y\sin\theta + \cos\theta(E_x\sin\phi + E_z\cos\phi)].$$

If one does not need such complete generality but still wishes the advantages of stereoscopic vision, a good approximation can be had with very simple apparatus. Even the sine-cosine resolving potentiometers become unnecessary.

Consider the case where both eyes look at a nearby object P on the axis of vision as projected

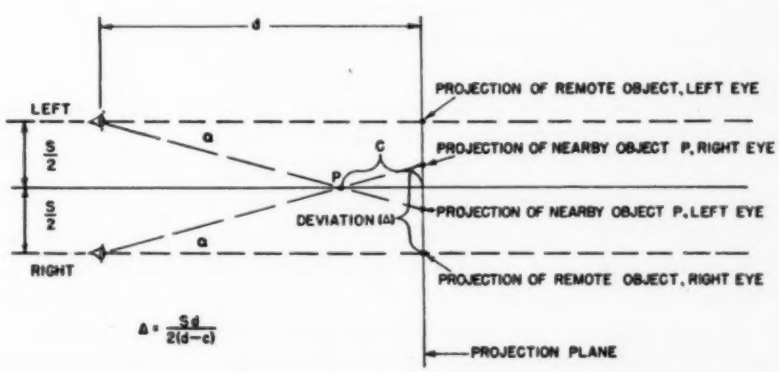

FIG. 9. Variation of binocular convergence angle with object distance.

on a plane perpendicular to the axis (Fig. 9). The convergence angle α for this point is determined solely by the proximity of the object to the eyes. The projection that represents this convergence must move to the right for the left

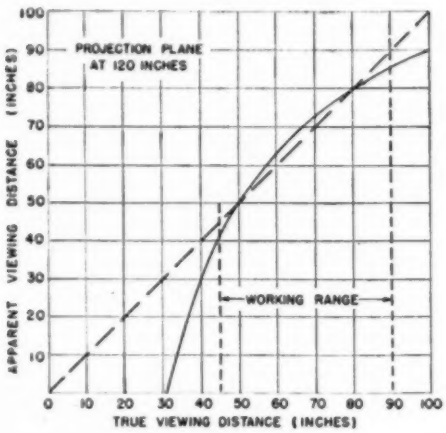

FIG. 10. Working range of simplified stereoscopic system.

eye and to the left for the right eye. The amount of deviation of each projection for an object to appear at a distance $d-c$ is given by

$$\Delta=\frac{Sd}{2(d-c)},$$

where Δ represents a deflecting voltage for application to the two cathode-ray tubes as X bias of opposite polarities.

S is a d.c. voltage representing interocular distance and can be regarded as constant; d, as it multiplies S, can be represented exactly by a linear potentiometer on the distance-of-view shaft, working as a voltage divider on S. The factor of 2 is, of course, a mere scale factor.

Since c is an instantaneous variable, it represents a reciprocal operation and requires a tube circuit; d, as it appears inside the parentheses with c in the denominator, is applied as a d.c. bias to c. This quantity $(d-c)$ is already available from the perspective circuits, leaving only a reciprocal of a voltage to be taken. As before, this is accomplished by means of a non-linear tube circuit.

As a surprisingly good practical approximation in the case where the object field is not too deep or too close to the observer, a fraction of $(d-c)$, taken with reversed polarity and with a bias added, can be substituted for the reciprocal $1/(d-c)$. This apparently poor approximation works well because an error in the Δ-voltage merely makes the object point appear stereoscopically a little nearer or farther than intended according to the perspective; this is an error that the eye can easily bear, as evidenced by its ability to understand perspective pictures on a flat sheet, where there is no correction at all. Figure 10 compares the apparent distance with the actual distance, using this simple stereoscopic system for a projection screen ten feet away and an object at various distances along the axis.

For objects off the axis the simplified stereoscopic method introduces small additional errors that increase as the object gets farther from the axis of view; however, these errors become important only for uncomfortably large angles of view.

If desired, the stereoscopic correction may be applied to simple projection data without the perspective correction. In this case the illusion of depth remains good, but objects seem to collapse as they approach and to expand as they recede in a very surprising manner.

In all these three-dimensional presentations the illusion is greatly enhanced if a few reference lines are sketched in to give the eye a comparison

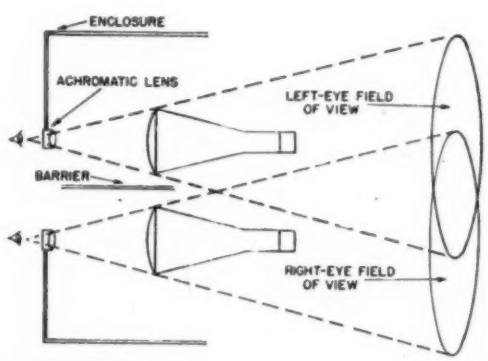

FIG. 11. Simple method for viewing stereoscopic images.

mesh with which to orient itself. There are many ways in which this can be done; one of the simplest is that of picture switching within the persistence period of the eye. It is relatively easy to commutate either mechanically or elec-

tronically between a sweep-circuit system and the picture data, and thus to draw in lines in any chosen direction and with any chosen spacing.

Though it is perfectly possible to superimpose such lines on the data, this may be difficult electronically in comparison with switching.

Again, it may be desired to measure the position of some intersection or other point in the picture space. This can be accomplished by a cursor system, using a calibrated set of controls to run a point or a line in a chosen orientation back and forth in the picture space.

The appearance on the market of multi-gun cathode-ray tubes offers an ideal solution to this problem of sketching in contour or grid lines, since it eliminates the need for any switching: with a two-gun tube, one gun paints in the data picture, and the other draws in the grid lines. Should one care to use the four-gun tube, the circuit is greatly simplified. Three of the guns can draw in three orthogonal coordinate-system grid lines in any of the conventional systems—Cartesian, polar, cylindrical—or even of the non-orthogonal systems.

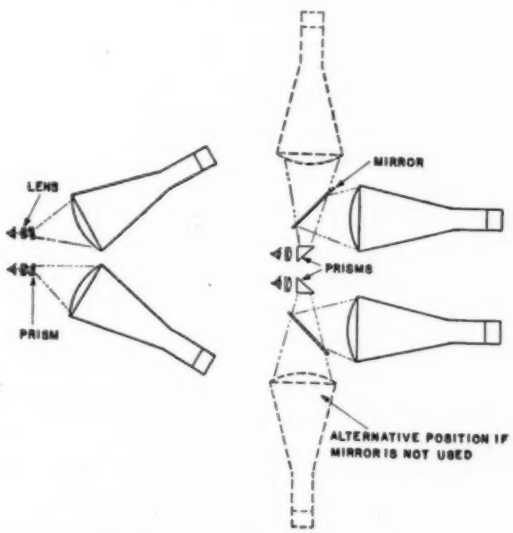

FIG. 12. Methods for viewing large cathode-ray tubes for stereoscopic presentation.

No special precautions need to be taken in viewing any of the monocular projections or the perspective pictures, whether they are viewed with one or with both eyes, since the eyes of a person used to reading such drawings are already completely conditioned to being deceived in these particular ways.

When viewing pictures that are mentally known to represent large objects, a little illusion

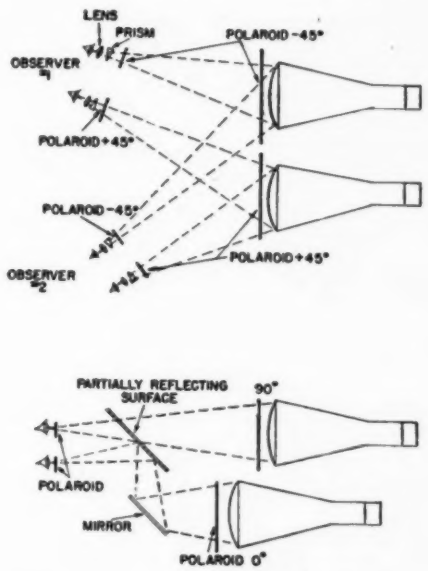

FIG. 13. (a) Use of Polaroid glasses to permit several observers to view stereoscopic presentation simultaneously; (b) Stereoscopic presentation for use in aircraft.

is added by fitting the observer with positive lenses of sufficient strength to place the viewed image just short of infinity. Seeing the face of the cathode-ray tube and its mount does not weaken the illusion appreciably as it becomes part of the "drawing board."

In contrast, data for stereoscopic viewing should be carefully presented to preserve the strong depth illusion of which this method is capable. The strength of stereoscopic reality found in the pictures varies markedly from observer to observer; airplane pilots, for example, are especially adept at perceiving it. That perception can be developed by learning is evident from the fact that a new observer seeing the stereoscopic CRO images for the first time may, if he is one of those least able to perceive the pictures, see almost no three-dimensional form to the images; however, after one hour of study, he will be able to see almost all the features. A very perceptive person will see all there is to see at first glance and will very likely be pointing

out faults in the perspective rendition within five minutes.

Several satisfactory methods of viewing the stereoscopic images have been worked out. The simplest of these uses two small CRO tubes of

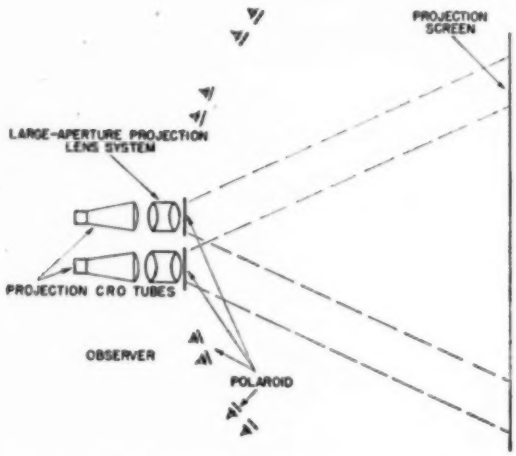

FIG. 14. Polarized projection for stereoscopic display.

diameter less than the interocular distance (Fig. 11). These tubes are viewed through simple achromatic lenses placed close to the eyes. The lenses make the tube face appear both at a distance and enlarged. An enclosure blocks out surrounding objects, and a partition prevents each eye from seeing the other's picture. This makeshift arrangement gives good results but permits seeing only such detail as can be presented on a three-inch tube. It also has the disadvantage that the eyes must be placed close to the viewing lenses.

If larger cathode-ray tubes are to be used, some optical arrangement must be made whereby each eye sees the center of one of the tubes directly ahead while the tubes are actually separated more than the interocular distance. Two of the easier ways of accomplishing this separation with prisms or mirrors are shown in Fig. 12.

By wearing Polaroid glasses it becomes possible to view the cathode-ray tubes over a reasonably wide angular range; consequently, several observers can see the presentation simultaneously (Fig. 13). If only the scopes are to be viewed, the observers can be fitted with prisms and enlarging lenses as well as Polaroids so that they can comfortably look at two tubes side by side and see them as superimposed because of the combined effect of the prism divergence and the Polaroid sorting out of the data. If this is undesirable, as in the case of data for an airplane pilot, the pictures can be shown superimposed with the aid of partially reflective surfaces. The Polaroid glasses are still worn but they do not interfere with ordinary vision.

Because of the selective reflection and transmission of plane polarized light by transparent sheets, proper choice of polarization plane will result in surprisingly little loss of light.

As a final and more elegant method, we may use polarized projection as a display means. Modern CRO projection techniques can provide a display several feet on an edge—a bright display that can be viewed by dozens of observers, each wearing ordinary 45° polarized Polaroid glasses (Fig. 14). By using highly directive projection screens, relatively little light is lost, and both images are displayed simultaneously on the same screen by simple polarization projection.

It is not my intention to enumerate here the many applications of three-dimensional cathode-ray presentation that can be made. I shall, however, list a few, chosen from widely separated fields, to illustrate its versatility.

The most general type of application is undoubtedly that in which three related quantities all vary simultaneously and where it is desired to visualize the whole complicated process. This visualization becomes especially important where the three interrelated quantities vary jointly as a function of still another parameter.

A case of this kind familiar to all of us is the common vacuum-tube characteristic. In its simplest three-variable form we have the covariation of grid voltage, plate voltage, and plate current as one or more of them change in some chosen manner. Going to the more complicated case, we can present plate-current, plate-voltage, and grid-voltage data for a pentode or tetrode while we slowly change another parameter, say suppressor or screen voltage.

From the field of internal combustion or steam engineering we can take the case of the thermodynamic cycle. Here we can plot pressure, volume, and temperature together.

Acoustic engineers will, I am sure, find it instructive to plot the reactive and resistive components of loudspeaker impedance against frequency, thus giving in one easily photographed picture a good instantaneous summary of the device's over-all performance.

From the field of biophysics I would cite the advantages of plotting the entire set of heart potentials from the standard three cardiograph leads as a single space figure whose shape would characterize the patient's heart action. Similar thinking leads to a corresponding electro-encephalographic application.

For studying a.c. phenomena, both low frequency and high, the device is unusually useful. Non-linear components can be made to trace their current-voltage or reactance-resistance characteristics as a function of frequency, temperature, or other variable at will. Simultaneous plots of both complex impedance components as a function of frequency are a familiar need in the field of matching networks and filter design.

A three-dimensional cosmic-ray telescope could be built whose principal cost would be the set of Geiger counters.

The close relationship between the development of the theory of the three-dimensional oscilloscope and the theory of drafting leads one to wonder whether it might not profitably be put to work in the drafting room.

For presentation of radar- and sonar-type data, provision must obviously be made for supplying information in proper sequence, since it is impractical to scan all three-dimensional space. Thus, if we are scanning in elevation and azimuth by radar, we must be prepared, at the instant when the x and y coordinates correspond to the elevation and azimuth of a target, to supply the range to the z circuit. Practicable pulse repetition frequencies do not permit scanning the z axis in addition to the x and y axes. In the radar case, the advantages of the telescopic feature and the rotatable viewing position become obvious: for example, we could choose an optimum viewpoint to see whether planes were near a collision course.

Though it is true that three-dimensional television data can be transmitted by this system, real advantages would accrue only if the original data contained range information directly. Otherwise regular double-channel stereoscopic television has the advantage of simplicity.

From the antenna designer's viewpoint, one can see the elegance of the system as applied to presentation of a whole three-dimensional antenna radiation pattern visible in space, to be examined from any direction at will.

As a last example, I should like to propose the use of the system for exploration of electrostatic or magnetic fields. In this case a probe would be moved about in the field, and a "vector" on the oscilloscope screen would point out the direction and magnitude of the field at successive positions.

A Least-Square Application to Relaxation Methods

O. L. Bowie
Watertown Arsenal, Watertown, Massachusetts
(Received April 24, 1947)

A least-square application to relaxation techniques is presented wherein the mean-square error is minimized in considering any corrections to a given set of values for the unknown function. A systematic procedure is, therefore, devised for weighting errors at various points of the lattice. The process has general applicability to various forms of equations and definitions of corresponding difference equations. As illustrations, Laplace's and the biharmonic equations are considered.

THE method of "relaxation" has recently come into prominence as a mathematical tool for overcoming the analytical difficulties encountered in the solution of partial differential equations from highly irregular shapes. Essentially, the differential equation is replaced* by a difference equation which may be solved either algebraically or by various iterative procedures. The iterative methods of solving the difference equation are known as relaxation techniques. It can be shown that if the mesh of the lattice used to cover the given region is made sufficiently fine, the solution of the difference equation approaches the solution of the original problem, and the difference quotients converge to the corresponding derivatives of the solution.

I. A LEAST-SQUARES PROCEDURE

Consider the class of partial differential equations whose solutions have the additive property. That is, if u_0 and u_1 are solutions, then $(c_0u_0+c_1u_1)$ is also a solution where c_0 and c_1 are arbitrary constants. The same property will also hold for the solutions of the corresponding difference equations.

Let the given region be covered by a lattice. Then for defined points on the lattice, the differential equation can be replaced by a difference equation of the form

$$L(u_i)=0, \tag{1}$$

where u_i are the values of the function at the points of the lattice and $L(u_i)$ is a relationship valid for each u_i, which, in general, involves linear combinations of the u_i. If $L(u_i)=0$, for all u_i of the lattice, and if the set of u_i satisfies the original boundary conditions set up in a modified difference equation form, then the set of u_i is a solution of the difference equation. In general, for a trial set, $\bar{u}_i$, it will be found that

$$L(\bar{u}_i)=p_i\not\equiv 0. \tag{2}$$

The p_i are called the residuals and are defined for each point of the lattice. The relaxation procedure consists in altering the values of $\bar{u}_i$ until $p_i\equiv 0$ for all p_i. In actual practice, sufficient accuracy is obtained by reducing the p_i so that they are all nearly zero.

It should be noted that from the nature of $L(\bar{u}_i)$ an adjustment in $\bar{u}_i$ at a point will affect the values of p_i at several points. The usual relaxation schemes (such as the Liebmann process) rely on smaller changes to the adjacent p's as compared with the correction of p_i. It can be seen that the rate of convergence of relaxation methods will be speeded up if the correction of a u_j is based on surrounding p_i as well as on p_j. The following method which can be used for this purpose will now be presented.

Let the measure** of error of a given set of $\bar{u}_i$ over the whole lattice be defined as

$$\sum_i [L(\bar{u}_i)]^2, \tag{3}$$

where the summation extends over all the points of the lattice. The approximate solution, $\bar{u}_i$, will be chosen to satisfy the given boundary conditions. Now consider a second set of values, $\langle u_i\rangle$, such that $\bar{u}_i+c\langle u_i\rangle$ obeys the boundary conditions for any constant c. The question is now raised as to what value of c will make the

* See reference 3.

** See reference 5.

total error a minimum for $\bar{u}_i+c\langle u_i\rangle$. Substituting into (3), one obtains for the total error

$$\sum_i [L(\bar{u}_i)+cL(\langle u_i\rangle)]^2. \tag{4}$$

Differentiation with respect to c yields for a minimum

$$c=-\sum_i L(\bar{u}_i)L(\langle u_i\rangle)/\sum_i [L(\langle u_i\rangle)]^2. \tag{5}$$

For the criterion on the best correction in the sense of (3) to add to a single $\bar{u}_j$, one would choose a set of $\langle u_i\rangle$ identically zero at all points except at the single point corresponding to $\bar{u}_j$. The correction would be given by (5) if $\langle u_j\rangle=1$. Similarly, the best uniform correction to add to a group of the values of the function can be determined by (5). In this latter case, the set $\langle u_i\rangle$ again must be chosen so that $c\langle u_i\rangle+\bar{u}_i$ satisfies the boundary conditions for any arbitrary c. In addition, by defining $\langle u_i\rangle$ as identically equal to one at all points at which corrections are to be made and, otherwise, as identically equal to zero, the uniform correction, c, can again be determined by (5).

The procedure indicated in (4) and (5) is restrictive in the sense that it provides for only a uniform correction to the given set of $\bar{u}_i$. This is evidently an unnecessary restriction, for one can choose several sets of $\langle u_i\rangle$ with several corresponding arbitrary constants and again derive conditions on the arbitrary constants by referring back to (3). This, however, would involve the solution of a set of simultaneous equations and the simplicity of the form of (5) would be lost.

II. APPLICATION TO LAPLACE'S EQUATION

The Dirichlet problem is that of finding a solution of Laplace's equation

$$(\partial^2 u/\partial x^2)+(\partial^2 u/\partial y^2)=0 \text{ in } R, \tag{6}$$

where u has specified values on the boundary of R. After R is covered with a square lattice, then in rectangular coordinates and in terms of neighboring points the difference equation corresponding to (6) becomes a set of relationships in the form

$$L(u_0)=u_1+u_2+u_3+u_4-4u_0=0, \tag{7}$$

where the notation is indicated in Fig. 1. One manner in which the $\bar{u}_0$ are adjusted so that the forms (7) are satisfied is to add iteratively to the quantities $\bar{u}_0$ the correction $\frac{1}{4}L(\bar{u}_0)$. The corrected $\bar{u}_0$ will then satisfy (7), to be sure, but $L(\bar{u}_1)$, $L(\bar{u}_2)$, $L(\bar{u}_3)$, and $L(\bar{u}_4)$ will be increased by an amount $\frac{1}{4}L(\bar{u}_0)$.

To illustrate the principle outlined in the first section, the criterion for the best correction will now be derived in terms of (7). The function $\langle u_i\rangle$ will thus be defined as unity at a single point and identically zero elsewhere. By (7) it is seen that $L(\langle u_i\rangle)$ has the values -4 at the point corresponding to the functional value of unity, 1 at four neighboring points, and zero elsewhere. A glance at Eq. (5) will show that for a single correction to $\bar{u}_0$ the best in the sense of (3) will be

$$c=-\frac{1}{20}[L(\bar{u}_1)+L(\bar{u}_2)+L(\bar{u}_3)+L(\bar{u}_4)-4L(\bar{u}_0)]. \tag{8}$$

Formulae similar to (8) can likewise be obtained for a single correction to several of the functional values.

For corrections of points adjacent to the boundary, it is necessary to define in some manner values for $L(\bar{u}_i)$ at boundary points in order to use (8). Such a definition is somewhat arbitrary as it imposes more conditions on the set of simultaneous difference equations than there are unknowns. At the same time a wise choice of the definition is important to insure rapid convergence of the iterative process. In most cases, it is sufficient to modify the form of

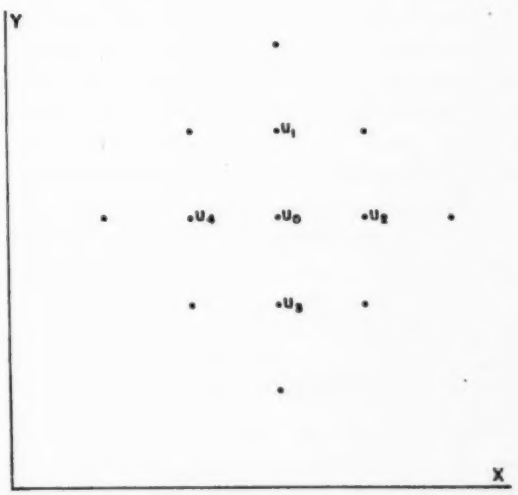

FIG. 1.

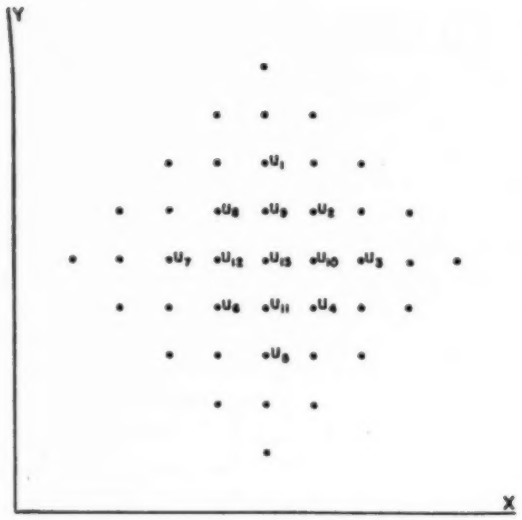

FIG. 2.

(7) by using forward differences when on the boundary. Then, during the process of iteration, a stage will be reached when the computer can vary the fictitious boundary $L(\bar{u}_i)$'s by visual inspection to speed the convergence.

It is interesting to note that a single correction based on (8) weights the values of $\bar{u}_i$ at the thirteen points shown in Fig. 1. Since the least-squares correction is based on adjacent residuals as well as the residual at the given point under consideration, it has a tendency to "smooth" the pattern of residuals. In general, this property has an advantage over usual "point by point" procedures. However, in some situations, the averaging effect slows down the rate of convergence. When the residuals are either predominantly positive or negative, the convergence is greatly speeded up by the larger corrections in the values of the function which one makes by using the usual "point by point" procedures. In practice, therefore, to obtain the full advantage of the least-square procedure, corrections should be made to the function at several points. It was found that a uniform correction, derived by the least-squares criterion, for small blocks of points proved very simple to handle and insured rapid convergence of the solution. For use of the least-squares method in the solution of the Dirichlet problem, therefore, it is recommended that the uniform correction to simple-shaped blocks of points be used in conjunction with the single-point correction.

III. APPLICATION TO THE BIHARMONIC EQUATION

The biharmonic problem involves the solution of the equation

$$[\partial^4 u(x, y)/\partial x^4]+2[\partial^4 u(x, y)/\partial x^2\partial y^2] +[\partial^4 u(x, y)/\partial y^4]=0 \text{ in } R, \quad (9)$$

subject to specified values of u and certain of its derivatives on the boundary of R. In terms of a square lattice of points, the difference equations involve thirteen points for each point of the lattice. With the notation of Fig. 2, the difference equations are in the form

$$L(u_{13})=(u_1+u_3+u_5+u_7)+2(u_2+u_4+u_6+u_8) -8(u_9+u_{10}+u_{11}+u_{12})+20u_{13}=0. \quad (10)$$

From Eq. (5) it is seen that for a single correction to $\bar{u}_{13}$ the best in the sense of (3) will be

$$c=-\frac{1}{676}\{[L(\bar{u}_1)+L(\bar{u}_3)+L(\bar{u}_5)+L(\bar{u}_7)] +2[L(\bar{u}_2)+L(\bar{u}_4)+L(\bar{u}_6)+L(\bar{u}_8)] -8[L(\bar{u}_9)+L(\bar{u}_{10})+L(\bar{u}_{11})+L(\bar{u}_{12})] +20L(\bar{u}_{13})\}. \quad (11)$$

Similarly, formulae for corrections to blocks of values of the function can be derived. Definitions must be set up for values of $L(u_i)$ where the lattice points are boundary points or points adjacent to the boundary. These may be set up by use of forward differences as in the previous section and adjusted as the computation progresses.

To obtain the full advantage of the least-squares procedure in the solution of the biharmonic equation, it is recommended that the uniform correction to simple-shaped blocks of points be used in conjunction with the single-point correction.

IV. DISCUSSION

The principle outlined in Section I can be applied to relaxation procedures involved in the solution of general types of equations of physics. The forms $L(u_i)=0$, themselves, may be defined in many ways. The difference equation may be set up using higher ordered differences, or differences using diagonal neighbors. A non-homogeneous equation can be likewise treated by suitably defining $L(u_i)=0$. In general, the form

of $L(u_i)$ should be chosen from the standpoint of the amount of weighting of errors possible with a minimum of calculation.

Although only a single-point correction has been explicitly derived in Sections II and III, the process for deriving similar formulae for corrections to blocks of points has been outlined. It would seem, in general, that such formulae for blocks of points should be derived only for the case of a uniform correction. More elaborate considerations would necessarily complicate the form of the correction formula.

Preliminary tests of this least-squares procedure have been found quite satisfactory when combining uniform corrections to blocks of points with single-point corrections. The advantage over usual "point by point" procedures increases as the process continues.

BIBLIOGRAPHY

1. G. H. Shortly and R. Weller, "The numerical solution of Laplace's equation," J. App. Phys. **9**, 334–348 (1938).
2. D. G. Christopherson and R. V. Southwell, "Relaxation methods applied to engineering problems," Proc. Roy. Soc. **A168**, 317–350 (1938). See also H. W. Emmons, "The numerical solutions of heat conduction problems," Trans. A.S.M.E. **65**, 607–615 (1943).
3. David Moskovitz, "The numerical solution of Laplace's and Poisson's equations," Quart. App. Math. **2**, 148–163 (July 1944).
4. I. S. Sokolnikoff, *Mathematical Theory of Elasticity* (McGraw-Hill Book Company, Inc., New York, 1946), Chapter V.

An X-Ray Diffraction Study of the Silver-Magnesium Alloy System

HAROLD R. LETNER* AND S. S. SIDHU**

Department of Physics, University of Pittsburgh, Pittsburgh, Pennsylvania

(Received April 29, 1947)

Four homogeneous solid solutions were found in the silver-magnesium alloy system. The α-primary solid solution of magnesium in silver has a f.c.c. structure. The β-solid solution has a b.c.c. structure. The γ-solid solution appears to have a complicated structure. While others have identified it as hexagonal, no definite structure could be assigned to it from our diffraction data. The δ-solid solution has a h.c.p. structure of magnesium.

The lattic parameter a_0 in the α-solid solution increases with increasing magnesium concentration but exhibits a marked negative deviation from Vegard's Law. The a_0 in the β-solid solution, however, increases linearly with increasing magnesium concentration.

Silver and magnesium atoms are distributed at random in the α-phase but take up preferred positions in the β-phase. The ordering process takes place throughout the β-phase, but is most nearly complete in the region of 50 atomic percent Mg.

INTRODUCTION

THE Ag-Mg alloy system presents an interesting crystal structure problem in that Ag is known to have a face-centered cubic (f.c.c.) structure,* while Mg is hexagonal close-packed (h.c.p.). Ag, atomic number 47, is monovalent and has an atomic radius of 1.44 angstrom units (A); Mg, atomic number 12, is divalent and has an atomic radius of 1.60A.[1] The purpose of the present work was to study by x-ray diffraction methods the changes which take place in the structure of Ag as Mg atoms are added to its lattice.

The phase equilibrium diagram of the Ag-Mg system was first determined by Zemczuznyj.[2] Subsequent investigations were carried out by Saeftel and Sachs,[3,4] Payne and Haughton,[5]

* Now at Mellon Institute of Industrial Research, Pittsburgh, Pennsylvania.

** On leave of absence now at Argonne National Laboratory, Chicago, Ill.

[1] W. Hume-Rothery, *The Structure of Metals and Alloys* (Chemical Publishing Company, Inc., Brooklyn, New York, 1939), Part III, pp. 30–49.

[2] S. F. Zemczuznyj, "Über die Leigerungen des Magnesiums mit Silber," Zeits. anorg. Chemie **49**, 400 (1906).

[3] F. Saeftel and G. Sachs, "Festigkeitseigenschaften und Struktur einiger begrenzter Mischkristallreihen," Zeits. Metallkunde **17**, 258 (1925).

[4] W. Guertler, "Neue Silberlegierungen," Zeits. Metallkunde **19**, 68 (1927).

[5] R. J. M. Payne and J. L. Haughton, "Alloys of magnesium, part IV.—The constitution of the magnesium-rich alloys of magnesium and silver," J. Inst. Metals **60**, 351–364 (1937).

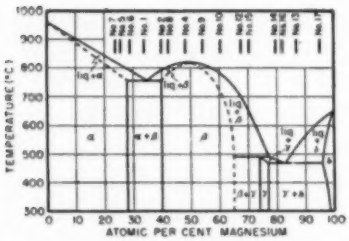

FIG. 1. Silver-magnesium phase equilibrium diagram showing compositions of the alloys studied.

Hume-Rothery and Butchers,[6] Owen and Preston,[7] Ageew and Kuznezow,[8] and George.[9] Figure 1 is the phase equilibrium diagram of Zemczuznyj as given by Hansen,[10] modified to include the more recent results of the other investigators for the Mg-rich portion of the system. The vertical lines with numbers 1 to 17 refer to this study.

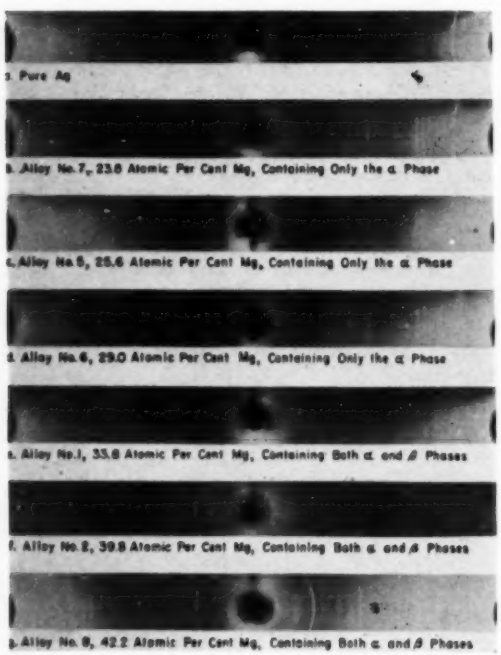
a. Pure Ag
b. Alloy No. 7, 23.8 Atomic Per Cent Mg, Containing Only the α Phase
c. Alloy No. 5, 25.6 Atomic Per Cent Mg, Containing Only the α Phase
d. Alloy No. 6, 29.0 Atomic Per Cent Mg, Containing Only the α Phase
e. Alloy No. 1, 33.8 Atomic Per Cent Mg, Containing Both α and β Phases
f. Alloy No. 2, 39.8 Atomic Per Cent Mg, Containing Both α and β Phases
g. Alloy No. 8, 42.2 Atomic Per Cent Mg, Containing Both α and β Phases

FIG. 2. X-ray photograms of pure silver and alloys containing the α-solid solution of magnesium in silver. Camera diameter 57.3 mm; copper K_α radiation.

EXPERIMENTAL PROCEDURE

Fifteen alloys having compositions indicated in Fig. 1 were prepared in an automatically temperature-controlled electric furnace under a commercial flux obtained from the Dow Chemical Company. Upon completion of the melting process, the resulting ingots, weighing approximately 50 grams each, were allowed to cool in the furnace. The cooling rate in the solidifying range of the alloys was approximately 3C° per minute.

Samples of filings were removed from the centers of the ingots with specially cleaned iron files and placed in evacuated hard glass tubes. After annealing for five hours at 525°C to remove mechanical strains set up in the crystal lattice by the filing process, the samples were analyzed chemically for both Ag and Mg. Portions of the

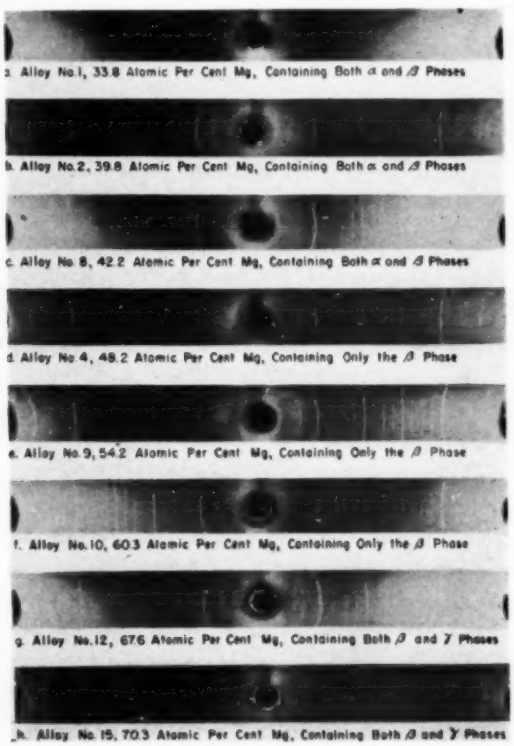
a. Alloy No. 1, 33.8 Atomic Per Cent Mg, Containing Both α and β Phases
b. Alloy No. 2, 39.8 Atomic Per Cent Mg, Containing Both α and β Phases
c. Alloy No. 8, 42.2 Atomic Per Cent Mg, Containing Both α and β Phases
d. Alloy No. 4, 48.2 Atomic Per Cent Mg, Containing Only the β Phase
e. Alloy No. 9, 54.2 Atomic Per Cent Mg, Containing Only the β Phase
f. Alloy No. 10, 60.3 Atomic Per Cent Mg, Containing Only the β Phase
g. Alloy No. 12, 67.6 Atomic Per Cent Mg, Containing Both β and γ Phases
h. Alloy No. 15, 70.3 Atomic Per Cent Mg, Containing Both β and γ Phases

FIG. 3. X-ray photograms of alloys containing the β-solid solution of magnesium in silver. Camera diameter, 57.3 mm; copper K_α radiation.

[6] W. Hume-Rothery and E. Butchers, "The solubility of silver and gold in solid magnesium," J. Inst. Metals **60**, 345–350.

[7] E. A. Owen and G. D. Preston, "The atomic structure of silver-magnesium and gold-zinc," Phil. Mag. **2**, 1266 (1926).

[8] N. Ageew and V. G. Kuznezow, "Roentgenographic study of alloys of magnesium and silver," Bull. Acad. Sci. U.R.S.S., Classe sci. math. nat., Ser. chem., 289–309 (1937).

[9] H. H. George, *X-Ray Investigation of Silver-Magnesium Alloys* (Thesis) (University of Pittsburgh, 1939).

[10] M. Hansen, *Der Aufbau der Zweistoff-Legierungen* (Julius Springer Verlag, Berlin, 1936), p. 38.

same samples were used in making powder x-ray-diffraction photograms to insure that the compositions of the filings used for diffraction studies and those used for chemical analyses were identical.[11]

Powder x-ray diffraction photograms were made with filtered Cu K_α radiation using a camera of 57.3-mm diameter. Lattice parameters for the f.c.c. and b.c.c. structures were calculated from the relation:

$$a_0=\frac{n\lambda}{2\sin\theta}(h^2+k^2+l^2)^{\frac{1}{2}}, \qquad (1)$$

where a_0 is the lattice parameter (i.e., the cube edge of the unit cell), n is the order of the diffracted ray, λ is the wave-length of the radiation used, $h\,k\,l$ are the Miller indices of the planes contributing to the diffracted ray, and θ is the angle between the incident x-ray beam and the diffracting planes. Lattice parameters for the h.c.p. structure were calculated from the corresponding expression:

$$a_0=\frac{n\lambda}{2\sin\theta}(4/3(h^2+hk+k^2)+(l/c)^2)^{\frac{1}{2}}, \qquad (2)$$

where a_0 and c_0 are the lattice parameters, and $c=c_0/a_0$ is the axial ratio.

Values of θ were obtained directly from the photograms by measuring the spans between corresponding lies of the diffraction pattern.[12] From these values the lattice parameters were calculated by means of Eqs. (1) or (2) and plotted against $\cot\theta$. The resulting curves were extrapolated to $\cot\theta=0$ to obtain final values of the lattice parameters, since the percentage error approaches zero as θ approaches 90°.[13–15]

[11] W. Hume-Rothery and P. W. Reynolds, "Application of the Debye-Scherrer method of x-ray crystal analysis," J. Inst. Metals **60**, 303–317 (1937).

[12] M. J. Buerger, "Design of x-ray powder cameras," J. App. Phys. **16**, 504 (1945).

[13] M. J. Buerger, "Precision determination of linear and angular constants of single crystals," Zeits. f. Krist. **97**, 433–468 (1937).

[14] Charles S. Barrett, *Structure of Metals, Metallurgy and Metallurgical Engineering Series* (McGraw-Hill Book Company, Inc., New York and London, 1943), pp. 134–138.

[15] B. E. Warren, "The absorption displacement in x-ray diffraction by cylindrical samples," J. App. Phys. **16**, 614 (1945).

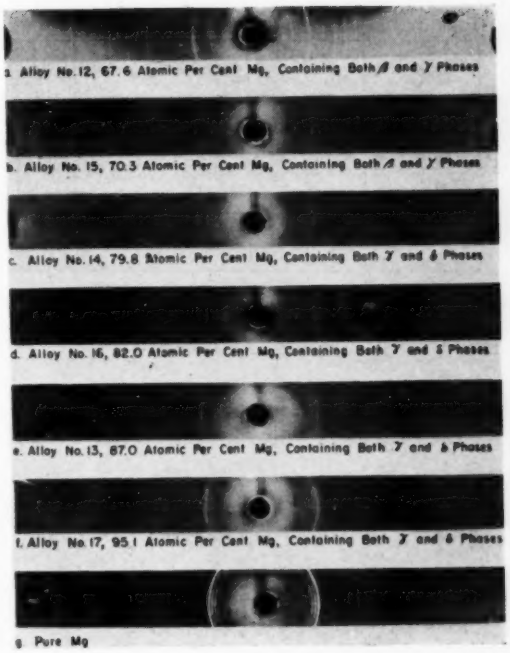
a. Alloy No. 12, 67.6 Atomic Per Cent Mg, Containing Both β and γ Phases
b. Alloy No. 15, 70.3 Atomic Per Cent Mg, Containing Both β and γ Phases
c. Alloy No. 14, 79.8 Atomic Per Cent Mg, Containing Both γ and δ Phases
d. Alloy No. 16, 82.0 Atomic Per Cent Mg, Containing Both γ and δ Phases
e. Alloy No. 13, 87.0 Atomic Per Cent Mg, Containing Both γ and δ Phases
f. Alloy No. 17, 95.1 Atomic Per Cent Mg, Containing Both γ and δ Phases
g Pure Mg

FIG. 4. X-ray photograms of alloys containing the γ- and δ-solid solutions of magnesium in silver and of pure magnesium. Camera diameter, 57.3 mm; copper K_α radiation.

The relative intensities of the diffraction lines were estimated and tabulated simultaneously with the lattice parameter measurements. Photograms of alloys containing the α- and β-phases were scrutinized for superstructure lines. For the α-phase, this amounted to a search for lines corresponding to reflecting planes having Miller indices $h\,k\,l$ which are mixed odd and even integers and for the β-phase, lines corresponding to planes for which the sums of the Miller

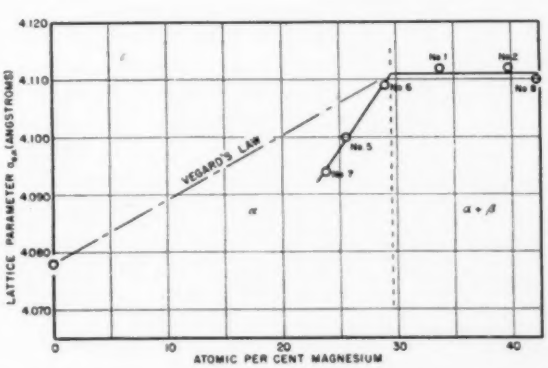

FIG. 5. Variation of lattice parameter $a_{0\alpha}$ with composition in α-phase silver-magnesium alloys.

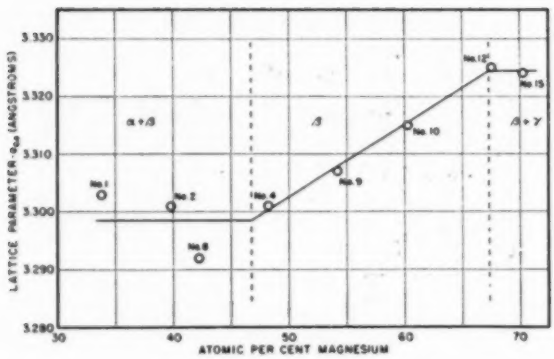

FIG. 6. Variation of lattice parameter a_{68} with composition in β-phase silver-magnesium alloys.

indices $h+k+l$ are odd integers.[16–18] No satisfactory analysis could be made for superstructure in the γ- and δ-phases because of the large number of extremely weak lines obtained on the photograms.

EXPERIMENTAL RESULTS

A. Phases and Phase Boundaries

Four types of crystal structure were found to exist in the Ag-Mg alloys investigated. These were a f.c.c. structure corresponding to the α-phase, a b.c.c. structure corresponding to the β-phase, an undetermined structure corresponding to the γ-phase and a h.c.p. phase belonging to the δ-phase. (See Fig. 1.) Attempts to determine the structure of the γ-phase were not successful; photograms of alloys containing this phase showed a multiplicity of very faint and indistinct lines. Ageew and Kuznezow have identified the structure as hexagonal.[8] X-ray photograms of the diffraction patterns corresponding to the various structures found are shown in Figs. 2–4.

Although no attempt was made to determine accurately phase boundaries, one point in this connection seems worthy of mention. Alloy No. 6 having a composition of 29.0 atomic percent Mg should, according to the phase equilibrium diagram in Fig. 1, contain both α- and β-phases. The photogram of this alloy, Fig. 2, shows only the f.c.c. lines of the α-phase. Similarly, alloy No. 8, also Fig. 2, having a composition of 42.2 atomic percent Mg, should contain only the β-phase according to Fig. 1. The photogram of this alloy shows unmistakably the f.c.c. and b.c.c. lines corresponding to both the α- and β-phases. Thus, while there is general agreement with the results of Zemczuznyj, the limited data available from the present work indicate that the

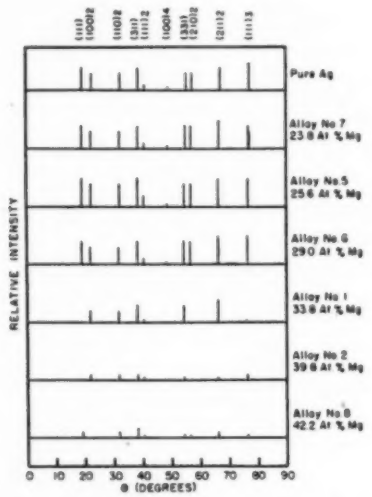

FIG. 7. Relative intensities of diffraction lines obtained from α-phase alloys of silver and magnesium.

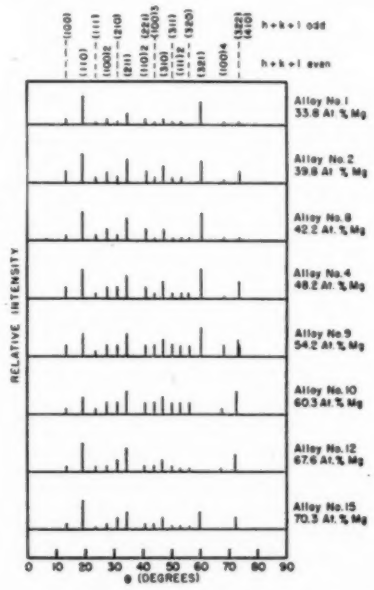

FIG. 8. Relative intensities of diffraction lines obtained from β-phase alloys of silver and magnesium.

[16] George L. Clark, *Applied X-Rays*, International Series in Physics (McGraw-Hill Book Co., Inc., New York and London, 1940).

[17] A. H. Compton and S. K. Allison, *X-Rays in Theory and Experiment* (D. Van Nostrand Company, New York, 1935).

[18] Charles S. Barrett, *Structure of Metals, Mettallurgy, and Metallurgical Engineering Series* (McGraw-Hill Book Company, Inc., New York and London, 1943), p. 127.

boundaries of the two-phase region between the α- and β-phases are not straight lines of constant composition as shown in Fig. 1 but are slightly displaced toward the Mg-rich end of the diagram.

B. Lattice Parameters

The lattice parameter $a_{0\alpha}$ varies with composition as shown in Fig. 5. The distribution of the alloy compositions studied does not permit the drawing of a complete curve for the entire phase; however, it is obvious that only a curve exhibiting a negative deviation from the linear relationship required by Vegard's law will fit the points obtained. This result is at variance with the work of Ageew and Kuznezow[8] who found that the lattice parameter increases linearly with increasing Mg content.

Within the precision of measurement, alloys of the β-phase show a linear variation of the lattice parameter $a_{0\beta}$ with change in composition. Rather wide discrepancies appear among alloys 1, 2, and 8 containing both the α- and β-solid solutions, all of which should have the same value of $a_{0\beta}$. In Fig. 6 the value chosen for $a_{0\beta}$ in the two-phase region is the arithmetic mean of the values for the three alloys. The resulting phase-boundary discontinuity, indicated by the dashed line, lies well to the Mg-rich side of alloy No. 8 as previously mentioned.

The indistinctness of the diffraction lines on photograms containing the γ-phase rendered impractical any attempt to observe lattice parameter variations in alloys 13, 14, 16, and 17. The lattice parameters of pure Mg were found to be $a_0=3.202$A and $c_0=5.199$A, in agreement with accepted values.

C. Superstructure

Photograms of alloys containing the α-phase show no evidence of superstructure. Figure 7 shows the relative intensities of all the diffraction lines observed on the photograms of each of the α-phase alloys. It will be noted that all of the lines correspond to reflections from planes which have either all odd or all even Miller indices; i.e., the (111), (100)2, (110)2, (311), (111)2, (100)4, (331), (210)2, (211)2, and (111)3 planes.

Photograms of the β-phase alloys, on the other hand, contain unmistakable evidence of superstructure lines. In Fig. 8 it will be noted that not only are lines corresponding to even values of the sum $h+k+l$ present, but relatively strong lines corresponding to odd values are also present. If the distribution of Ag and Mg atoms in the b.c.c. lattice were random, lines corresponding to the (100), (111), (210), (221), (311), (320), (322), and (410) planes would not appear on the photograms. Hence it is quite evident that the Ag and Mg atoms take up preferred positions in the β-solid solution to form an ordered structure. Comparison of superstructure lines corresponding to the various β-phase alloys reveals that they are strongest near the middle of the β-phase, indicating that the segregation of the Ag and Mg atoms into cube centers and cube corners is most nearly complete when equal numbers of each atom are available; i.e., in the region of 50 atomic percent Mg.

Erratum: The Torsion of a Rubber Cylinder

[J. App. Phys. **18**, 444 (1947)]

R. S. Rivlin
National Bureau of Standards, Washington, D. C.

Equations (4) should read

$$\Theta=2\psi r\left(\frac{\partial W}{\partial I_1}+\frac{\partial W}{\partial I_2}\right)$$

and $$Z=-2\psi^2a^2\left(\frac{\partial W}{\partial I_2}\right)_{r=a}+2\psi^2\int_a^r r\left\{\left(\frac{\partial W}{\partial I_1}-2\frac{\partial W}{\partial I_2}\right)-2\left[\frac{\partial^2 W}{\partial I_1^2}+(3+\psi^2r^2)\left(\frac{\partial^2 W}{\partial I_1\partial I_2}\right)\right.\right.$$
$$\left.\left.+(2+\psi^2r^2)\frac{\partial^2 W}{\partial I_2^2}\right]\right\}dr+2\left[\frac{\partial W}{\partial I_1}-\left(\frac{\partial W}{\partial I_1}\right)_{r=a}\right]+4\left[\frac{\partial W}{\partial I_2}-\left(\frac{\partial W}{\partial I_2}\right)_{r=a}\right].$$

Preliminary Analysis of Microwave Transmission Data Obtained on the San Diego Coast Under Conditions of a Surface Duct

C. L. Pekeris* and M. E. Davis**

(Received May 6, 1947)

The transmission data for 63 Mc and 170 Mc obtained by the U.S.N.E.L. on the San Diego coast on April 4, 1945, when a strong duct was formed near the ground, were analyzed by wave theory. The average observed M-curve was fitted with a linear-exponential term, and the electromagnetic field beyond the horizon was computed by the theory of normal modes. Good agreement between theory and experiment was obtained for both frequencies at a range of 32 miles (see Figs. 7 and 8). In the ranges between 32 and about 70 miles the observed variation of intensity with height agrees with theory, but the theoretical horizontal decrement is less than the observed by about 0.1 d.b./n. mile for 63 Mc, and by about 0.2 d.b./n. mile for 170 Mc. Beyond about 80 miles the observed field tends to assume a uniform distribution with height and shows little horizontal attenuation. Such an effect had been observed by the U.S.N.R.L. expedition to Antigua for 9-cm waves under conditions of an oceanic surface duct. Its interpretation is still wanting.

1. INTRODUCTION

IN this paper is given a preliminary analysis of transmission data for 63 Mc and 170 Mc obtained by the U.S.N.E.L. along the San Diego coast under atmospheric refraction conditions which produce a so-called surface duct. The set-

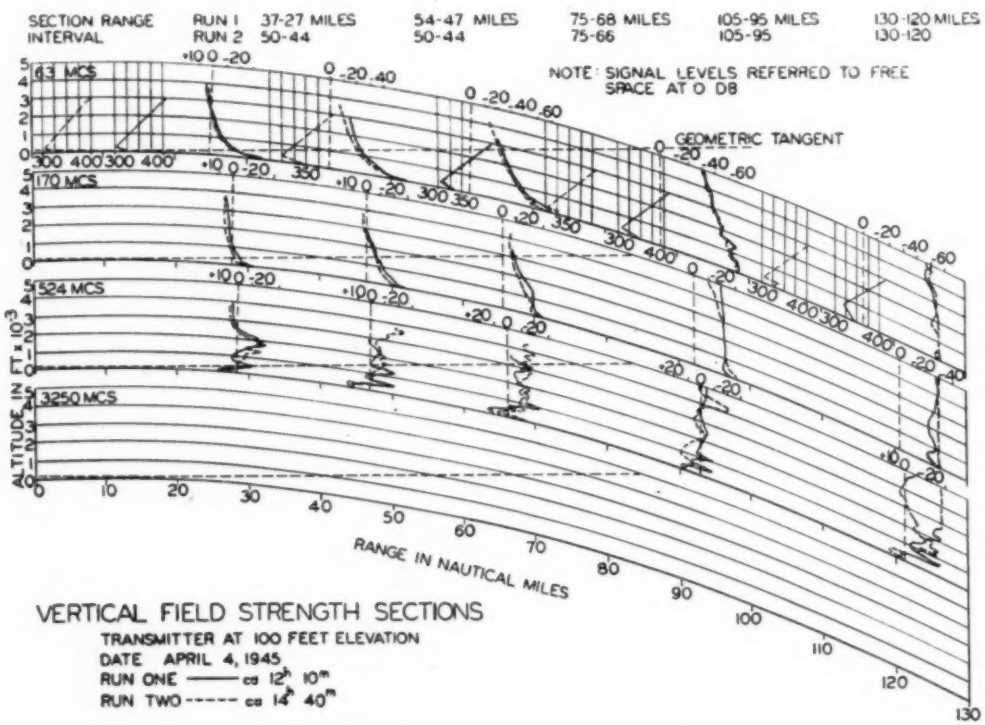

Note: Run 2 should read 37–27 instead of 50–44.

FIG. 1.

* Columbia University Mathematical Physics Group, on leave of absence from Massachusetts Institute of Technology. This paper is based on work done for the Naval Research Laboratory under contract N6ori-110, task order #3 with the Navy's Office of Research and Inventions. Publication assisted by the Ernest Kempton Adams Fund for Physical Research of Columbia University.

** U. S. Navy Electronics Laboratory, San Diego, California.

up of the experiment and the observed M-curves, as well as the measured cross sections of field intensity at various ranges from the transmitter are shown in Fig. 1. The average observed M-values based on 12 soundings are shown by curve A in Fig. 2. Of the 12 soundings, the two taken at the maximum range of 115 miles deviate markedly from the others; another of the soundings taken about 2 hours before the experiment at a range of 10 miles also appears anomalous. This may be caused by both spacial and temporal variation of the M-curves. Leaving out these three soundings one obtains an average M-curve shown by curve B of Fig. 2.

Taking the M-curve B as characteristic of the average atmospheric refraction condition over the relevant portion of the transmission path, we attempt to represent it by a linear-exponential term. Various such representations are shown in Fig. 3, with curve E appearing to give the best fit. This theoretical curve has a surface value for $(M-M_0)$ of 72.3, which is probably considerably in excess of the actual value. However, as has been pointed out by Professor Hartree, transmission is not seriously affected by the detailed distribution of M near the surface because of the vanishing of the field intensity at the surface.

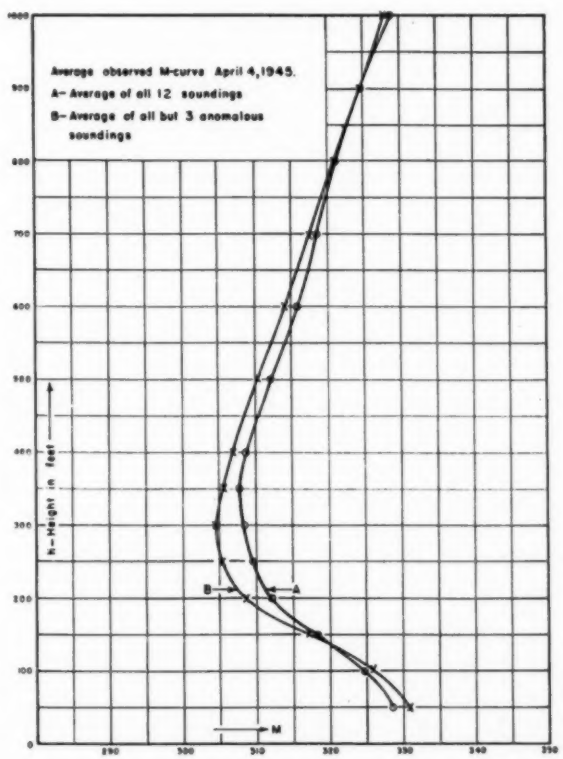

FIG. 2.

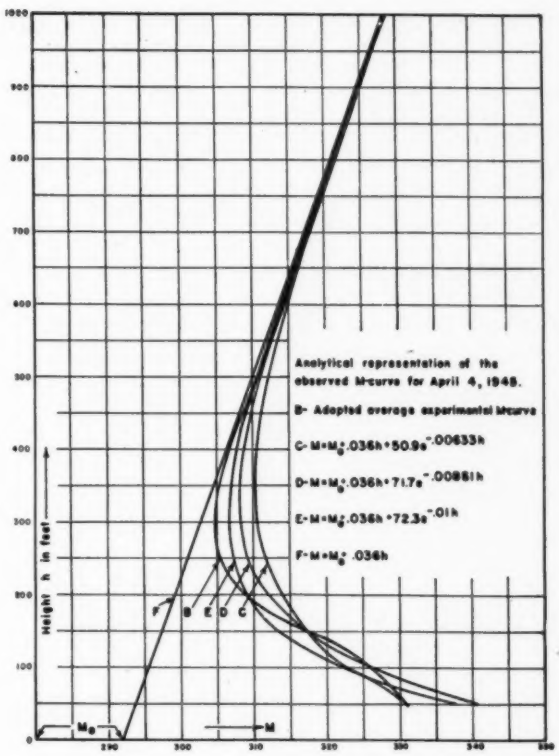

FIG. 3.

The surface duct under discussion, as represented by curve E

$$M = M_0 + 0.036h + 72.3e^{-0.01h}, \qquad (1)$$

with its surface M, excess of 72.3, and duct height of 300 feet is to be contrasted with curve C' of the Antigua oceanic surface duct previously analyzed,[1]

$$M = M_0 + 0.036h + 12.06e^{-0.0714h}, \qquad (2)$$

where the surface M, excess, and duct height had values of only 12.06 and 45 feet, respectively. It is therefore of interest to test how wave theory can predict the electromagnetic field under such vastly different conditions. It turns out that when expressed in natural units, curve E for 170 Mc (176 cm) is close to curve C' for 9 cm, that is, the San Diego duct had about the same trapping power for 176 cm waves as the Antigua duct[2] had for 9 cm waves.

[1] C. L. Pekeris, Proc. I.R.E. **35**, 435 (1947).
[2] M. Katzin, R. W. Bauchman, and W. Binnian, Proc. I.R.E. **35**, 891 (1947).

TABLE I. Data for 63 Mc, $\lambda=476$ cm, $H=442$ feet, $L=25.8$ n. miles. Curves C, D, and E are shown in Fig. 3.

Curve	α	λ	D_1	Theor. decrement d.b./n. mile	Obs. decrement d.b./n. mile	Obs. decrement range miles
C	3.21	2.80	$-1.03+1.82i$	0.61	0.79	32–71
D	4.52	3.80	$-1.02+1.88i$	0.63	0.73	32–100
E	4.56	4.42	$-0.99+1.98i$	0.67	0.66	71–100

TABLE II. Data for 170 Mc, $\lambda=176$ cm, $H=228$ feet, $L=18.5$ n. miles.

Curve	α	λ	D_1	Theor. decrement d.b./n. mile	Obs. decrement d.b./n. mile	Obs. decrement range miles
C	6.23	1.44	$-1.84+0.69i$	0.32	0.61	32–71
D	8.77	1.96	$-1.48+0.72i$	0.34	0.41	32–100
E	8.84	2.28	$-1.22+0.94i$	0.44	0.17	71–100

2. ANALYSIS OF THE FIELD BY THE THEORY OF NORMAL MODES

According to the theory of normal modes, the field FS relative to free space due to a dipole radiating in a horizontally stratified atmosphere is given by[1]

$$FS=20\log_{10}\left[2(\pi x)^{\frac{1}{2}}\left|\sum_{m=1}^{\infty}e^{-A_m x+iB_m x}U_m(z_1)\,U_m(z_2)\right|\right]\text{d.b.} \quad (3)$$

Here x denotes horizontal distance from transmitter expressed in natural units L, z_1, and z_2 the heights of transmitter and receiver above ground expressed in natural units H, where

$$L=3.304\lambda^{\frac{1}{3}}\text{ n. miles},\quad H=7.243\lambda^{\frac{1}{3}}\text{ feet}, \quad (4)$$

and λ is the wave-length in centimeters. The height-gain functions $U_m(z)$ and the characteristic constants A_m and B_m can be computed by known methods[2] for the case of the linear-exponential M-curve given in Eq. (1). These depend on the values of the parameters a and c in the expression

$$M=M_0+0.036h+ae^{-ch}. \quad (5)$$

Again, it is convenient to use instead of a and c the natural parameters

$$\alpha=3.85a\lambda^{-\frac{1}{3}},\quad \lambda^{***}=Hc, \quad (6)$$

whereby the exponential term in (5) is transformed into $\alpha e^{-\lambda z}$.

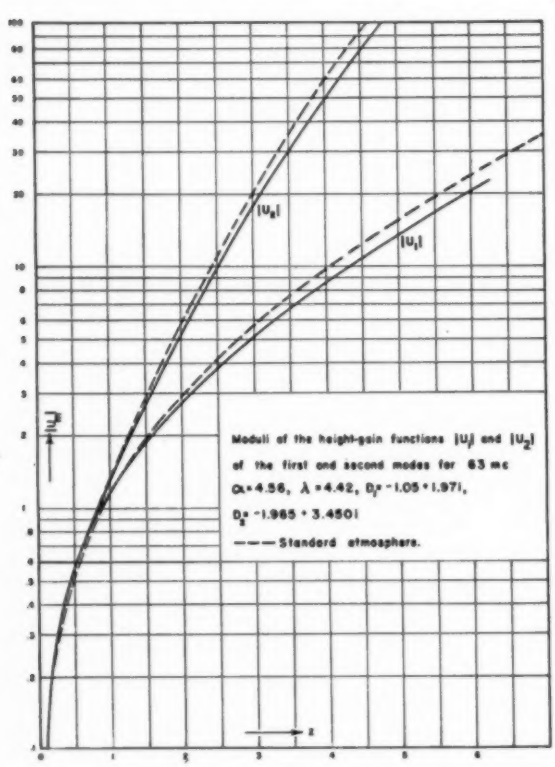

FIG. 4.

Tables I and II show the results of the analysis for the 63 Mc and 170 Mc, respectively. The characteristic values $D_1=B_1+iA_1$ of the first mode were obtained by interpolation from the values given in reference (3).[3] In the case of curve E and 63 Mc the value of D_1 shown in Table I required extrapolation beyond the maximum value of 4 for λ treated in reference (3). As a check, D_1 was recomputed by the perturbation method and a value of $-1.05+1.97i$ was obtained. This method also yielded a convergent value for $U_1(0)$ of $-0.043+1.17i$. With these constants the differential equation for the height-gain function of the first mode $U_1(z)$

$$\frac{d^2U(z)}{dz^2}+Q(z)\,U(z)=0,\quad Q(z)=z+D+\alpha e^{-\lambda z} \quad (7)$$

was integrated using an interval $\Delta z=0.1$ and the

*** Not to be confused with the λ in (4) which denotes wave-length.

[3] See a forthcoming paper by C. L. Pekeris and W. S. Ament. To be published in Phil. Mag.

recursion formula

$$\left[1+\frac{(\Delta z)^2 Q_1}{12}\right]U_1=2U_0-U_{-1}$$
$$-\frac{(\Delta z)^2}{12}(10U_0Q_0+U_{-1}Q_{-1}), \quad (8)$$

which is correct to within $[(\Delta z)^2/240]\delta^4(QU)$, where δ^4 denotes the fourth difference. The perturbation method also gives for the second mode $D_2=-1.965+3.450i$, $\dot{U}_2(0)=0.041+1.084i$, and these were used to obtain $U_2(z)$ by (7) and (8). The results for the first two modes are shown in Figs. 4 and 5. Clearly, for 63 Mc the trapping of the modes is small, so that for the application in view it would have been sufficient to use the solutions for a standard atmosphere.

In the case of 170 Mc and curve E, values of $D_1=-1.22+0.94i$ and $\dot{U}_1(0)=1.14+1.04i$ were obtained by interpolation from the "method II" values tabulated in reference (3). With these, the height-gain function $U_1(z)$ was integrated using (7) and (8), and the result is shown in Fig. 6. Here the trapping is considerable, the theoretical

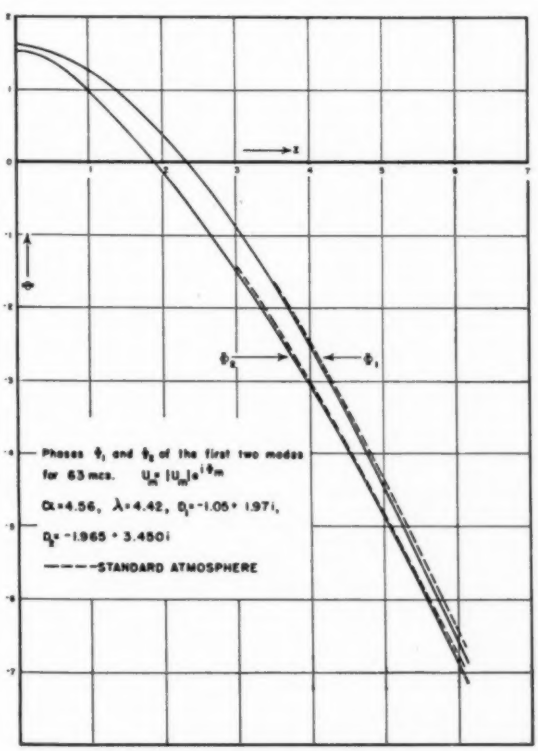
Phases ϕ_1 and ϕ_2 of the first two modes for 63 mcs. $U_m=|U_m|e^{i\phi_m}$
α=4.56, λ=4.42, D_1=-1.05+1.97i,
D_2=-1.965+3.450i
----STANDARD ATMOSPHERE

FIG. 5.

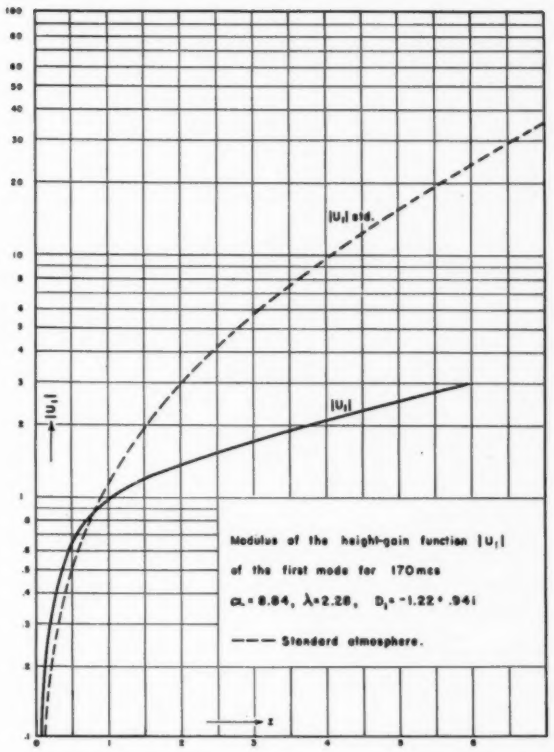
$|U_1|$ std.
$|U_1|$
Modulus of the height-gain function $|U_1|$ of the first mode for 170 mcs
α=8.84, λ=2.28, D_1=-1.22+.94i
---- Standard atmosphere.

FIG. 6.

decrement being less than half the standard value. From the perturbation method one obtains the approximate values $D_2=-2.01+3.12i$, $\dot{U}_2(0)=-0.36+1.05i$.

3. DISCUSSION OF RESULTS

Figure 7 shows a comparison of observed field intensities relative to free space with theoretical. The first two modes were used in the calculations, and where the second mode contributed more than 50 percent to the total field the theoretical curves were terminated. The observed increase of intensity with height, as well as the detailed distribution of intensity with height, shows satisfactory agreement with theory out to a range of 71 miles, but the observed decrement is greater than the theoretical (which is close to the standard value) by about 0.1 d.b./n. mile. In the case of 170 Mc shown in Fig. 8 there is again good agreement at a range of 32 n. miles, and satisfactory agreement in the variation of intensity with height out to 49 n. miles. The observed

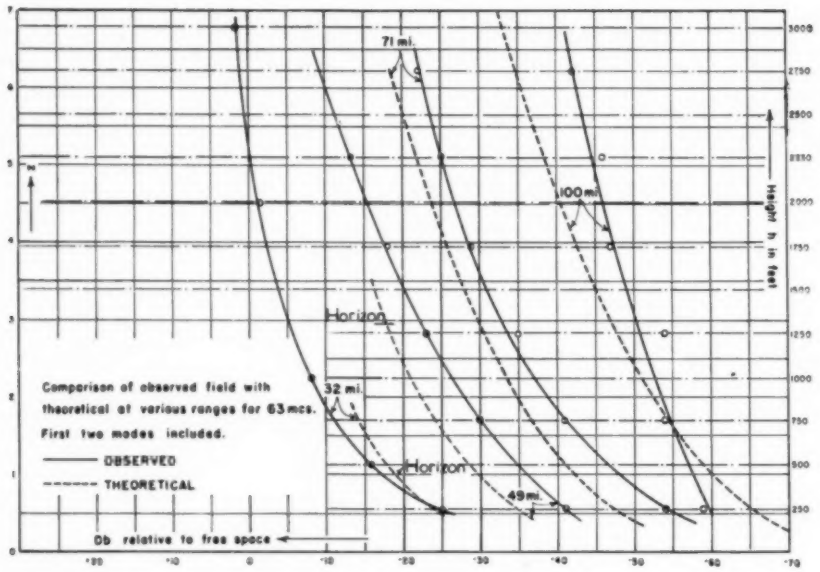

FIG. 7.

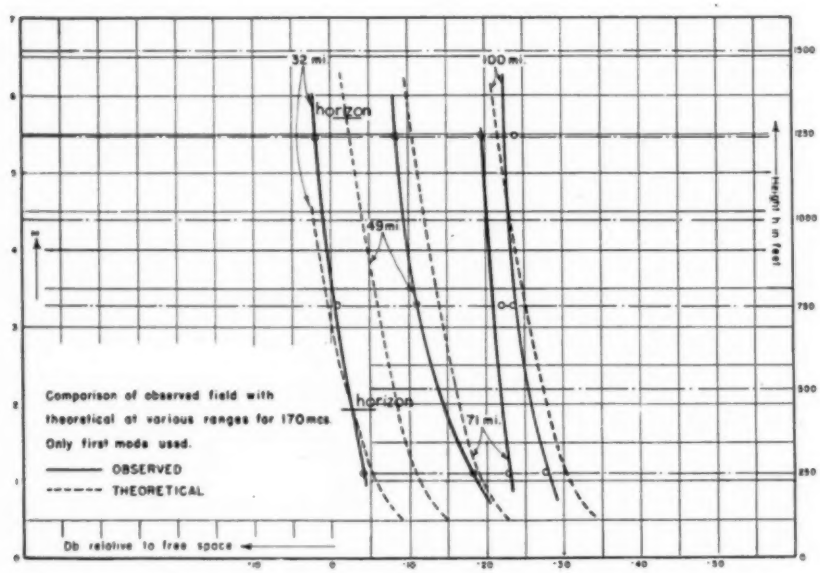

FIG. 8.

decrement, however, while only 0.7 of standard, exceeds the theoretical value by about 0.3 d.b./n. mile at this range.

It is possible that a weaker surface duct than the one adopted in this preliminary analysis would bring the theoretical decrements to closer agreement with observation, while not materially affecting the shape of the height-gain curve. Part of the excessive observed attenuation no doubt originates from scattering by inhomogeneities in the atmosphere. However, the tendency of the observed field to assume a uniform distribution with height, with little horizontal attenuation beyond about 70 miles, is probably an effect which cannot be accounted for by the present formulation of the normal mode theory.

Letters to the Editor

Modified Cavity Oscillator for the Generation of Microwaves

GEORGE G. BRUCK
Specialties, Inc., Syosset, New York
March 13, 1947

THE cavity consists of two co-axial cylinders and two end-plates. N longitudinal slots in the wall of the inner cylinder are used to create the proper type of field. This layout resembles the well-known "turbator." A qualitative picture of the field can be given easily although an exact calculation is rather laborious. Figure 1 shows a probable aspect related to the π-mode of the magnetron. Figure 2 is a probable configuration similar to the TE_{01} mode of a cylindrical guide.

Electrons may be made to describe circular orbits in the region between the two cylinders by applying a positive potential to the inner one. As in the orbital beam tube (RCA) there is no need for a magnetic field. Because of progressive sorting, N-electron clouds are formed. This is explained in the following way: the fringing field near the slots has an electric component in the direction of the flight-path of the electrons. This component of the field accelerates or decelerates the electrons. The accelerated ones, which absorb energy from the field, fly outward, while the decelerated ones, which give up energy to the field, approach the inner cylinder because of loss in velocity. At the following slot the unfavorable electrons, the faster ones, pass through a weaker fringing field than the favorable ones. They extract less energy from the field than the favorable ones are adding to it. The effect obtained is quite pronounced because the intensity of the fringing field declines exponentially with the distance from the slot. The in-phase electrons spiral inward. The out-of-phase electrons spiral outward. There exists an added tendency of proper phasing because of the difference in path length for the fast and slow electrons. The angular displacement required to give proper phasing can be progressively approached by the faster electrons because of the increasing radius of their orbit.

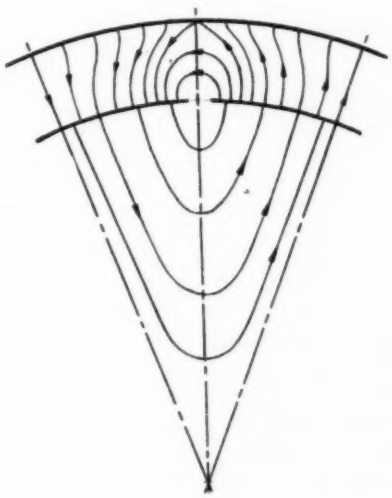

FIG. 1. Probable electric field π-mode.

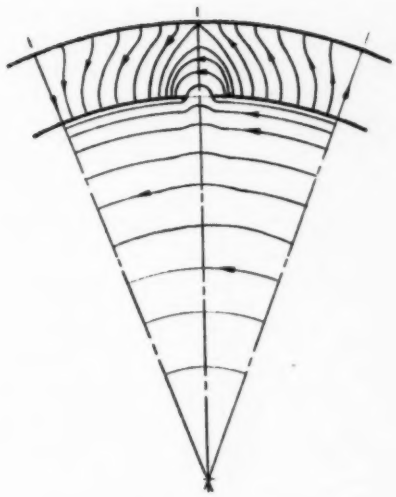

FIG. 2. Probable electric field corresponding to TE_{01} mode.

The cathode and accelerating grid are both parallel to the cylinder axis. Their location is such as to create minimum interference with the orbits of the electron. There are no slots provided in their immediate neighborhood (Fig. 3). The voltage on the accelerating grid is related to the potential between the inner and outer cylinders in order to produce initially circular orbits.

Microwave power is extracted from the inner cavity by any approved method probe, loop, or window.

For modes of the TE_{01} type, the cavity may be split along a plane, perpendicular to the axis. This permits the insertion of a dielectric vacuum-tight window and location of the electron stream in the sealed and evacuated part. The output iris and simple means for frequency adjustment are located in the non-evacuated section.

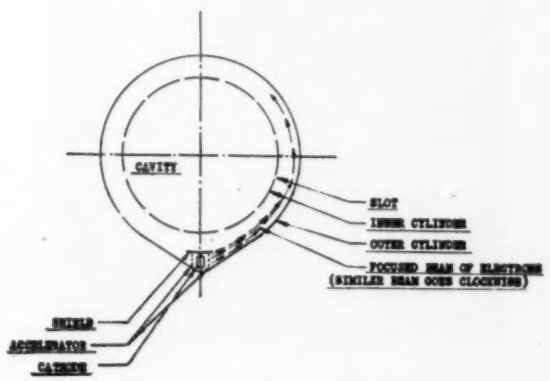

FIG. 3. Potential distribution: cathode, shield, outer cylinder . . . negative; accelerator, inner cylinder . . . positive.

No evaluation of the specific properties of this tube has as yet been made. It is anticipated that high output at higher frequencies will be obtainable, particularly above 30 kmc. It is further believed that this type of oscillator may be made to work at frequencies exceeding 100 kmc.

Particle "Growth" in the Electron Microscope

V. E. Cosslett*
Cavendish Laboratory, Cambridge, England
June 9, 1947

IT has recently been observed by Watson[1] that carbon black particles appear to increase in size when used as objects in an electron microscope. He rightly stresses the importance of this disturbing effect in particle-size determinations, and calls for an exchange of experience in order to clear it up.

We observed a similar effect some months since with the smallest zinc-oxide crystals obtainable by burning zinc in air in a coal-gas flame (see Fig. 1); they were being used as test specimens in investigating the performance of a Siemens electron microscope. We have now obtained similar results with zinc, molybdenum, and magnesium oxides in the RCA Type-B microscope. Figure 2 shows a typical series of photographs from zinc oxide supported on an RCA nickel grid. Plates (a), (c), and (e) were taken at intervals of 2 minutes after bringing the needles into the field of view, in critical illumination, i.e., with the source imaged on the specimen, which was thus exposed to maximum energy flux. Plate (b) is of a field lying within 10 microns of that first examined, and plate (d) is of a field lying on the opposite side of the grid hole containing these two fields, i.e., about 75 microns from them and outside the focused image of the source. It is clear that the effect is confined to the region covered by the latter, and its very immediate neighborhood.

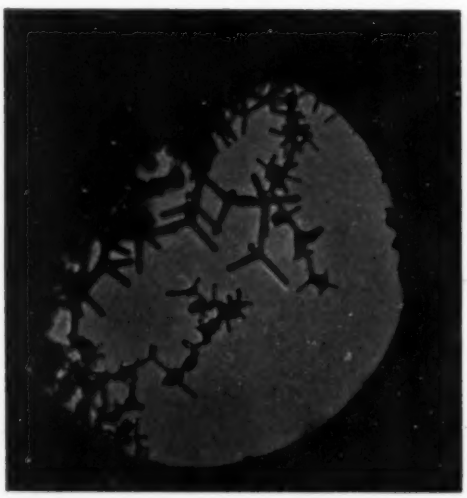

FIG. 1. Zinc-oxide smoke particles (20,000×) after *ca.* 3-minutes exposure to electron beam in Siemens electron microscope (on nickel grid).

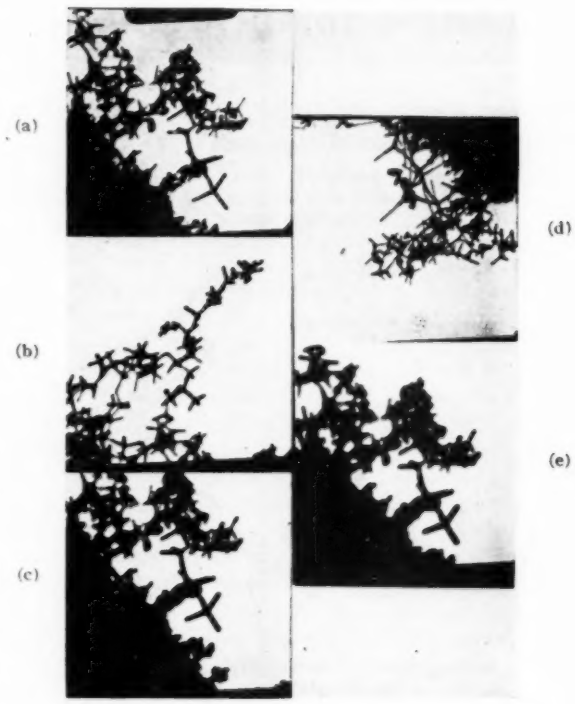

FIG. 2. Zinc-oxide smoke particles in RCA Type-B electron microscope 12,000× (on nickel grid).
a. After *ca.* 2 minutes in beam.
b. Adjacent field to (a) (within 10μ), after *ca.* 3 minutes in beam.
c. Field (a) after a further 2 minutes in beam.
d. Field *ca.* 75μ distant from field (a).
e. Field (a) after a further 2 minutes in beam.

Observation of crystals supported on long chains of their like from the opposite side of a grid hole, or by adventitious, loosely-adhering material on the near side, shows that such growth does not occur when there is a poorly conducting path between specimen and grid. Watson found little effect on particles supported in the center of a grid space on a collodion film, but considerable effect after shadowing with chromium. We find little effect at all in such supported specimens, wherever they be with respect to the grid, and no enhancing influence of a thick gold deposit (*ca.* 100 atomic layers). This is of importance for the estimation of the size of virus and 'phage particles, which cannot be observed otherwise than on a supporting film. We have not been able to find any increase in size of gold-shadowed turnip virus particles, nor of the flagella of bacteria, after exposures in the beam up to 10 minutes.

In contradistinction to Watson, who suggests that the growth arises from the deposition of organic material from the vapor state in the form of ion clusters, we incline to the view that the effect is due to ejection of adsorbed matter, and perhaps of metal itself, from the grid wires under electron bombardment. The local temperature, since the beam image is of the order of 10 microns only in diameter, will be very high and may well reach 1000°C; in the Siemens microscope it is possible to fuse the nickel

grid if the filament is a little over-run. Prior cleaning of the grids with organic solvents, and heating in the electron beam in vacuum before depositing the specimen, bring about a small improvement only, making it very doubtful that organic impurities on the grid are responsible. The fact that magnesium oxide, a highly refractory material, shows more rapid growth than either zinc or molybdenum oxides, suggests that it cannot be due to recrystallization or the growth of some crystals at the expense of others; in any case a diminution in size is never observed.[2] We have used copper and platinum-gold object holders, as well as nickel, and find the growth slightly less rapid on the platinum-gold and slightly more so on the copper disks. This gradation is in the order of the melting points of these metals, but it is not necessarily the case that this is the same as that of ease of sputtering. As a working hypothesis, however, we put forward the view that the observed increase in size of particles in good electrical contact with the grid arises from the deposition of charged metal and other particles ejected from the supporting holder by the electron beam. If it were from organic vapors, it should be observable in gold-shadowed viruses and similar specimens. In Watson's case it may be that contamination comes also from the carbon black itself under electron bombardment, and hence affects gold-shadowed specimens.

* I. C. I. Research Fellow.
[1] Watson, J. App. Phys. **18**, 153 (1947).
[2] The original plates of Figs. 1 and 2 show the accretions of material to be of lower opacity to electrons than the zinc-oxide needles; this may, however, arise from loose agglomeration rather than from a smaller physical density.

Ultrasonic Modulation of a Light Beam*

R. F. Humphreys, W. W. Watson, and D. L. Woernley**
Sloane Laboratory, Yale University, New Haven, Connecticut
June 23, 1947

THE use of a light beam as a carrier of intelligence has the obvious military advantage of high collimation, hence a low probability of detection by an enemy not in the direct line of the beam. If the wave-length of the light is outside the visible region, the chance of direct line-of-view detection by an enemy is still further reduced. However, there are three major limitations to the use of such a communication device: (a) attenuation of the carrier light beam by atmospheric absorption, (b) attenuation by the infra-red (or ultraviolet) filter, and (c) the difficulty in obtaining a satisfactory signal-to-noise ratio. Evidently, these limitations are somewhat interdependent. If, furthermore, it is desired that the equipment be portable, the limitation of power and space must be considered. This note is concerned with the performance of an experimental infra-red communication unit designed for the Army Signal Corps.

The most direct method of light modulation involves varying the intensity of the source of light in accord with the signal frequency. The very appreciable thermal inertia of light sources, however, permits only a relatively small signal-to-noise ratio. That an ultrasonic grating, formed by a traveling sound wave in a liquid medium, will serve as an almost inertia-less modulator has been pointed out by Jeffree[1] and Becker,[2] and the method has been employed successfully in the Scophony Television system.[1]

A beam of parallel light falls on a glass cell (Fig. 1) at the bottom of which is a 7-megacycle quartz crystal. The cell is filled with xylol and capped with a plug of glass wool to prevent the formation of standing sound waves. (The cell performs equally well as a modulator with either traveling or standing waves; however, it is not desirable to have a mixture of the two.) The waves traveling up the cell form moving regions of increased and decreased density, hence, are similar to a moving diffraction grating. The diffraction pattern which results when light is directed normally to the sound waves has an order spacing proportional to the wave-length of the crystal excitation (approximately 0.4° for the frequency used). The distribution of light intensity in the various orders depends on the amount of crystal excitation; the light in the zero order is nearly inversely proportional to the excitation of the crystal.[3] Thus, an ultrasonic grating corresponds somewhat to an optical grating whose groove shapes are variable at will. If the crystal excitation is modulated by a signal, the light received in the zero order will have the same modulation. It should be noted that orders higher than zero are likewise modulated, though 180° out of phase with the undeviated light; the advantage gained by using the zero order lies in its greater intensity.

The light source found most satisfactory was a 6-volt

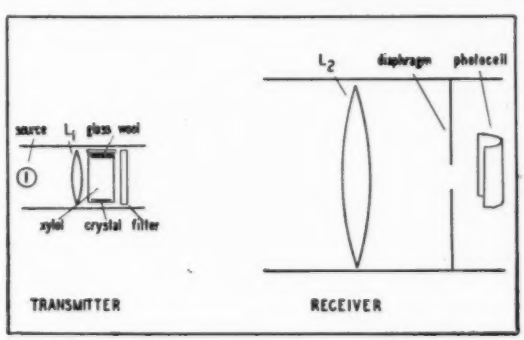

FIG. 1. Schematic diagram of the transmitter-receiver unit for modulating an infra-red light beam.

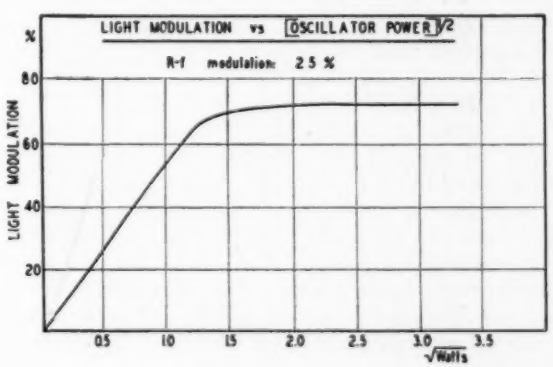

FIG. 2. Light modulation of the zero-order diffraction image as a function of sound intensity (assumed proportional to the voltage on the crystal).

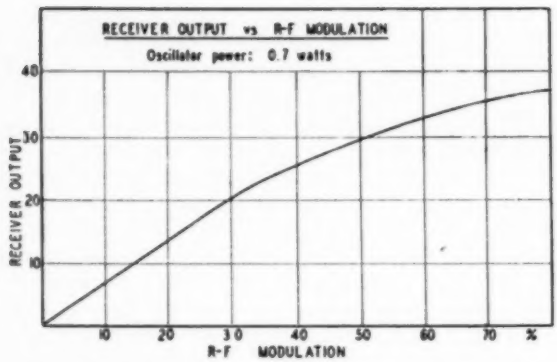

FIG. 3. The curve of audio-signal output as a function of percentage r-f modulation indicates the approximate linearity of the ultrasonic modulator. At 70 percent modulation the deviation is only 2 db.

Mazda ribbon lamp, operated at 8 volts; at this latter voltage the infra-red energy was doubled, while the life of the lamp was not seriously shortened. An achromatic lens (L_1), of 60-mm diameter, formed parallel light which completely filled the cell. The infra-red filter (Corning "Heat Resistant") was made removable to allow daytime signaling. The collection lens (L_2) at the receiver should be as large as conveniently possible to obtain the maximum signal-to-noise ratio. An eight-inch diameter lens was used in the present work with a quarter-inch diaphragm placed at its principle focus, slightly in front of the photocell. A rifle telescope (magnification 4×) was mounted on the unit to aid initial contact between the two communicators.

A 7-megacycle x-cut quartz crystal rested on the stainless-steel base of the liquid cell; on the crystal's upper surface was evaporated copper and then a layer of gold. Contact with this electrode was made with a spring-bronze fork, soldered to the gold surface with Wood's metal to eliminate contact sparking. The crystal was driven at its fundamental frequency by a conventional electron-coupled oscillator with one stage of amplification; a 6V6GT tube served to plate-modulate the amplifier stage. The receiver contained an RCA 918 photo-cell with three 6Sj7 stages of audio-amplification; earphones were used in the output circuit. For the portable unit a 6-volt vibrator pack supplied the necessary power; the vibrator, transmitter, receiver, and optical system were contained in a single, well-shielded unit. The total power consumption was approximately 40 watts. The r-f power delivered to the crystal was of the order of one watt.

The linearity of the ultrasonic cell as a modulator is indicated in Fig. 2, where the sound intensity is taken to be proportional to the square root of the oscillator power. The degree of r-f modulation is held constant (25 percent). It is seen that from zero to 70 percent the modulation is reasonably linear. A curve of r-f modulation (constant r-f power) *versus* receiver output confirms this relation (Fig. 3). The shape of the curve conforms with that predicted by the theory of Raman and Nath.[4]

The most severe operating conditions occur, of course, in bright sunlight, where the signal-to-noise ratio is low. With the red filter removed, the limiting distance for satisfactory two-way conversation was found to be about 3000 yards. Night communication using the filter was very clear at 3000 yards and was still possible at 5000 yards. Beyond this the background noise became prohibitive. If the restriction of low power consumption is removed, a more intense source of light and a larger modulating crystal should easily double this maximum range.

* This paper is based on work done for the Signal Corps Engineering Laboratories under Contract W-1077-SC-1077 in 1942.
** Present address: Cornell Aeronautical Laboratory, Buffalo, New York.
[1] J. H. Jeffree, Television (London) **9**, 260 (1936).
[2] H. E. R. Becker, Zeits. Hochfrequenztech. **48**, 89 (1936).
[3] H. E. R. Becker, Ann. Physik (Leipzig) **25**, 373 (1936).
[4] C. V. Raman and N. S. N. Nath, Proc. Ind. Acad. Sci. **2**, 406, 413 (1935).

Films, Resistant to Organic Solvents, for Use in the Electron Microscope

S. G. ELLIS
Department of Physics, University of Toronto, Canada
June 28, 1947

FILMS of Alkathene,* insoluble in ether and suitable for specimen supports in the electron microscope have been made from hot xylene solutions of the plastic.

A suitable strength for the solution is 0.2 g of Alkathene grade 2 in 100 cc of xylene. It is convenient to use the solution in such a quantity (75 cc) that, when placed in a bottle with a wide neck, a clean glass microscope slide can be half-immersed in the bottle, and a ground glass stopper inserted. The bottle is heated in a water bath at 100°C until the solution is clear. The bottle may then be removed from the bath, the slide lifted from the solution and held vertically just above its surface for a few seconds and then removed from the bottle. The film of Alkathene left on the slide is suitably cut with a needle and then floated off on the clean surface of some hot distilled water at a

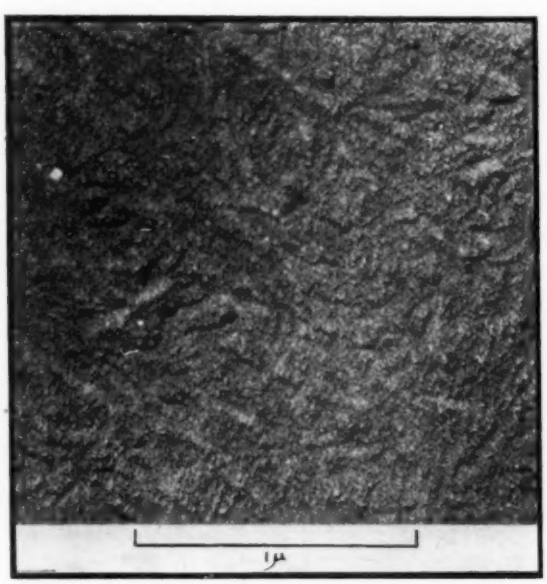

FIG. 1. Alkathene film shadow cast with chromium

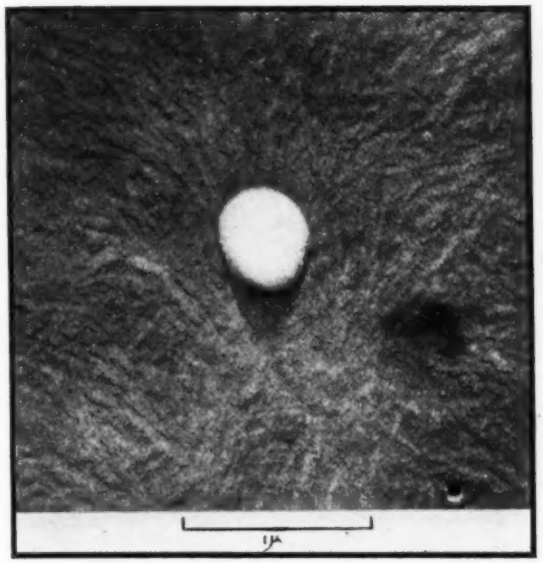

FIG. 2. Unidentified particle on Alkathene film shadow cast with chromium.

temperature above 50°C. A mesh can then be placed on the film and mesh lifted from the water and allowed to dry in the usual manner. When another microscope slide has been placed in the Alkathene solution it should be allowed to come to the temperature of the solution before being removed.

These Alkathene films, when examined in the electron microscope, show a characteristic structure (see Fig. 1). There are many applications in which the structure will not interfere with the observations since adequate contrast can be obtained in the micrographs (Fig. 2). The strength of these films, for a given transparency to the electron beam, is comparable with that of Formvar films. The films, when mounted on a mesh, have been flooded with either suspensions, both of soaps and carbons, without any apparent solvent action on the Alkathene.

In the studies made to date it has not been possible to prevent the formation of the characteristic structure in these films either by varying the strength of the xylene solution or by changing the conditions under which the xylene evaporates. Attempts to form a film by rapidly dipping and withdrawing a cold microscope slide into the hot xylene solution failed.

Similarly attempts to cast the films on the surface of hot water failed, since with the solvents used the solutions of the plastic spread in an irregular and unsatisfactory manner.

We are indebted to Mr. F. G. Rice of Canadian Industries Limited, for samples of Alkathene and for information on its use.

* "Alkathene" (registered trademark of I.C.I. in Canada and most of the important countries in the world) is a straight low polymer of ethylene formed at high pressure. Its properties are described in a series of papers by E. Hunter and W. G. Oakes, R. B. Richards and E. L. Midwinter, in British Plastics for March, April, and May, 1945. It is available from: Plastics Division, Canadian Industries, Ltd., P. O. Box 10, Montreal, Canada, for delivery in Canada only, and Plastics Division, Imperial Chemical Industries, Ltd., Welwyn Garden City, Hertfordshire, England.

Note on the Reduction of Microphonics in Triodes[1]

VICTOR W. COHEN AND ABRAHAM BLOOM
Ordnance Development Division, National Bureau of Standards, Washington 25, D. C.
June 2, 1947

UNDER the above title, Mr. Waynick has considered the behavior of a simple triode with a vibrating grid and developed, as a consequence of the motion, a relationship between the microphonic output and the grid bias. This relationship indicates that under certain conditions the microphonic response can be appreciably reduced by a suitable choice of grid bias. The application of this effect to high gain amplifiers with fixed bias may be of importance. In the application of the theory however to the 6A3 tube, he has failed to consider two very important factors both of which pertain to this type of tube. These are: (a) The effect of symmetry in a plane symmetrical triode, and (b) the importance of motion of the cathode in filamentary tube types.

Consider an idealized symmetrical plane triode with the cathode in the center and two grid planes attached to a pair of side rods so that they vibrate with their separation fixed. Then as the grid-cathode distance *increases* on one side, it will *decrease* on the other. To a first-order approximation, therefore, the vibration of the grid side rods will result in no change in I_p. For a more accurate evaluation of the microphonic output, one must consider the second-order approximation. We have made such a calculation and find that, depending upon the spacings, there may or may not be a point between negative cut-off and zero grid bias at which the microphonic output is zero. A rough approximation of the second-order term is:

$$I-I_0=\Delta I=G_m\Delta d^2\left[\frac{4}{d^2}\left(E_g+\frac{K}{b}E_p\right)+\frac{(d-2b)}{bd}\,\frac{2}{b^2}KE_p+\tfrac{1}{2}\frac{K^2E_p^2}{b^4}\left(E_g+\frac{K}{b}E_p\right)^{-1}\right],$$

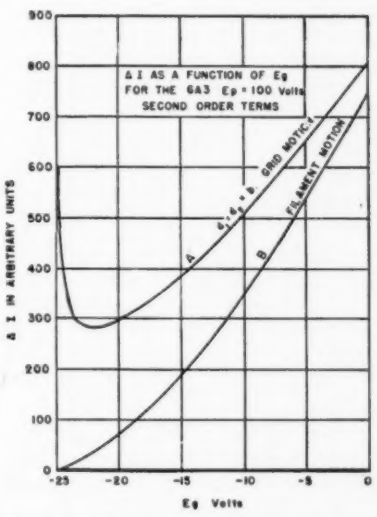

FIG. 1. The second-order term for the change in plate current due to (A) grid motion and (B) filament motion, as a function of grid bias. The curves are calculated for the 6A3, with 100 volts applied to plate.

where $G_m = 3C/2d^3[E_g + (KE_p/b)]^{\frac{1}{2}}$, where d = grid-cathode spacing, b = grid-plate spacing, $C = 2.33 \times 10^{-6} A$ amperes, Δd = grid displacement, and $K = 1/2\pi n \log 1/2\pi np$.

The behavior of this second-order term for ΔI as a function of grid bias is shown in Fig. 1 curve A, where the term $\Delta I d^4/C(\Delta d)^2$ is plotted against E_g, for the special case of the 6A3 in which $d = b$, $u = 4$, $E_p = 100$ v.

This function goes to infinity at cut-off and has a minimum not far from cut-off.

Since in practice the tube is not perfect in its assembly, the symmetry may not be exact. The microphonic output due to grid vibration may, therefore, contain components of both first and second orders. The first-order term will obey a function similar to Waynick's but will have an amplitude dependent upon the degree of asymmetry.

For a single plane triode the first-order term of ΔI as a function of E_g is shown in Fig. 2 curve A, in which $\Delta I d^3/C\Delta d$ is plotted against E_g for the same case as Fig. 1A. If the vibration is harmonic, the first-order term of the output will be a sine wave which will reduce to zero amplitude at a particular bias as shown. The second-order term, however, since it depends upon the square of the grid displacement, will have a wave form of the second harmonic of the vibration frequency since $\sin^2\omega t = \frac{1}{2} - \frac{1}{2}\cos 2\omega t$.

While it is true that for indirectly heated cathodes the important cause of microphonics will be the grid vibration, in filamentary types the resonant vibration of the cathode is very important. We have subjected a 6A3 to vibration tests and find very distinct resonant vibration of the filament legs visible with the naked eye. Each leg had its own resonant frequency, most of these being near 800 cycles. The grid vibration was of smaller amplitude and was not visible in a binocular microscope of 36×, using stroboscopic illumination. It was detectable with a r-f capacity vibration pick-up.

The cathode of each section of the 6A3 is formed from a narrow ribbon, in the shape of a letter M. The plane of the ribbon in each leg is designed to be perpendicular to the idealized cathode plane. One would expect, therefore, that appreciable vibrations would occur only in the cathode plane. However, since in assembly the cathode ribbon may be warped slightly, there may be a component of vibration normal to the cathode plane. A rough calculation of the change in plate current due to filament motion gives to a second-order approximation:

$$I - I_0 = \Delta I = -2\frac{C}{d_1^3}\left(E_g + \frac{K}{b_1}E_p\right)^{\frac{1}{2}} d_1 + \frac{2C}{d_2^3}\left(E_g + \frac{KE_p}{b_2}\right)^{\frac{1}{2}} d_1 + 3\frac{C}{d_1^4}\left(E_g + \frac{K}{b_1}E_p\right)^{\frac{1}{2}} (d_1)^2 + \frac{3C}{d_2^4}\left(E_g + \frac{K}{b_2}E_p\right)^{\frac{1}{2}} (d_2)^2,$$

where the subscripts 1 and 2 refer to opposite sides of the triode.

Clearly all four terms of this expression are $\frac{3}{2}$ power curves and have minima only at cut-off, i.e., where $E_g = -K/bE_p$. The form of the second, and first-order terms are illustrated in Fig. 1 curve B and Fig. 2 curve B, respectively.

With the foregoing considerations in mind, one can explain some of Waynick's observations on the 6A3 which appear to depart from his theory.

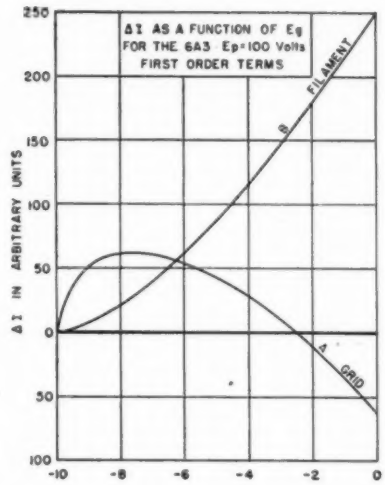

FIG. 2. The first-order term for the change in plate current due to motion of (A) grid and (B) filament as a function of grid bias. The curves are calculated for the 6A3, with 100 volts applied to plate.

1. Case 2 and 8 may be explained as due to resonances either of a filament leg or of the grid in a symmetrical section of the tube.

2. Case 6 was undoubtedly due in part to a second-order term giving rise to a second harmonic of the vibration frequency which did not pass through zero as the fundamental component did.

3. The residual output near the minima which appeared to contain the second harmonic of the driving frequency was probably due to second-order effects.

The apparent close agreement observed in some cases may have been due to a grid vibration in a highly asymmetrical section of the tube.

A more detailed discussion of calculations of the effects of vibration of triode elements as well as experimental methods and observations is contained in a manuscript now nearing completion.[2]

[1] Waynick, J. App. Phys. **18**, 239 (1947).
[2] Paper delivered at Winter Convention of the I.R.E., March 1947.

Comments on "Sound-Velocity Determination of Molecular Weights"

G. J. DIENES
Development Laboratories, Bakelite Corporation, Bound Brook, New Jersey
June 24, 1947

IN a recent paper in this journal, A. Weissler, S. W. Fitzgerald, and I. Resnick[1] described a method of molecular-weight determination for liquid polymers based on sound-velocity, density, and refractive-index measurements. The essential relation for calculating molecular weights by their method is an empirical linear correlation between molar sound velocity and molar refraction.

It occurred to the writer that there is no necessity for making the sound-velocity measurements since the mo-

TABLE I.

Glycol	Theoretical mole wt.	No. ave. mole wt. from specific refractivity	Deviation, %
Ethylene	62.1	62.1	0.0
Diethylene	106.1	101.5	−4.3
Triethylene	150.1	144.8	+3.5
Tetraethylene	194.2	192.9	+0.7
Pentaethylene	238.2	245.7	−3.1
Poly 200	200±10	193.0	0.0
Poly 300	300±15	316.9	+0.6
Poly 400	400±20	408.6	0.0
Poly 600	600±30	576.2	0.0
			Ave: 1.4%

lecular weights are easily calculable from molar refractions, as pointed out recently by E. Warrick.[2] Calculation of molecular weights from molar refractions is based on the well-accepted concept of group additivity and the additional step of an empirical correlation between molar velocity and molar refraction is eliminated. Since the molar-refraction method is physically analogous to a chemical end-group determination, the resulting molecular weight, in the case of a heterogeneous polymer, will evidently be a number average. This can also be readily shown mathematically using additivity of molar refractions on the basis of mole fractions.

In the system of polyethylene glycols, treated by the above authors, the average experimental molar-refraction increment for each $-CH_2-CH_2-O-$ structural unit, based on the first five pure members of the series, is 10.97. From the general formula for the polyethylene glycols, $HO-(CH_2-CH_2-O-)_n-H$, the molecular weight, M, of any member may be written

$$M=44.05i+62.07, \tag{1}$$

where

i = number of CH_2-CH_2-O units in compound, 44.05 = molecular weight of CH_2-CH_2-O unit, and 62.07 = molecular weight of ethylene glycol.

Similarly, the molar refraction, on the basis of additivity of groups, may be expressed

$$R=(n^2-1/n^2+2)M/d=rM=10.97i+14.47,$$

or

$$r(44.05i+62.07)=10.97i+14.47, \tag{2}$$

where

$r=(n^2-1/n^2+2)1/d$ = specific refractivity of compound, and 14.47 = molar refraction of ethylene glycol.

Equation (2) is easily solved for i, and substitution of i in Eq. (1) gives the molecular weight. From the density and refractive-index data reported by Weissler, Fitzgerald, and Resnick, the molecular weights given in Table I were calculated.

The agreement between theoretical molecular weight and molecular weight calculated from the experimental specific refractivities is actually better than that obtained by the molar-velocity method (1.4 percent *vs.* 2.0 percent). Since the molar-refraction method depends essentially on differences between the molar refractivity of the chain and the end-groups, it is evidently only applicable to compounds of relatively low degree of polymerization. This same limitation, however, applies to the molar-velocity method. For low molecular-weight liquid polymers the molar-refraction method is very useful and convenient as the necessary density and refractive-index measurements are easily made to a high degree of accuracy.

[1] A. Weissler, S. W. Fitzgerald, and I. Resnick, J. App. Phys. **18**, 434 (1947).
[2] E. Warrick, J. Am. Chem. Soc. **68**, 2455 (1946).

Preliminary Measurements Relative to the Onset of Thermal Convection Currents in Unconsolidated Sands*

H. L. MORRISON
North Carolina State College of Agriculture and Engineering, Raleigh, North Carolina
July 10, 1947

TO assess a recently advanced theory[1] for the minimum temperature gradient necessary to cause the onset of convection in a viscous liquid in a porous medium, a series of appropriate measurements has been initiated using several different liquids separately in unconsolidated sands of known permeability. These measurements are reported here in a preliminary form because of their interesting bearing upon the theory itself and upon its application to geophysical problems. The measurements were made on mixtures (depth 10 cm) of liquid and sand in a 400-cc beaker (diameter 7.0 cm) which was heated from below; temperatures were observed at various depths in the mixture, as functions of time; and microscopic observations were made of the onset of motion in small suspended solid particles (impurities) which were visible near the wall of the beaker. Precautions were taken to assure the horizontal uniformity of temperature (maximum deviation about ¼°C to ½°C) throughout the mixture; and subsidiary measurements of upward motions of the liquids, caused by diffusion, were made using suitable soluble dyes so as to assure that this possible disturbing effect was negligible. A further subsidiary series of measurements was made using a beaker of 15.0-cm diameter, to exhibit the effects of vessel radius; there were no appreciable effects on the temperature gradient required for onset of convection. Typical observations are recorded in Table I. In Table I, the data in columns 4 to 6 are cast in the form used in reference 1, so that z column 4+column 6 = $z+\theta$; the column 3 refers to the gradient at z (distance into mixture

TABLE I.

Liquid	Permeability of sand (d'Arcy's)	Temperatures and gradients at onset of convection: Local gradient (°C/cm) estimated	β-gradient (°C/cm)	Temperature at $z=0$ (°C)	Approximate θ temperature function (°C)
Glycerol	95	−80	−8.4	125	$-47\frac{1}{2}\sin(\pi z/10)$
CCl_4	127	−0.8	−0.8	31½	0
H_2O	127	−6.0	−6.0	57	0

from bottom) = 2 cm, the usual point of location of the microscope.

In attempting to compare the data in Table I with the theory,[1] one meets definite difficulties. Thus, the θ-function for the CCl_4 and H_2O data, does not accord with the sinusoidal one assumed in developing the theory, though this may not be too significant, for the theory might use a more general series of sine functions which could correlate with the zero used in the measurements. Again, the theory does not contemplate a variation of viscosity with temperature, a situation which is far from acceptable for the liquids used in these measurements. Finally, the finite horizontal extent of the mixture in these measurements implies, at least in principle, boundary conditions which the theory does not contemplate. Nevertheless, any attempted application of the Eq. (26) in reference 1 to these experiments appears to indicate that for the glycerol test, the calculated gradient is at least on order of magnitude in excess of the observed, and for the other two, the calculated gradient is slightly in excess of the observed. Apart then, from the possibility that it is not correct to identify the onset of motion in suspended matter in the present series of measurements with the onset of convection, it can only be concluded at the moment that the theory[1] predicts excessive values for the minimum temperature gradient but that it deserves such extensions as to render it applicable to materials, dimensions, and θ-function having actual, rather than ideal, characters.

This work was suggested to the author by Dr. F. T. Rogers, Jr., to whom, with Mr. C. W. Horton, the author is also indebted for continuing conversations and correspondence relating to it. Further measurements are in progress, and will be reported when and if it is possible to extend the theory suitably.

* An earlier report on this work was presented at the April 1947 meeting of the Southeastern Section of the American Physical Society at Salisbury, North Carolina. See Phys. Rev. **71**, 834 (1947).

[1] C. W. Horton and F. T. Rogers, Jr., J. App. Phys. **16**, 367 (1945).

Attachments for Aligning a Console Electron Microscope

HENRY C. FROULA
Armour Research Foundation of Illinois Institute of Technology, Chicago, Illinois
July 8, 1947

THE alignment of the electron gun and anode aperture in our RCA console electron microscope was greatly simplified through the use of the two devices described below.

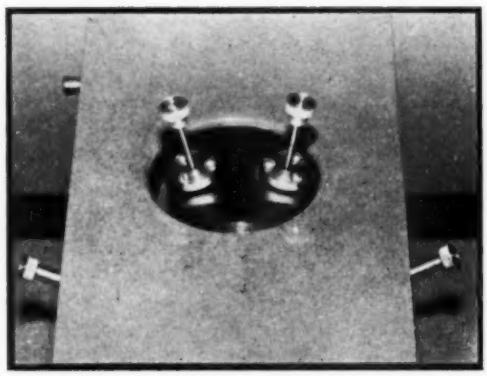

FIG. 1. Rear view of console electron microscope, showing external controls for alignment of electron gun and anode aperture.

The first of these two devices provides for the alignment of the electron gun. Three arms mounted 120° apart on the front rim of the gun extend forward to overhang the fixed column by about one-half inch. One of these arms (on the underside of the gun) is a flat spring whose free end presses upward against the column, tending to lower the gun. Each of the other two arms has a tapped hole through which a screw is driven against the fixed column. Manipulation of the screws provides a two-dimensional adjustment of the gun position. The two screws can be turned externally by means of the removable extension shafts which project through the sides of the hood as shown in Fig. 1.

The second of the two devices provides for the external adjustment of the anode aperture. The regular cover of the specimen chamber is replaced temporarily by one having two sealed passages holding a pair of metal rods. These rods can be seen projecting upward in the figure. Their lower ends are articulated with the two screws which adjust the anode aperture. The vacuum seals through which the rods pass, permit a liberal amount of movement of the rods so that adjustments can be made during actual operation of the microscope.[1]

Both of these devices have had considerable use in our laboratory and have given very satisfactory service in establishing and maintaining suitable alignment of the microscope.

[1] The seals are of the type described by D. B. Cowie, Rev. Sci. Inst. **15**, 46 (1944).

New Books

Radium Therapy; Its Physical Aspects.

By C. W. Wilson. Pp. 224, Figs. 97, 30 tables, and 4 mathematical appendices. Chapman and Hall, Ltd., London, 1945. Price $6.00 plus postage.

This book supplies an excellent practical survey of the physical aspects of radium therapy, more complete and detailed than anything hitherto available. The basic theories of radioactivity are passed over rather briefly, but the interaction of high energy radiations with matter is discussed in detail. The development of methods and theory of dosimetry receives considerable attention. Detailed descriptions are given of the air-wall ionization chamber, and of various practical vacuum-tube dosimeters, with instructions for their use.

A large part of the book is devoted to dosage calculations, with many examples. For surface therapy, the Paterson and Parker charts are followed. In intracavitary treatments, various systems for treatment of cancer of the cervix are compared in detail. For interstitial dosage calculations, the Memorial Hospital and Paterson and Parker techniques are discussed, with numerous examples for the latter. A chapter devoted to dosage in teleradium therapy will find few readers in America, since this method is now little used here. The matter of protection is adequately covered.

One might wish that more attention had been devoted to the matter of integral dose, or total energy absorbed by the patient, since this had been more thoroughly studied in England than in the United States.

Each chapter contains a good list of references, specific and general. The appendix consists of useful mathematical tables.

Radiologists have long felt a need for such a book; there has been no satisfactory text covering this field. It should be welcomed by students, teachers, and all practicing radiologists and radium therapists.

Edith H. Quimby
Columbia University

Introduction to Atomic Physics

By Henry Semat. Revised Edition. Pp. 412+xi, Figs. 169, Tables 27, 23×15.5 cm. Rinehart and Company, Inc., New York, 1946. Price $4.50.

The first edition of Semat, appearing in 1939, at once became a standard undergraduate text on atomic physics and won a place of respect on the shelves and desks of physicists and chemists of experience. This second edition is substantially the earlier Semat, though it presents an altered appearance. The page size, type, paper, and some of the subdivision of text into chapters have been changed along with the corporate title of the publisher. The effect of the new format is one of increased elegance and modernity, but not all users will approve the change to paper of half the former thickness.

Getting down to subject matter, one finds that a large number of small, first-edition errors have been corrected, data have been brought up to date, several diagrams have been redrawn, and new paragraphs inserted to clarify or supplement previous treatments. This piecemeal modernization has been accomplished smoothly without serious impairment of the unity of the book. Some new problems have been constructed and some old ones improved. The statement that 94 elements are found in nature is not yet correct.

The book begins and ends with nuclear energy, the frontispiece comprising photographs of the first atomic bomb explosion, and the final chapter being devoted entirely to a discussion of nuclear energy. This chapter, the only completely new one in the book, starts with the stellar energy reactions of Bethe and proceeds through a careful history of nuclear fission researches to nuclear chain reactions, fast and slow. Some of the latter discussion is taken sentence for sentence from the Smythe report, without quotation marks, but with a preceding statement that the discussion is based on the report. The reviewer dislikes and disbelieves statements that mass is converted into energy, or even "other forms of energy." This common stereotype will do no harm to physicists but may interfere with students' understanding of the equivalence equation since it suggests that after the event the total mass is less than it was before.

Other topics which make their first appearance in this edition are the measurements of nuclear magnetic moments, the discovery and production of new elements, electron optics, and the design and use of the betatron. Semat's first edition was distinguished by an unpretentious clarity of statement and a consistent awareness of the capacity and limitations of the chosen audience. These characteristics are preserved in the current modifications and extensions. It is a sad circumstance that enables a book on atomic physics to be brought up to date after seven years with no more enlargement than Semat has found necessary. It is to be hoped that the third edition will require the inclusion of much more new material.

Paul Kirkpatrick
Stanford University

New Booklets

The National Research Council calls attention to *Mathematical Tables and Other Aids to Computation*, a quarterly journal published by the Council at 2101 Constitution Avenue, Washington 25, D. C. It is edited by Raymond C. Archibald and Derrick H. Lehmer and is an international publication which serves as an information center of published and unpublished mathematical tables and material dealing with other aids to computation. Because of the continuous pagination in each volume and a system of constant cross references, new subscribers will find it desirable to begin their subscriptions with the first issue of the year. Subscription is $4 per year; single issues $1.25.

Jarrell-Ash Company, 165 Newbury Street, Boston 16, Massachusetts, announce their new 20-page catalog *I-3* describing their stigmatic grating spectrographs and accessories.

Interchemical Review, 432 West 45th Street, New York 19, New York, features in its Spring 1947 issue articles on the application of filters in photography, methods of printing on vinyl film, and the wartime development in Britain of a non-metallic conductive coating for paper.

The most recent issue (Volume 9, Number 2) of *Philips Technical Review*, published by Philips Laboratories in Holland, contains the following articles, according to North American Philips Company, Inc., 100 East 42 Street, New York 17, New York: "A new electron microscope with continuously variable magnification," by J. B. le Poole; "Electronic conductivity of non-metallic materials," by E. J. W. Verwey; "Installations for improved broadcast reception," by P. Cornelius and J. van Slooten.

RCA Victor Division, Camden, New Jersey, has issued a 16-page booklet, for distribution to consumers, entitled *What's Your Television I.Q.?*

Dover Publications, 1780 Broadway, New York 19, New York, has published a new 1947 catalog of scientific books published by it. 38 pages.

Burrell Technical Supply Company, 1942 Fifth Avenue, Pittsburgh 19, Pennsylvania, has issued an *Announcer* of scientific equipment. It is published quarterly and describes various laboratory instruments and equipment. Each edition also contains a dissertation on the history of some instrument or process now used in industrial research.

Cannon Electric Development Company, 3209 Humboldt Street, Los Angeles 31, California, has issued *Cannon Plugs*, a 78-page booklet containing many photographs and describing the uses of its products in industry.

Microfilm Service, a new affiliate of the American Council on Public Affairs, located at 2153 Florida Avenue, Washington 8, D. C., is publishing through the microfilm medium scholarly manuscripts on specialized subjects, documents of historical value, and out-of-print studies.

The Editorial Service Bureau of Kodak, 343 State Street, Rochester 4, New York, has issued the first edition of *Shorts*, a 4-page digest of new uses of photography.

Foster D. Snell, Inc., 29 West 15th Street, New York 11, New York, has released a 1947 edition of its brochure under the heading *The Chemical Consultant and Your Business*. Available without charge.

Distillation Products, Inc., 755 Ridge Road West, Rochester 13, New York, has published a 16-page booklet entitled *Information on High Vacuum Distillation*.

Fischer and Porter Company, Hatboro, Pennsylvania, has released a new, larger catalog section No. 95-D describing the company's line of precision bore glass specialties. Address Department 6F-D in requesting a copy.

Here and There

New Appointments

Cleveland Norcross, formerly executive secretary of the Office of Scientific Research and Development, is now assistant director of the American Institute of Physics.

Captain Robert D. Conrad, U. S. Navy retired, has been named assistant director of Brookhaven National Laboratory for atomic research.

Effective September 1, T. Keith Glennan, recently an executive of Ansco Division of General Aniline and Film Corporation and wartime director of the U. S. Navy Underwater Sound Laboratory, became president of Case Institute of Technology, Cleveland, Ohio, succeeding William E. Wickenden, who has retired.

Science reports that Henry N. Russell, professor of astronomy and director of the observatory, Princeton University, retired July 1. Lyman Spitzer, Jr., professor of astrophysics, Yale University, has been appointed director of the observatory, and Martin Schwarzschild, Columbia University, has become professor of astronomy.

William E. Good has been granted a year's leave of absence from the Westinghouse Research Laboratories to aid in atomic energy investigation at the Argonne National Laboratory near Chicago.

Louis N. Ridenour, formerly assistant professor of physics, University of Pennsylvania, has been appointed dean of the Graduate School, University of Illinois.

New Casting Resin

P. J. Franklin and M. Weinberg of the National Bureau of Standards issued recently a report on a casting resin developed by the Bureau. Their report says, "During the war, exacting mechanical and electrical stability requirements of special electronic applications—such as the radio proximity fuze—necessitated the potting of the circuit components. Because of the high impedance of the circuits involved, the electrical loss factor or the dissipation of the available energy in the casting or 'potting' compound became a matter of major importance. An extensive investigation of various available casting resins at the National Bureau of Standards revealed none suitable for the particular applications because of the high loss factor. The few materials with adequate electrical properties were deficient mechanically. In addition, the applications required a resin of such viscosity that the potting compound would encompass all the circuit elements when poured into

a container housing the electronic device, and then harden to a rigid solid without adversely affecting circuit operation.

"Many casting resins have been developed, but few have the vital electrical properties for proper operation of high-impedance, high-frequency equipment. As a result of experience gained in the fuze-development program at the National Bureau of Standards, a new casting resin embodying the required properties of mechanical and electrical stability, was formulated through a systematic variation of resin constituents. Various applications at the Bureau indicate that, with slight modifications to suit the intended use, the new potting compound—known as NBS Casting Resin—can be readily employed in many high-frequency devices requiring such mechanical-electrical insulation.

"The most important properties specifically desired of a casting resin when utilized at high frequencies in high-impedance circuits are low power factor, low dielectric constant, short polymerization period at low temperature and atmospheric pressure, high impact strength, small volume shrinkage on polymerization, dimensional and electrical stability, and low moisture absorption. The NBS Casting Resin not only meets these requirements but fulfills the additional requirements of low viscosity and low surface tension, and hence may be poured through small openings."

New Research Laboratory in Texas

In April a new research laboratory was officially opened on a 3000-acre strip eight miles west of San Antonio, Texas. The project, made possible by the gift of a valuable oil property by Tom B. Slick, San Antonio oil and ranch man, consists of two separate but closely associated units: the Foundation of Applied Research, utilizing the Essar Ranch as part of its laboratory, and the Institute of Industrial Research, including a development service for inventors. While the Foundation of Applied Research was incorporated by its trustees as a non-profit undertaking, it has been designed to make its own way financially, after a development period, from sales of Essar Ranch's blooded cattle and from earnings by the Institute of Industrial Research through fees and patent proceeds.

Dr. Gregory Pincus, head of the Worcester Foundation for Experimental Biology at Worcester, Massachusetts, is selecting the research men and scientists who will staff the Foundation and the Institute.

Objectives of the projects have been outlined by Mr. Slick as follows: "The only limitation to the scope of work to be undertaken by the Foundation is that it has in view a distinctly practical application. The value of pure scientific study is fully realized, but it is felt that the Foundation's greatest contribution can be realized by concentration on the field lying between pure scientific study as carried out by universities and similar institutions, and completely industrial research of limited range as conducted by the average industrial corporation."

The Institute of Industrial Research, under separate management from the Foundation, will undertake, on a fee basis for industrial corporations, programs similar to the services rendered by the Mellon, Armour, and Midwest Institutes, and in addition will provide inventors with a complete processing service should their projects be determined worthy of development.

New Computer at California Institute of Technology

Science reports that an electric analog computer will be part of the new analysis laboratory now being established at the California Institute of Technology. Gilbert D. McCann, Associate Professor of Electrical Engineering at the Institute, is setting up the laboratory.

The new calculator, which will be made available to all interested industrial and engineering organizations as well as being used for research at the Institute, is expected to be completed by August. Weighing approximately 33,000 pounds, the machine, including its control desk, will occupy some 1000 square feet of floor space. The device was designed for the solution of complex mathematical problems in the field of algebra and calculus requiring an accuracy of the order of 1 percent. It is particularly suited to solving engineering problems, including those of electrical circuits; applied mechanics; self-induced mechanical oscillations, such as airplane structure flutter, car shimmy, rail car stability; problems in thermodynamics, such as a general analysis of heat flow problems; speed controllers, voltage regulators; and angle position controllers, such as airplane stabilizers, guided missiles, gyro pilots, etc.

Physical Society Acoustics Group

The Acoustics Group of the Physical Society was formed at an inaugural meeting at the Royal Institute of British Architects in February 1947. Dr. Alex Wood gave an address entitled "The Contribution of Acoustical Science to Allied Studies." The meeting was attended by some 170 persons. The principal object of the Group is to provide an opportunity for the varied types of workers engaged on acoustical problems to meet and discuss the scientific and technical implications of their work. Membership is open both to members and also to non-members of the Physical Society. For further particulars inquire of the Joint Honorary Secretaries of the Acoustics Group, The Physical Society, 1 Lowther Gardens, Prince Consort Road, London S. W. 7.

Sound Apparatus Company

The Sound Apparatus Company announces the opening of its production plant in Stirling, New Jersey. The company's research laboratories are in Millington, New Jersey, and the main offices are at 233 Broadway, New York City.

High Vacuum Symposium

National Research Corporation, in cooperation with the Division of Industrial and Engineering Chemistry, American Chemical Society, has announced plans for a High Vacuum Symposium to be held in Cambridge, Massachusetts, October 30 and 31. Secretary for the event is Stanley Heck, National Research Corporation, Boston 42, Massachusetts.

Kodak Fellowships

Sixteen educational institutions have been offered one or more of twenty-two Eastman Kodak fellowships in chemistry, physics, engineering, and business administration for the school year 1947–48. In addition six similar fellowships are to be sponsored by Tennessee Eastman Corporation, Kodak subsidiary.

National Electronics Conference

A National Electronics Conference will be held at the Edgewater Beach Hotel, Chicago, Illinois, November 3–5, 1947. Dr. George D. Stoddard, new president of the University of Illinois, will deliver the keynote address. The complete program for the Conference includes twenty technical sessions with a total of about fifty papers.

Taylor Elected Radiology Fellow

Lauriston S. Taylor, chief of the x-ray section at the National Bureau of Standards, has been elected an associate fellow in the American College of Radiology.

Institute of Navigation Officers

The institute of Navigation has elected the following national officers for the academic year 1947–48: president, Commodore G. G. McLintock, USMS, Special Assistant to the Commandant, U. S. Maritime Service; vice president, Captain P. V. H. Weems, USN (*Retired*), Annapolis, Maryland; technical adviser, Paul Rosenberg, president of Paul Rosenberg Associates, New York City; executive secretary, Samuel Herrick, professor of astronomy, University of California at Los Angeles.

Chicago Physics Club Officers

The following are the new officers of the Physics Club of Chicago, elected May 1947: president, W. F. Einbecker; vice president, H. A. Carter; treasurer, J. W. Juvinall; secretary, H. C. Froula.

Conference on Administration of Research

A conference on "Administration of Research" will be held at The Pennsylvania State College on Monday and Tuesday, October 6 and 7. The main purpose of the conference is to provide free discussion on the organization, administration, and operation of research laboratories.

Discussion will be led by Prof. Philip M. Morse, Brookhaven National Laboratories, and Dr. Jesse E. Hobson, Armour Research Foundation. The following men will be the principal speakers:

Dr. Maurice Holland, New York, Consultant
Dr. R. L. Jones, Bell Telephone Laboratories
Dr. G. H. Young, Mellon Institute of Industrial Research
Dr. Dwight E. Gray, Applied Physics Laboratory
Dr. L. Warrington Chubb, Westinghouse Electric Corporation
Dr. Edw. U. Condon, National Bureau of Standards
Hon. James H. Duff, Governor, Commonwealth of Pennsylvania
Commodore Henry A. Schade, Director, Naval Research Laboratory
Dr. Paul D. Foote and Dr. Blaine B. Westcott, Gulf Research Laboratories
Dr. Albert W. Hull, General Electric Company

For further information and a copy of the program, address Dr. Eric A. Walker, Head, Electrical Engineering Department, The Pennsylvania State College, State College, Pennsylvania.

Calendar of Meetings

October

2–4	Society of Automotive Engineers, Los Angeles, California
15–18	American Society for Civil Engineers, New Orleans, Louisiana
20–24	American Society for Metals, Chicago, Illinois
23–25	Optical Society of America, Cincinnati, Ohio
30–31	National Research Corporation and American Chemical Society, Cambridge, Massachusetts (High Vacuum Symposium)

November

3–5	National Electronics Conference, Chicago, Illinois
3–7	American Institute of Electrical Engineers, Chicago, Illinois
6–7	Society of Automotive Engineers, Tulsa, Oklahoma (Fuels and Lubricants Meeting)
7–8	Conference on X-Ray and Electron Diffraction, Mellon Institute of Industrial Research, Pittsburgh, Pennsylvania
17–19	Institute of Radio Engineers and the Radio Manufacturers Association, Engineering Department, Rochester, New York
28–29	American Physical Society, Houston, Texas

December

1–3	Society of Automotive Engineers, Kansas City, Missouri (Air Transport Engineering Meeting)
1–5	American Society of Mechanical Engineers, New York, New York
26–31	American Association for the Advancement of Science, Chicago, Illinois
29–31	American Physical Society, Chicago, Illinois